

Replies to review comments

We thank all the reviewers and the co-editor for the time and effort spent on the manuscript.

Considering all suggestions from three reviewers, we made the following major changes in the revision of the manuscript:

1. A detailed description of our MIPAS aerosol measurements is added.
2. The Sect. 3.2 that introduces the meteorological background is moved to Sect. 3.1. And Fig.4 that shows the meteorological background is the new Fig. 1.
3. In Fig. 1, ACI values no larger than 8 instead of 7 is shown to allow in a little more measurements, and it is moved to the new Fig. 5.
4. The Fig. 6 that shows the latitude and height cross section of the MIPAS median ACI values is removed, because contaminated by the background aerosol, the change of aerosol load after the Merapi eruption in 2010 and the poleward transport of the volcanic aerosol is not clear.
5. MIPAS aerosol measurements during the relatively volcanic eruption quiescent period in the Southern Hemisphere from 11/2007 to 03/ 2008 are used as the reference state to derive the change of aerosol load in the Southern Hemisphere after the Merapi eruption in 2010, so that the seasonal variations are removed. And the Fig.7 (the new Fig. 6 in the revised manuscript) and the Fig. 10 (the new Fig. 9 in the revised manuscript) are updated accordingly. Reference time period from November 2003 to March 2004 is also tested and they all showed qualitatively comparable results.
6. An appendix is added to compare the aerosol load in the tropical stratosphere during the selected reference period (11/2007 to 03/ 2008) and the time period of investigation (11/2010 to 03/ 2011).
7. The “transport efficiency“ may not be the accurate term to describe the proportion of sulfur that originated from the Merapi eruption and was transported to the Antarctic upper troposphere and lower stratosphere (UTLS), so we rephrase it in the abstract, discussion and conclusion..

Please find our point-by-point replies below in blue color. Other amendments can be found in the revised manuscript with tracked changes.

Anonymous Referee #1

Received and published: 1 June 2018

The Editor will have to decide if there is enough new science here to accept this paper. The paper needs some revisions, but the question is whether it is important science. This paper is well written and presents a new analysis of the poleward transport of the Merapi sulfur. But I'm not sure what is surprising in the conclusions. It is already known that stratospheric sulfur from volcanic eruptions gets transported to the poles, as we find it in ice cores.

Both the sulfate in the ice core record and observation of Antarctic ozone depletion have verified that major volcanic eruptions at low latitudes and volcanic eruptions at the Southern Hemisphere high latitudes may contribute to the sulfate in Antarctica, for instance, the low-latitude major eruptions of Agung in 1963 (Nicolas Patris, 2000), El Chichón in 1982 (Hofmann and Rosen, 1985), Pinatubo and Cerro Hudson in 1991 (Pitts et al., 1993) and high-latitude eruption Calbuco (Solomon et al., 2016; Ivy et al., 2017; Stone et al., 2017). However, there are discussions about the contributions over Antarctica from long range transport and local volcanic sources.

Meanwhile, due to the limit of spatial and temporal resolution of satellite data, and the spatial coverage of in-situ observations, it is difficult to investigate the transport process. We were not able to estimate the influence of the location of the eruption, the height of plume, and the atmospheric background conditions on the transport pathway, and thus not able to judge whether a volcanic eruption will contribute to the sulfate in Antarctica or how much if it does.

It is reasonable to believe that major low-latitude eruptions inject SO₂ directly into the upward branch of the BDC, and the SO₂ or aerosol ascend and flow slowly poleward along the BDC, which could be the main pathway of long-range transport from the tropics to the poles. The Merapi eruption in 2010 was a moderate eruption in the tropics that showed a poleward dispersion of aerosol to Antarctica whereas most other tropical eruptions did not. The fast dispersion of volcanic aerosol for the Merapi case did not seem to be caused by BDC.

This study is one step forward to reveal the transport process and the influence of background atmospheric conditions by combining satellite observations with model simulations in a case study. By carrying out model simulations, it was found that the transport of the volcanic aerosol from the Merapi eruption in 2010 was mainly driven by the relatively quick quasi-horizontal transport from the tropical tropopause layer to the upper troposphere and lower stratosphere at mid- and high latitudes. Based on simulations, the mechanism that influences the transport pathway could be analyzed, and the amount of sulfur transported could be quantified.

Is it that so little of the sulfur made it to the poles?

Based on our simulation and calculation, there was a maximum 8.80×10^3 tons of sulfur went to the south of 60°S between the isentropic surfaces of 350 and 480 K at the end of February 2011. If these were in form of a 75–25% $\text{H}_2\text{SO}_4\text{-H}_2\text{O}$ solution, the total aerosol mass loading adds up to 2.15×10^4 tons. As seen in Fig.1 (Fig. 5 in the revised manuscript), except for the high-latitude volcanic eruptions, the moderate tropical eruption, Merapi eruption in 2010, made a most prominent contribution to the stratospheric aerosol at mid- and high latitudes.

Are there any observations to validate the model simulation?

In our study, MIPAS data are compared with model results. The altitude-resolved MIPAS aerosol observations are the best data to validate our model results. The CALIOP measurements captured some signals of sulfate aerosol and ash (not shown in the manuscript), but because the CALIOP aerosol data is very limited during the polar daytime, it did not complement to the MIPAS observations. We did not obtain ice core data later than 2001 to verify the disposition of sulfate.

Fig. 7 (confusing because the units are not defined) actually shows that the aerosol load was reduced at the South Pole.

Figure 7 shows the change in median ACI values in the tropics and the Southern Hemisphere corresponding to the same time period as Fig. 6. It is to demonstrate the increase in the aerosol load due to the eruption of Merapi. To calculate the values in Fig. 7, we first define the “reference state” of the aerosol load by calculating the median ACI in 1–4 November 2010 when there was no aerosol from the Merapi eruption. Then the median ACI values in Fig. 6 are subtracted from this “background” ACI. Since in the MIPAS retrievals, smaller ACI values represent larger aerosol extinction coefficients, in Fig. 7, the positive values indicate an increase in aerosol load and negative values indicate a decrease of the aerosol load. The values do not have units.

The negative values in the South Polar Region above 10 km are not caused by the transport of the volcanic aerosol. Because time period of 1–4 November 2010 is not an ideal “reference state” aerosol load, so there are seasonal variations in the Fig.7. Inspired by suggestions of referees, we used another time period to define the “reference state”. We removed the seasonal cycle in the aerosol data by using data from 11/2007-03/2008 (a relatively volcanically quiescent period in the Southern Hemisphere) instead of 4 days reference period. In this way, the change of the aerosol load after the Merapi eruption and the poleward transport of aerosol are clearer. For more details, please see reply to major comment 1 of referee #2 and the revised manuscript.

I am also confused about the initial stratospheric transport of the volcanic plume. If there was a westerly phase of the QBO, why was the transport toward the west?

Trajectory calculations of each air parcel in Lagrangian transport simulations are driven by wind fields at the location of each air parcel. Figure R1 shows the monthly mean zonal wind in November 2010. If the air parcels were in the area with easterlies, they would be transported towards west. The QBO index in Fig. 4f only shows the zonal wind anomalies over the Equator at 30 or 50 hPa, but can not show the wind directions at the location of each air parcels. Please note that in the revised manuscript, Fig. 4 is move to Fig. 1.

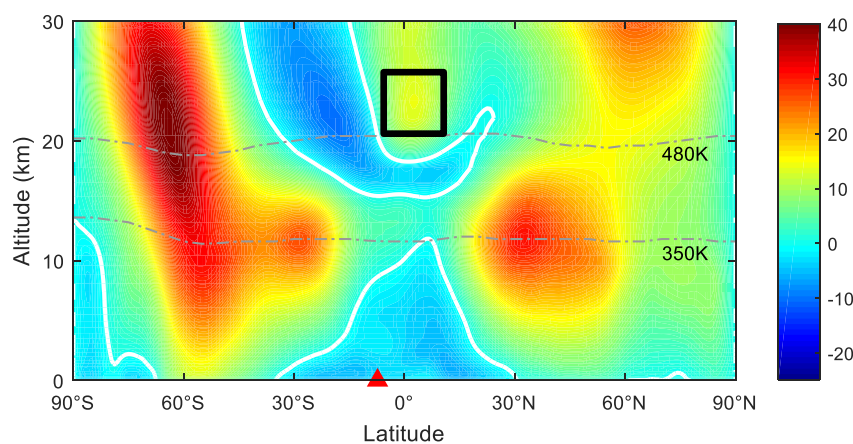


Figure R1: Monthly mean zonal wind (unit: m/s) in November 2010, overlapped the potential temperature of 350K and 480K. The thick white contour indicates the value of 0. The rectangle indicates the region over the equator between 30 hPa (~ 25 km) and 50hPa (~21 km). QBO indices (monthly mean zonal wind anomalies over the Equator) are usually defined at pressure levels of 30 and 50 hPa. The red triangle denotes the latitude of Mount Merapi.

I am confused by the discussion of transport barriers on page 12. The authors say there are PV boundaries, but never explain how this works nor what values of PV are used. Then they use potential temperature values to define transport boundaries. They have to explain how this works and make clear what “boundaries” are and why they chose the values of PV or potential temperature for those boundaries.

Rossby wave breaking is an important mechanism for the exchange of air masses between the tropical upper troposphere and the extratropical lower stratosphere. Potential vorticity (PV) streamers (e.g., poleward-moving filaments with low PV originating in the tropics) are indicators of Rossby wave breaking (RWB) and constitute important atmospheric transport pathways between the tropics and extratropics.

Kunz et al. (2015) derived a climatology of PV streamer boundaries on isentropic surfaces between 320 and 500K using ERA-Interim reanalyses for

the time period from 1979 to 2011. This boundary is defined as the maximum product of the meridional PV gradient and zonal wind speed on isentropic surfaces, which identifies a PV contour that best represents the dynamical discontinuity on each isentropic surface. It can be used as an isentropic transport barrier and to determine the isentropic cross-barrier transport related to Rossby wave breaking. There are seasonal variations in the location of PV boundaries as shown in Fig. R2 and the specific values of the PV boundaries on isentropic surfaces in each season can be found in Table R1.

In this study, the horizontal transport along the subtropical jet associated with Rossby wave breaking is a long-range transport mechanism from the tropical tropopause layer to the Southern Hemisphere lower stratosphere. The volcanic plume was transported along the subtropical jet and at the same time entered the extratropical lower stratosphere driven by Rossby wave breaking. The PV contours shown with gray dashed lines in Fig. 8 (the Fig. 7 in the revised manuscript) represent the isentropic transport barrier on 350 K isentropic surface (-3.33 PVU during November and -4.78 PVU during December) based on the climatology of the PV streamer boundaries derived by Kunz et al. (2015). Isentropic transport of air masses across these contours is due to Rossby wave breaking. In the polar stratosphere, PV boundaries on isentropic surfaces, e.g., around 480 K, can be considered as a barrier for cross polar vortex transport of air masses between the mid-latitudes and polar regions.

We have added more detailed explanations to Sect. 3.4 in the revised manuscript to make this term clearer.

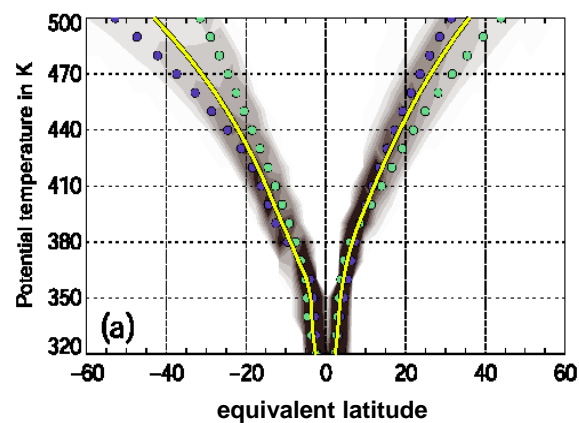


Figure R2. Probability density function of the 1979–2011 daily values of the (a) dynamically relevant contour of PV on isentropes between 320 and 500 K. The bin size is 3 PVU for PV and 5° for equivalent latitude. Blue and green dots represent the mean PV or mean equivalent latitude of the dynamically relevant contour in June, July and August (JJA) and December, January and February (DJF) respectively. The solid yellow line represents an annual mean. (Kunz et al., 2015)

Isentrope	Northern Hemisphere				Southern Hemisphere			
	MAM	JJA	SON	DJF	MAM	JJA	SON	DJF
320 K	2.22	2.44	2.60	2.21	-2.98	-2.25	-2.37	-2.53
330 K	2.59	3.08	3.28	2.65	-3.80	-2.52	-2.77	-3.59
340 K	2.85	3.62	3.74	2.91	-3.92	-2.79	-3.00	-4.48
350 K	2.98	4.46	4.10	3.24	-3.83	-3.17	-3.33	-4.78
360 K	3.64	5.51	4.91	3.80	-4.43	-3.93	-5.62	-5.18
370 K	4.63	6.36	5.99	4.65	-5.50	-6.20	-9.54	-6.24
380 K	5.88	7.24	7.20	6.07	-6.69	-9.57	-11.47	-7.61
390 K	7.76	8.56	8.54	8.58	-8.67	-12.52	-13.34	-9.23
400 K	9.63	10.04	9.99	11.36	-11.08	-14.37	-15.47	-10.92
410 K	11.50	11.67	11.51	13.93	-13.07	-16.20	-17.73	-12.64
420 K	13.53	13.44	13.21	16.55	-15.12	-18.39	-20.10	-14.51
430 K	15.68	15.33	15.15	19.20	-17.20	-21.17	-22.55	-16.51
440 K	17.85	17.28	17.26	21.94	-19.29	-24.60	-25.15	-18.50
450 K	20.15	19.28	19.52	24.95	-21.56	-28.61	-28.02	-20.50
460 K	22.55	21.38	22.01	28.17	-24.11	-32.81	-31.30	-22.52
470 K	25.09	23.65	24.82	31.69	-27.00	-37.38	-35.27	-24.52
480 K	27.80	26.08	27.85	35.46	-30.19	-42.20	-39.75	-26.64
490 K	30.62	28.55	31.16	39.47	-33.80	-47.35	-44.47	-28.93
500 K	33.64	31.44	34.80	43.90	-37.78	-52.86	-49.46	-31.47

Table R1 Seasonal Mean of the PV boundaries (in PVU) in isentropic surfaces between 320 and 500 K (Kunz et al., 2015)

It is not clear to me how the values of 8800 tons of sulfur (and are they sure this is S, and not SO₂ or SO₄?) and 4% were derived for transport into the south polar cap. The figures did not show much arriving south of 60°S at all.

As Figure 10a (Fig. 9a in the revised manuscript) showed with black dots, it is calculated that there was a maximum of 4% of the plume south of 60°S between isentropic surfaces of 350 and 480 K at end of February 2011. The percentage is roughly calculated by dividing the number of SO₂ parcels between 350 and 480 K south of 60°S by the total number of SO₂ parcels released.

Based on previous research on the Merapi case, we assigned a total mass of SO₂ to all parcels released. There is not a chemical scheme in the Lagrangian particle dispersion model we used, so we assume that when the plume went to the high latitudes, the SO₂ are all converted to sulfate acid. And we multiplied the percentage of air parcels south of 60°S between isentropic surfaces of 350 and 480 K with the total mass of sulfur in the released plume and only calculated the mass of the part of sulfur (not SO₂ or sulfate acid). This result (8800 tons) is under the assumption that sulfate aerosol converted from SO₂ remained in the plume. And there are other factors that can affect this number have been discussed in Sect. 4.

It is possible that the confusions above came up because it was not very clearly explained in the manuscript. So we have added a further explanation

for each of them in the revised manuscript.

The authors need to address the 56 comments in the attached annotated manuscript, paying particular attention to issues with the figures.

Please see the supplement with comments.

Anonymous Referee #2

Received and published: 25 June 2018

General comments

This study investigates the transport of volcanic sulfur emissions from the 2010 eruption of Merapi. It uses both model simulations and satellite observations to investigate the poleward transport of sulfur to high latitudes. The topic is well suited to ACP.

Major comments

1. The study claims “good agreement” between the simulated trajectories and the MIPAS aerosol index measurements, and uses this “agreement” to underpin the conclusions of the work. Unfortunately, I just don’t see a good agreement between the satellite observations and the model results. The model results (Fig 5) show a strong sulfur presence at and above the tropical tropopause, and strong poleward transport along the 380 K PT surface. From Fig. 7, the observations show almost no aerosol above the tropical tropopause, and slight aerosol increases in the high latitude upper troposphere. If this slight high latitude aerosol increase is from the Merapi eruption, the transport pathway does not appear to be via the 380 K PT surface, as in the model simulation.

Plus, the observations show a highly elevated aerosol index in the SH high latitude stratosphere before the eruption, and some apparent descent of these aerosols, which could contribute to the elevated aerosol signal just below the tropopause in Jan and Feb 2010. I also worry about the choice of a very small reference period in the calculation of the anomalies in Fig 7, it seems likely that the anomalies shown might contain the influences of seasonal variations in aerosol and transport, for instance there are strong variations in UT aerosol in the NH, not associated with volcanic activity in Fig 6. The simulations presented here produce some clear results, but much more work would be required to be able to say that these results are supported or “validated” by the observations, this is simply not true.

We agree that we messed up a clear presentation of the satellite data showing the Merapi plume transport in Fig.7. We thank referee #2 for pointing out that 4 days before the eruption are too short for a reference period as there are seasonal variations in the aerosol signal. In order to bring the aerosol signal of the Merapi into the foreground, we selected a time period from 11/2007 to 03/2008 with no major SO₂ emission in the Southern Hemisphere UTLS (as shown in Fig. 5 in the revised manuscript) as a “reference state”, calculated the biweekly median ACI of the “reference state” and subtracted the biweekly ACI median between 11/2010 and 03/2011 from it. Now the aerosol signal due to the Merapi aerosol is shown clearly.

To test for inter-annual variations, we tested a second time period 11/2003 to 03/2004 without large or moderate volcanic eruptions in the Southern

Hemisphere and found qualitatively comparable results.

The Fig.6 does not show the poleward transport of the aerosol clearly with seasonal cycle in it, so we remove the Fig. 6 and the Fig.7 is the new Fig. 6 in the revised manuscript.

2. The authors claim to have investigated the transport efficiency of volcanic aerosol, for example stating that “the most efficient pathway for the quasi-horizontal mixing was in between the isentropic surfaces of 360 and 430 K”. They do not however define what they mean by “efficiency”—usually efficiencies correspond to some sort of ratio, e.g., the proportion of transported to injected material, but the analysis seems only to be based on the vertical levels where the largest numbers of trajectories existed, which is obviously strongly connected to the vertical level of the injections. It is also stated that transport from quasi-horizontal mixing is “more efficient” than the slow residual mass circulation of the Brewer-Dobson circulation, but this is a rather obvious result for an injection into the tropical UTLS especially when only short term simulations are performed. Is transport to Antarctica from a tropical UTLS injection more efficient than transport of background sulfate via the BDC? Such questions cannot be answered with this study.

Thank you for pointing this out. We agree that we can not compare the in-mixing with BDC in our study. We have rephrased the statement throughout the manuscript. Instead of “efficiency”, it is more accurate to say it is the proportion of sulfur that originated from the Merapi eruption and was transported to the Antarctic UTLS.

3. The connection between the aspects of the simulated aerosol transport and different dynamical regimes—the phase of the QBO or the strength of the subtropical jet—are not tested in any way, and so cannot be linked in a causal way. For example, the study does not show in any way that the transport of aerosol “was facilitated by the weakening of the subtropical jet during the seasonal transition from austral spring to summer and linked to the westerly phase of the quasi-biennial oscillation (QBO)” as stated in the conclusions. This is an assumption based on prior work, not a conclusion of the experiment presented here.

We agree that the role of QBO in the transport cannot be considered as the conclusions of this study. The influence of the QBO phase is rather described as the meteorological background. We have removed the statement of the QBO in the abstract and conclusions.

Specific comments:

P1, l16: usually present tense (“estimate”) is used to describe work done in the presented study. Check here and throughout.

Fixed. Thank you.

P1, I19: See major comment 1: “good agreement” is never quantified, and there is little evidence that the observations suggest a significant amount of aerosol transported to the SH high latitudes.

[Please refer to the reply to major comment 1. The agreement between the simulations and the observations is significantly improved after we applied a new reference state.](#)

P1, I26: Most efficient or strongest? Most efficient would imply calculation of some sort of efficiency index, which does not seem to have been done. These heights may have been where the strongest transport occurred just because of the height of the injection, not because the transport there is stronger than other heights.

[We agree that most of the poleward transport is due to the in-mixing because the top of SO₂ injection is in the tropical tropopause layer. The words have been rephrased. Please also refer to the reply to major comment 2.](#)

P1, I28: I guess less than 4% of the SO₂ was transported to high SH latitudes since SO₂ is decaying with a 1-month timescale, you probably mean 4% of the injected sulfur.

[Yes, the 4% is the fraction of sulfur. It is fixed in the abstract.](#)

P2, I8: The study by Aquila et al. (2014) presents model results of a geoengineering scenario: this is not strong proof for the kind of strong statement given here.

P2, I9: Similarly, the Pausata et al. (2015) study is also based on modeling results; this statement needs to be less conclusive to properly reflect current scientific understanding.

[Because the QBO is not directly related to our results in this study, we removed these sentences in the introduction.](#)

P2, I11: The impact of aerosol on polar ozone has been known about for a long time; a handful of references from 2008-2016 don't properly support the statement made here.

[A few earlier references are added here.](#)

P2, I17: “a new record of the size...” is awkwardly phrased.

[It is replaced with “an Antarctic ozone hole with the largest daily average size”.](#)

P3, I11: Kravitz and Robock (2011) describe the impact of season on the impact of high latitude eruptions, and say little about the impact of the variation of quasi-horizontal mixing with season. Toohey et al. (2011) would be a more appropriate reference here.

Toohey, M., Krüger, K., Niemeier, U. and Timmreck, C.: The influence of

eruption season on the global aerosol evolution and radiative impact of tropical volcanic eruptions, *Atmos. Chem. Phys.*, 11(23), 12351–12367, doi:10.5194/acp-11-12351-2011, 2011.

The reference is replaced. Thank you.

P4, I12: “product is sensitive: : :”

Fixed.

P6, I12: Some indication of what kinds of measurements have been used to build the “chronology of the Merapi eruption” would be useful for the reader here.

Thank you very much for your suggestion. We added the data source here as follows:

“According to the chronology of the Merapi eruption that combined satellite observations from AIRS, the Infrared Atmospheric Sounding Interferometer (IASI), the ozone monitoring instrument (OMI) and a limited number of Ground-based ultra-violet Differential Optical Absorption Spectroscopy (DOAS) measurements...”

P6, I25: The reconstructed SO₂ injection between Nov 1 and Nov 3, which shows injection above the tropopause but little anywhere else—seems unlikely given the reported eruption chronology. This portion of the injection time series seems very uncertain, and the implications of possible errors here should be discussed.

Thank you for pointing this out. The SO₂ above the tropopause is quite robust in our simulation. We have checked the CALIOP profiles from 27 October 2010 to 10 November 2010 and found a few profiles that show some dust appeared over the location of Mount Merapi at the height from about 14 to 18 km on 2, 3, 5 November 2010 (no tracks over volcanic plume on 4 November 2010), and 3 to 17 km on 6 November 2010. It could be a fraction of the volcanic plume elevated by the updraft in the convection appeared with the tropical storm Anggrek. The center of the tropical storm Anggrek was on the Indian Ocean about 1000 km southwest of the Mount Merapi. So we consider this small fraction of SO₂ as real and prefer to keep it in our results. The fraction of SO₂ plume above the tropopause very small and our conclusions are not affected with or without it.

We have added some explanation in Sect. 3.2.

P7, I2: One should be clear that you are neglecting the impact of sedimentation completely, i.e., for all sulfate particles—it reads now like you are neglecting sedimentation for the small aerosol. Secondly, you need some words on the applicability of this assumption.

To avoid the ambiguity, this sentence is removed from Sect. 3. A few sentences are added in Sect.4 to discuss this assumption.

P7, I7: “parcels in the upper troposphere: : :”
Fixed.

P7, I21: The two sentences starting with “A more negative...” seem to be referring to conclusions from prior studies, which should be referenced. Also, the first sentence especially is confusing since the post-Merapi anomalies in Fig 4d imply a less negative eddy heat flux, best would be to adjust the description to be consistent with what is seen in Fig 4.

References are added.

P8, I21: please be clear that you refer to “the simulated plume” here and elsewhere.

It is fixed here and throughout the manuscript.

P8, I25: Till-> Until
Fixed.

P8, I30: I don't see the “secondary upward transport” commented on here, either the description needs to be clearer, or this statement cut. P8, I31: Using the word “observable” when presenting simulation results is confusing.

This paragraph is rephrased. An appendix is added to show the upward transport of aerosol in the tropical stratosphere.

P9, I9: I don't think you can conclude with all certainty that the transport was suppressed by the subtropical jets—it is likely, but you didn't test it in any way in your analysis.

This paragraph has been removed together with the Fig. 6.

P9, I17: Four days is a very small sample to base a reference state on. How sensitive are the results to the choice of a reference? Better might be to define a clean climatology from prior years and subtract a seasonally varying climatology.

We changed the reference period. Please see reply to major comment 1 for the details.

P9, I22: Why does the zonal averaging “degrade” the ACI signal? Is this related to incomplete sampling and the plume being localized? What about the 1 month timescale of the conversion of SO₂ to sulfate, does that play a role?

The global MIPAS measurements cover longitudes from -180 to 180° each day. After an eruption, only measurements around the longitude of the volcano indicate aerosol. When there are more than about 30 MIPAS measurements

between the Equator and 5°S, but only one or two of them sample the plume and the others sample clear air, the median and often the mean signal indicate clear air. Of course, the sampling also plays a role. In the tropics, MIPAS measures only down to about 12 km. Hence, the first eruption phase of Merapi (26 Oct - 3 Nov) will be missed. At higher altitudes, if the plume falls between the measurement tracks, it will be missed. The aged aerosol is usually dispersed, so the plume will not be missed due to the sampling.

The conversion of SO₂ to sulfate starts with the moment when the SO₂ enters the atmosphere, and the converted aerosol particles are present in detectable amounts right after the SO₂ injection.

The sentence in the manuscript "No significant change was observed during the first half month after the eruption due to the zonal averaging degrading the aerosol signal (Fig. 7a)" has been changed to:

"In the first half of November, the zonal median (Fig. 6a) does not show a signal of the Merapi eruption, because during the initial time period, the plume was confined to longitudes around the volcano (see Fig. 3), and the MIPAS tracks did not always catch the maximum concentration, so the median ACI values are large (low concentration or clear air). In the second half of November the plume was transported zonally around the globe and hence, the largest aerosol increase appeared in the upper troposphere at the latitude of the Mount Merapi (Fig. 6b) and then moved quasi-horizontally southward into the UTLs region at ~30–40°S (Figs. 6c–d), consistent with what Fig. 5c–d shows."

P9, I24: The strongest signal in the SH high latitudes is a large decrease in ACI, what is this?

This is a seasonal effect we observe every year in the MIPAS data. We followed your suggestion of using more data to define the reference state and to remove seasonal variations. For details and changes on the manuscript please see reply to the major comment 1.

P9, I25: How was the significance of this increase tested?

This paragraph is removed and new texts are added to describe the new Fig. 6.

P10, I2: "comparable" is a rather weak adjective, and in fact there are many important differences between the model results and observations (see major comments).

This sentence has been removed.

P10, I4: "in the surf zone"

Fixed.

P10, I6: What is “our data”? The statement here seems based on the simulation results, but not strongly supported by the observations.

It refers to the simulations. It is replaced with “The simulations”.

P10, I7: The conclusion regarding the main transport pathway stated here should apply only to the Merapi eruption—a large eruption like Pinatubo with a higher injection height will certainly have a different main transport pathway.

It is corrected in the manuscript

P11, I5: “the simulated poleward...”

Fixed.

P11, I14: observed->simulated

Fixed.

P11, I25: The impact of the QBO was not shown in any way by this study, only assumed based on prior work.

We have removed the statement of the QBO in the abstract and conclusions. Please refer to the reply to major comment 3.

P11, I28: No, Figure 4 shows there was weaker than usual wave activity after the eruption, and a colder, more stable vortex until the end of February.

The longitudinally averaged poleward eddy heat flux between 45 and 75° S was smaller than the long-term mean, indicating that the vortex was relatively unperturbed from mid-September to December. However, the polar vortex elongated and weakened gradually through November and was displaced off the pole in mid-December and broke down by mid-January 2011 as shown in Fig. R3. This decay of the polar vortex could also be seen in the Fig. 8 (the Fig. 7 in the revised manuscript), marked by the grey solid contour.

In Fig. R3, the breakdown was marked when the winds around the vortex edge decreased below 15 ms^{-1} on the 475 K potential temperature surface. Figure R4 shows the final warming started in mid-October with the development of strong zonal asymmetries in temperature. The cold pool over the South Pole declined and displaced. A warm pool with temperatures of 230–240 K dominated Antarctica from the end of December. This warming can also be observed in Fig. 4b (the new Fig.1b in the manuscript). Consistent with the warming, the zonal wind speed at 60°S at 150 hPa (Fig. 4c) showed a pronounced reduction in wind speed from 40 ms^{-1} at the beginning of October to less than 20 ms^{-1} from beginning of January.

In the revised manuscript, we add the temporal variations of the area of the polar vortex in Fig. 1 in the revised manuscript to show the change of intensity of the polar vortex.

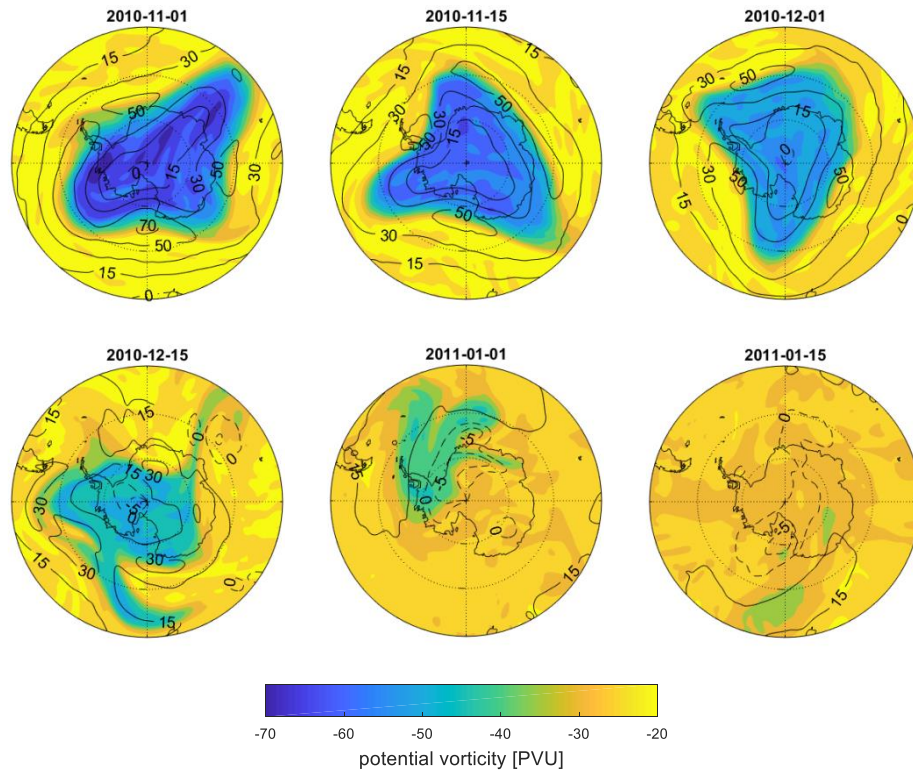


Figure R3: ERA-Interim potential vorticity ($1\text{PVU}=10^{-6}\text{Km}^2 \text{ s}^{-1} \text{ kg}^{-1}$; shaded) and zonal wind contours (m s^{-1} ; black curves) on the 475 K isentropic surface. Data are shown for 00:00UTC on selected days. Outer circles of the polar maps indicate the latitude of 45°S. The prime meridian is oriented towards the top of the map.

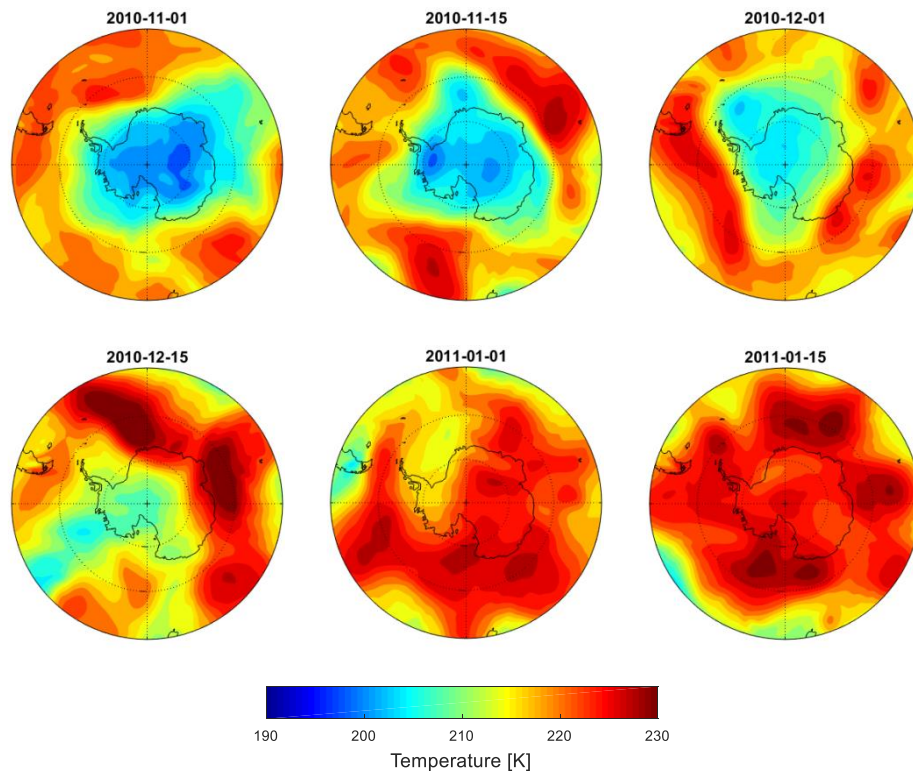


Figure R4: ERA-Interim temperature on the 150hPa pressure level. Data are shown for

00:00UTC on selected days. Outer circles of the polar maps indicate latitude of 45°S. The prime meridian is oriented towards the top of the map.

P12, l1: This paragraph is irrelevant, unless the authors have some evidence that the aerosol from Merapi was enough to produce enough heating to perturb the QBO.

This paragraph is removed.

P12, l9: This sentence, with the use of the word “contributed” is a rather strong statement given the observations don’t really support the strong degree of transport in the model.

The simulations agree much better to the observations after using a new reference state. But the assumptions in our simulation may overestimate the amount of aerosol transported to the Antarctica UTLS, so we rephrased this sentence and this estimation of the transported aerosol may be considered as an upper limit.

P12, l23: Again (see major comments), I don’t agree that the “MIPAS aerosol detections confirmed the MPTRAC simulations”.

Please refer to reply to major comment 1.

P13, l12: “validated” is too strong.

It is rephrased.

Anonymous Referee #3

Received and published: 5 July 2018

The paper contains a comparison between results of trajectory calculations for longrange transport of volcanic aerosol and a satellite derived qualitative quantity for aerosol, the aerosol cloud index (ACI). It might be of interest for ACP but it needs a lot of improvements to be useful.

1 General comments

It is often not clear what is from previous work or the actual study. Concerning the comparison and for model validation it would be much better to use the actual observations of H₂SO₄ aerosol and SO₂ given in Günther et al., 2018 (ACP!) instead of the aerosol cloud index which cannot distinguish between PSCs and volcanic aerosol (e.g. Fig. 1) and where also important definitions are not provided. The figures are difficult to understand and contain too many frames. There are also several times contradictions between text and figures. The remarks on the interactions with the QBO should be corrected and shortened.

We agree that the current presentation of the MIPAS ACI data is not ideal for the comparison with the model results and we appreciate the suggestion to compare with the aerosol and SO₂ retrievals by Günther et al. (2018). However, after thorough analysis, we decide not to replace the ACI for the comparison but to improve the presentation of the ACI data. The reasons that lead to our decision are:

Before the retrieval of H₂SO₄ aerosol and SO₂, Günther et al. (2018) pre-processed the MIPAS data by filtering out optically thick clouds using the cloud index (CI) with a threshold of 1.7 and after the retrieval they filtered out thin ice clouds using with threshold ACI<7 and the same ice filter method as we did (Griessbach et al., 2016), and also the same ash filter to remove volcanic ash and mineral dust (Griessbach et al., 2014). In addition, Günther et al. (2018) removed all retrieved data points that were up to 4 km above any detected ice cloud. This was not necessary for the ACI as it is given on MIPAS 1.5 km vertical sampling grid in the UTLS, but the retrievals by Günther et al. (2018) had a vertical resolution of 3-4 km. Furthermore, Günther et al. (2018) filtered out PSCs based on latitude, time, and temperature criteria, i.e., if the temperature between 17–23 km dropped below the NAT existence temperature (195 K) poleward of 40° in NH winter (15 November to 15 April) and SH winter (1 April to 30 November) the retrieval results were discarded. But we would like to keep the non-ice PSC data in our figures to give an impression on the temporal and spatial extent of the PSCs. The PSC signal usually is stronger than the aerosol signal. It means that aerosol retrievals below PSCs are not possible.

Hence, generally our ACI data is representing the raw aerosol signal before

the volume density retrieval of Günther et al. (2018), with the main difference that we did not filter out PSCs. Filtering out PSCs based on time, latitude, and temperature criteria may also lead to a loss of clear air profiles, e.g., when the synoptic temperature is sufficiently low but no PSCs are present.

So instead of replacing our ACI data with retrievals of Günther et al. (2018), we first added a detailed description of the ACI and the filter methods we used in Sect. 2. Second, we significantly improved the representation of the ACI data in Fig. 7 (the new Fig. 6 in the revised manuscript) for the comparison with the simulations. Now the simulations agree much better with the MIPAS observations, and the poleward transport of the plume can be seen clearly.

2 Specific comments

Abstract: Please correct or remove the statements on QBO. Most of the calculations are for polar summer without vortex. Please mention the aerosol cloud index explicitly if you like to keep the main focus on it, just saying aerosol observations is misleading here.

The role of QBO in the transport cannot be considered as the conclusions of this study. The influence of the QBO phase is rather described as the meteorological background. We have removed the statement of the QBO in the abstract and conclusions. The aerosol cloud index is added in the abstract.

Introduction, L48: This might have some effect on ozone depletion in the next ozone hole season (2011).

It is added in the introduction. Thank you.

Section 2.1: Include more details on ACI from the Griessbach paper if you like to use this, including their Eq.3. The second paragraph is messy concerning the wavelength.

We revised Section 2.1 and described the ACI and what it is used for in our study in more detail. The paragraphs on the ACI read now:

"ACI is the maximum value of the cloud index (CI) and aerosol index (AI):

$$ACI = \max(CI; AI), \quad (1)$$

The CI method is an established method to detect clouds and aerosol with MIPAS data. The CI is the ratio between the mean radiance around the 792 cm^{-1} where a CO₂ line is located and the atmospheric window region around 833 cm^{-1} (Spang et al., 2001):

$$CI = \frac{\overline{I}_1([788.25, 796.25 \text{ cm}^{-1}])}{\overline{I}_2([832.31, 834.37 \text{ cm}^{-1}])}, \quad (2)$$

where \bar{I}_1 and \bar{I}_2 are the mean radiances of each window. The AI is defined as the ratio between the mean radiances around the 792 cm^{-1} CO₂ band and the atmospheric window region between 960 and 961 cm^{-1} :

$$AI = \frac{\bar{I}_1([788.25, 796.25 \text{ cm}^{-1}])}{\bar{I}_3([960.00, 961.00 \text{ cm}^{-1}])}, \quad (3)$$

where \bar{I}_1 and \bar{I}_3 are the mean radiance of each window.

For the CI, Sembhi et al. (2012) defined a set of variable (latitude, altitude, and season) thresholds to discriminate between clear and cloudy air, and the most advanced set of altitude and latitude dependent thresholds allows for the detection of aerosol/clouds with IR extinction coefficients larger than 10^{-5} km^{-1} .

The ACI is a continuous unitless value, small values indicating a high cloud or aerosol particle load and higher values indicating a smaller cloud or aerosol particle load. For the CI, Sembhi et al. (2012) defined a set of variable (latitude, altitude, and season) thresholds to discriminate between clear and cloudy air. The most advanced set of altitude and latitude dependent thresholds allows for the detection of aerosol and clouds with IR extinction coefficients larger than 10^{-5} km^{-1} . For the ACI, a comparable sensitivity is achieved when using a fixed threshold value of 7 (Griessbach et al. 2016). Variations in the background aerosol are also visible with larger ACI values.

To remove ice clouds and volcanic ash from the MIPAS aerosol measurements, we first separated the data into clear air ($ACI > 7$) and cloudy air ($ACI \leq 7$). Then we applied the ice cloud filter (Griessbach et al., 2016) and the volcanic ash and mineral dust filter (Griessbach et al., 2014) to the cloudy part and removed all ice or ash detections. However, since the ice and ash cloud filters are not sensitive to non-ice PSCs, the resulting aerosol retrieval results still contain non-ice PSCs (supercooled ternary solutions and nitric acid trihydrate). We keep the non-ice PSCs in the MIPAS retrieval results in this study to show the temporal and spatial extent of the PSCs, when and where the identification of volcanic is not possible.

Section 2.3: Is the reanalysis ERA Interim (mentioned too late)?

Yes, the MPTRAC model in this study is driven by the ERA-interim reanalysis. The MPTRAC model can also be driven by other reanalyses. We added this information at the beginning of Sect. 2.3.

Section 3.1: Figure 2 and the text are in contradiction to each other and the given reference (Suroño).

We checked the texts to fix a few mistakes in the description. Some sentences are added to explain the SO₂ around the tropopause during 1–3 November 2010. To avoid ambiguities, one sentence that describes the degassing in the chronology provided by Suroño et al. (2012) is removed.

Section 3.2, L256ff: Effect on late spring or summer circulation?

The paragraph about the role of QBO that starts from Line 256 is removed in the revised manuscript.

Section 3.3: Figure 3 is difficult to read and interpret, especially in connection with the zonal wind (Singapore data). There is also some contradiction to Fig. 6 which does not contain $ACI < 7$ in the regions of interest. Comparing Fig. 5 and 6 is like comparing apples and oranges. Here the clear poleward plume shown in Günther et al., 2018 would be much more useful.

Figure 3 compares the altitude of air parcels in the plume simulated with MPTRAC model and the latitude of the MIPAS ACI measurements. Both the simulations and observations use the same color scheme but the observations are marked additionally with circles. In this way, when the simulations do not agree with the observations, different colors may be observed.

In the MPTRAC model, trajectory calculations are driven by wind fields at the location of each air parcel. Air parcels at various altitudes may disperse towards different directions. Please refer to the reply to referee #1.

Figure 6 shows the median value of the MIPAS ACI in each latitude-altitude bin across all longitudes. The ACIs in each bin may contain small values that indicate large aerosol extinction and large values that indicate small aerosol extinction or even clear air. The median ACI value in each bin is probably larger than 7 when the majority of the ACI values in that bin are large.

We have used a new definition of the reference state to derive the change of aerosol load after the Merapi eruption. Please see Fig. 6 in the revised manuscript. The poleward transport is clearer and the simulations and observations agree better.

Section 4, line 403: It might be of interest to compare the sulfate input from Merapi to the Antarctic lower stratosphere with the contribution of the Puyehue-Cordon Caulle eruption in June 2011.

The Puyehue-Cordon Caulle is a mid-latitude eruption (40.59°S) that has a higher chance to influence Antarctica than a volcanic eruption in the tropics. Although the amount of SO_2 injected was only 0.2 Tg, it is not difficult to estimate that the Puyehue-Cordon Caulle added more aerosol to Antarctica than Merapi based on Fig. 1 (Fig. 5 in the revised manuscript). It erupted during austral winter, had a direct influence on the formation of PSCs and affected the ozone concentration in the following austral spring, which can be seen in Fig. 4 in the study of Solomon et al. (2016). The Puyehue-Cordon Caulle eruption is one of the important cases that should definitely be investigated if we would like to study the influence of volcanic eruption on the Antarctic aerosols. So the accurate estimation of the effect of the Puyehue-Cordon Caulle eruption could be a whole new study.

3 Technical corrections

Please correct the plenty typos and grammar errors. In line 444 it should be 2011. Use consistent units. Don't use words like 'data', 'observed' for model results.

We have checked the typos and try to improve the grammar throughout the manuscript.

Figure 2, caption: Strange units. Is the time UTC or local? Longitude and latitude range for integration?

It is UTC. The explanation is added in the caption.

The spatial range for integration is within the radius of 75 km to the location of the Mount Merapi as described in Sect. 2.3.

Figure 4: For what latitude range is frame f? It would be more useful to provide data for 100hPa instead of 30hPa.

The QBO index is defined as the zonal wind anomalies over the Equator (0°) at 30 hPa or 50 hPa. But since the QBO is not directly related to the conclusion, the QBO index is removed from the figure. The temporal variation of the area of the polar vortex is added instead.

Figure 5: The labels are too small and the color scale is for large portions out of range.

The color scheme is improved. As the Southern Hemisphere is the area of interest, we only keep the figures for the Southern Hemisphere.

Figure 6, caption: Spell out ACI.

The Fig. 6 is removed in the revised manuscript.

Figure 7, caption: Is aerosol load here equal to ACI (without unit)?

Yes, the "aerosol load" in the caption is replaced with "MIPAS ACI values".

Figure 10: Labels missing.

The labels are added.

References:

Griessbach, S., L. Hoffmann, R. Spang and M. Riese: Volcanic ash detection with infrared limb sounding: MIPAS observations and radiative transfer simulations, *Atmos. Meas. Tech.* 7, 1487-1507, doi: 10.5194/amt-7-1487-2014, 2014.

Griessbach, S., Hoffmann, L., Spang, R., von Hobe, M., Müller, R., and Riese, M.: Infrared limb emission measurements of aerosol in the troposphere and stratosphere, *Atmos.*

- Meas. Tech., 9, 4399-4423, doi:10.5194/amt-9-4399-2016, 2016.
- Günther, A., Höpfner, M., Sinnhuber, B. M., Griessbach, S., Deshler, T., von Clarmann, T., and Stiller, G.: MIPAS observations of volcanic sulphate aerosol and sulphur dioxide in the stratosphere, *Atmos. Chem. Phys.*, 2017, 1-32, doi: 10.5194/acp-18-1217-2018, 2018.
- Hofmann, D. J., J. M. Rosen and W. Gringel: Delayed production of sulfuric acid condensation nuclei in the polar stratosphere from El Chichon volcanic vapors, *J. Geophys. Res. Atmos.*, 90(D1), 2341-2354, doi: doi:10.1029/JD090iD01p02341, 1985.
- Ivy, D. J., Solomon, S., Kinnison, D., Mills, M. J., Schmidt, A., and Neely, R. R.: The influence of the Calbuco eruption on the 2015 Antarctic ozone hole in a fully coupled chemistry-climate model, *Geophys. Res. Lett.*, 44, 2556-2561, 10.1002/2016GL071925, 2017.
- Kunz, A., Sprenger, M., and Wernli, H.: Climatology of potential vorticity streamers and associated isentropic transport pathways across PV gradient barriers, *J. Geophys. Res. Atmos.*, 120, 3802-3821, doi: 10.1002/2014jd022615, 2015.
- Nicolas Patris, R. J. D., Jean Jouzel Isotopic signatures of sulfur in shallow Antarctic ice cores, *J. Geophys. Res. Atmos.*, 105, 7071-7078, doi:10.1029/1999JD900974, 2000.
- Patris, N., R. J. Delmas and J. Jouzel: Isotopic signatures of sulfur in shallow Antarctic ice cores, *J. Geophys. Res. Atmos.*, 105(D6), 7071-7078, doi: 0.1029/1999JD900974, 2000.
- Pitts, M. C. and L. W. Thomason: The impact of the eruptions of Mount Pinatubo and CERRO Hudson on Antarctic aerosol levels during the 1991 austral spring, *Geophys. Res. Lett.*, 20(22), 2451-2454, doi: doi:10.1029/93GL02160, 1993.
- Solomon, S., Ivy, D. J., Kinnison, D., Mills, M. J., Neely, R. R., and Schmidt, A.: Emergence of healing in the Antarctic ozone layer, *Science*, 10.1126/science.aae0061, 2016.
- Stone, K. A., Solomon, S., Kinnison, D. E., Pitts, M. C., Poole, L. R., Mills, M. J., Schmidt, A., Neely, R. R., Ivy, D., Schwartz, M. J., Vernier, J.-P., Johnson, B. J., Tully, M. B., Klekociuk, A. R., König-Langlo, G., and Hagiya, S.: Observing the Impact of Calbuco Volcanic Aerosols on South Polar Ozone Depletion in 2015, *J. Geophys. Res. Atmos.*, 122, 11,862-811,879, 10.1002/2017JD026987, 2017.



1 Long-range transport of volcanic aerosol from the 2010 Merapi 2 tropical eruption to Antarctica

3 Xue Wu^{1,2}, Sabine Griessbach¹, Lars Hoffmann¹

4 ¹Jülich Supercomputing Centre, Forschungszentrum Jülich, Jülich, Germany

5 ²Key Laboratory of Middle Atmosphere and Global Environment Observation, Institute of Atmospheric
6 Physics, Chinese Academy of Sciences, Beijing, China


7 *Correspondence to:* Xue Wu (xu.wu@fz-juelich.de)

8 Abstract


9 Volcanic sulfate aerosol is an important source of sulfur for Antarctica where other local sources of
10 sulfur are rare. Mid- and high latitude volcanic eruptions can directly influence the aerosol budget of the
11 polar stratosphere. However, tropical eruptions can also enhance polar aerosol load following
12 long-range transport. In the present work, we analyze the volcanic plume of a tropical eruption, Mount
13 Merapi in October 2010, using the Lagrangian particle dispersion model Massive-Parallel Trajectory
14 Calculations (MPTRAC), Atmospheric Infrared Sounder (AIRS) SO₂ observations and Michelson
15 Interferometer for Passive Atmospheric Sounding (MIPAS) aerosol observations. We investigate the
16 pathway and transport efficiency of the volcanic aerosol from the tropical tropopause layer (TTL) to the
17 lower stratosphere over Antarctica. We first estimated the time- and height-resolved SO₂ injection time
18 series over Mount Merapi during the explosive eruption using the AIRS SO₂ observations and a
19 backward trajectory approach. Then the SO₂ injections were tracked for up to 6 months using the
20 MPTRAC model. The Lagrangian transport simulation of the volcanic plume was compared to MIPAS
21 aerosol observations and showed good agreement. Both ¹ of the simulation and the observations
22 presented in this study suggest that a ² significant amount of aerosols of the volcanic plume from the
23 Merapi eruption was transported from the tropics to the south of 60°S within one month after the
24 eruption and even further to Antarctica in the following two months. This relatively fast meridional
25 transport of volcanic aerosol was mainly driven by quasi-horizontal mixing from the TTL to the
26 extratropical lower stratosphere, which was facilitated by the weakening of the subtropical jet during the
27 seasonal transition from austral spring to summer and linked to the westerly phase of the quasi-biennial
28 oscillation ³ (QBO). When the plume went to southern high latitudes, the polar vortex was displaced from
29 the ⁴ south pole, so the volcanic plume was carried to the ⁵ south pole without penetrating the polar vortex.
30 Based on the model results, the most efficient pathway for the quasi-horizontal mixing was ⁶ between
31 the isentropic surfaces of 360 and 430 K. Although only 4% of the initial SO₂ load was transported into


Summary of Comments on acp-2018-332-RC1-supplement.pdf


Page: 1

 Number: 1 Author: Subject: Highlight Date: 5/31/2018 8:53:47 PM
delete


 Author: Administrator Subject: Sticky Note Date: 6/2/2018 4:12:04 PM
fixed

 Number: 2 Author: Subject: Highlight Date: 5/31/2018 8:54:31 PM
needs to be quantified. Significant by what standard?

 Author: wuxue Subject: Sticky Note Date: 8/27/2018 1:56:55 AM
The sentence is rephrased.


 Number: 3 Author: Subject: Highlight Date: 5/31/2018 8:55:25 PM
delete. Acronym is not used again.


 Author: Administrator Subject: Sticky Note Date: 6/2/2018 4:12:19 PM
fixed

 Number: 4 Author: Subject: Highlight Date: 5/31/2018 8:55:59 PM
South Pole

 Author: Administrator Subject: Sticky Note Date: 6/2/2018 4:14:31 PM
fixed

 Number: 5 Author: Subject: Highlight Date: 5/31/2018 8:56:06 PM
south pole

 Author: Administrator Subject: Sticky Note Date: 6/2/2018 4:14:48 PM
fixed

 Number: 6 Author: Subject: Highlight Date: 5/31/2018 8:56:29 PM
delete

 Author: Administrator Subject: Sticky Note Date: 6/2/2018 4:14:54 PM
fixed



32 the lower stratosphere south of 60°S, the Merapi eruption contributed about 8800 tons of sulfur to the
33 Antarctic lower stratosphere. This indicates that the long-range transport under favorable
34 meteorological conditions enables tropical volcanic eruptions to be an important remote source of sulfur
35 for the Antarctic stratosphere.

36 1 Introduction

37 Over the past two decades, multiple volcanic eruptions injected sulfur into the upper troposphere and
38 lower stratosphere, which has been the dominant source of the stratospheric sulfate aerosol load
39 (Vernier et al., 2011), preventing true background levels from other sources ever being seen (Solomon
40 et al., 2011). Stratospheric sulfate aerosol mainly reflects solar radiation and absorbs infrared radiation,
41 causing cooling of the troposphere and heating of the stratosphere. contributes to the largest
42 uncertainties to estimates and interpretations of the Earth's changing energy budget (Boucher et al.,
43 2013). Further, by modulating the stratospheric and tropospheric temperature it has an impact on
44 stratospheric dynamics, e. g. it can lead to dramatic phase changes of the quasi-biennial oscillation
45 (Aquila et al., 2014) and alter the spatiotemporal characteristics of the El Niño–Southern Oscillation
46 (ENSO) on both short (few years) and long (decades) timescales (Pausata et al., 2015). Stratospheric
47 sulfate aerosol also has an impact on chemical processes in the lower stratosphere (Jäger and Wege,
48 1990; Solomon et al., 1993), in particular on polar ozone depletion (Tilmes et al., 2008; Drdla and
49 Müller, 2012; Solomon et al., 2016). The presence of H₂SO₄ in the polar stratosphere in combination
50 with cold temperatures facilitates the formation of polar stratospheric clouds (PSCs), which increase
51 heterogeneous ozone depletion chemistry (Solomon et al., 1999; Zuev et al., 2015). Recent healing of
52 Antarctic ozone depletion was constantly disturbed by moderate volcanic eruptions (Solomon et al.,
53 2016). Mid- and high latitude explosive volcanic eruptions may directly influence the polar stratosphere.
54 For example, the aerosol plume from the Calbuco eruption in 2015, including various volcanic gases,
55 penetrated the polar vortex and caused a new record of the size of the Antarctic ozone hole after the
56 eruption (Solomon et al., 2016; Ivy et al., 2017; Stone et al., 2017).
57 Usually, Antarctica is relatively free of local aerosol sources, but aerosols from low latitudes can reach
58 Antarctica through long-range transport (Sand et al., 2017). Some of the sulfate found in the ice cores
59 can be attributed to volcanic eruptions (Mazzera et al., 2001; Gao et al., 2007; Sigl et al., 2015).
60 Measurements of enhanced aerosol in the lower Antarctic stratosphere right above the tropopause were
61 made in October/November 1983, 84 and 85. These enhanced aerosol number concentrations were

T Number: 1 Author: Subject: Highlight Date: 5/31/2018 8:57:19 PM
But we already know this happens for large eruptions. What is new here?

S Author: Administrator Subject: Sticky Note Date: 6/3/2018 12:04:58 PM
Please refer to the reply for details.

T Number: 2 Author: Subject: Highlight Date: 5/31/2018 8:58:18 PM
Not correct. What do you mean by "uncertainties?" Largest compared to what?

S Author: Administrator Subject: Sticky Note Date: 6/3/2018 3:56:45 PM
This sentence is removed from the texts.

T Number: 3 Author: Subject: Highlight Date: 5/31/2018 8:59:20 PM
dynamics;

S Author: Administrator Subject: Sticky Note Date: 6/2/2018 4:15:59 PM
fixed

T Number: 4 Author: Subject: Highlight Date: 5/31/2018 9:01:00 PM
new record size [record for what? Monthly mean? All time size?]

S Author: Administrator Subject: Sticky Note Date: 8/27/2018 10:47:27 PM
Fixed. The sentence is rewritten as: ... in October 2015 caused a Antarctic ozone hole with the largest daily averaged size in record.

T Number: 5 Author: Subject: Highlight Date: 5/31/2018 9:01:38 PM
aerosols [you use both singular and plural in the paper. Choose one and stick to it.]

S Author: Administrator Subject: Sticky Note Date: 6/2/2018 4:16:37 PM
fixed

T Number: 6 Author: Subject: Highlight Date: 5/31/2018 9:02:52 PM
Most

S Author: Administrator Subject: Sticky Note Date: 6/2/2018 4:17:45 PM
fixed

T Number: 7 Author: Subject: Highlight Date: 5/31/2018 9:03:02 PM
in ice

S Author: Administrator Subject: Sticky Note Date: 6/2/2018 4:19:19 PM
fixed

T Number: 8 Author: Subject: Highlight Date: 5/31/2018 9:03:32 PM
1984 and 1985

S Author: Administrator Subject: Sticky Note Date: 6/2/2018 4:18:36 PM
fixed





62 attributed to aerosol transported to Antarctica from the eruption of the tropical volcano El **1** **Unichon** in
63 1982 (Hofman and Rosen, 1985; Hofmann et al., 1988). Tropical volcanic eruptions can also enhance
64 polar aerosols by long-range transport. Model results indicate that numerous moderate eruptions have
65 affected ozone distributions over Antarctica, including the Merapi tropical eruption in October 2010
66 (Solomon et al., 2016). However, the transport mechanism is not well represented in present global
67 climate models, and the uncertainties in modeled AOD in both polar regions are large (Sand et al.,
68 2017).


69 **2** **he** Mount Merapi (7.5°S, 110.4°E, elevation: 2930 m) is an active stratovolcano located in Central
70 Java, Indonesia. Merapi has a long record of eruptive activities. The most recent large eruption with a
71 volcanic explosivity index **3** **VEI** of 4 occurred between 26 October and 7 November 2010 (Pallister et
72 al., 2013), with SO₂ emission rates being a few orders of magnitude higher than previous eruptions.
73 Following the Merapi eruption in 2010, evidence of poleward transport of sulfate aerosol towards
74 southern hemisphere high latitudes was found in time series of aerosol observations by the Michelson
75 Interferometer for Passive Atmospheric Sounding (MIPAS) (Günther et al., 2017) and Cloud-Aerosol
76 Lidar with Orthogonal Polarization (CALIOP) (Khaykin et al., 2017) .


77 There are three main ways for transport out of the tropical tropopause layer (TTL): the deep and shallow
78 branches of the Brewer-Dobson circulation (BDC) and horizontal mixing (Vogel et al., 2011). There is
79 considerable year-to-year seasonal variability in the amount of irreversible transport from the tropics to
80 high latitudes, which is related to both the phase of the **4** **QBO** and the state of the polar vortex (Olsen et
81 al., 2010). The BDC plays a large role in determining the distributions of many constituents in the
82 extratropical lower stratosphere. And the faster quasi-horizontal transport between the tropics and polar
83 regions also significantly contributes to determining these distributions. The efficiency of transporting
84 constituents quasi-horizontally depends on wave breaking patterns and varies with time of year (Kravitz
85 and Robock, 2011; Wu et al., 2017). Better knowledge of the transport pathways and an accurate
86 representation of volcanic sulfur injections into the upper troposphere and lower stratosphere (UTLS)
87 are key elements for understanding the global stratospheric aerosol budget is key to understanding the
88 cooling effects and ozone loss linked to volcanic activity.


89 The aim of the present study is to investigate the quasi-horizontal transport by tracing the volcanic
90 plume of the Merapi eruption from the tropics to Antarctica and quantifying its contribution to the
91 sulfur load in the Antarctic lower stratosphere. In Sect. 2, the new Atmospheric Infrared Sounder (AIRS)
92 SO₂ observations (Hoffmann et al., 2014), the MIPAS aerosol observations (Griessbach et al., 2016)
93 and the method for reconstructing the SO₂ injection time series of the Merapi eruption are introduced. In

 Number: 1 Author: Subject: Highlight Date: 6/2/2018 4:18:47 PM
Chichón


 Author: Administrator Subject: Sticky Note Date: 6/2/2018 4:19:10 PM
fixed


 Number: 2 Author: Subject: Highlight Date: 5/31/2018 9:04:25 PM
delete

 Author: Administrator Subject: Sticky Note Date: 6/2/2018 4:19:36 PM
fixed

 Number: 3 Author: Subject: Highlight Date: 5/31/2018 9:05:43 PM
delete [not used again]

 Author: Administrator Subject: Sticky Note Date: 6/2/2018 4:19:45 PM
fixed

 Number: 4 Author: Subject: Highlight Date: 5/31/2018 9:05:18 PM
needs to be defined in the text [not abstract] before using.

 Author: Administrator Subject: Sticky Note Date: 6/2/2018 4:20:20 PM
fixed




94 Sect. 3 the results are presented: first, the reconstructed time series of the Merapi eruption is discussed;
95 second, the dispersion of the Merapi plume is investigated using up to 6 months long Lagrangian
96 forward trajectories initialized with the reconstructed SO₂ time series; third, the simulation is compared
97 to MIPAS volcanic aerosol measurements and the plume dispersion is investigated using MIPAS
98 aerosol detections. In Sect.4 the results are discussed with the background of the meteorological
99 conditions and conclusions are given in Sect. 5.


100 2 Satellite data, model and method


101 2.1 MIPAS instrument and aerosol measurements


102 MIPAS (Fischer et al., 2008) is an infrared limb emission spectrometer aboard the European Space
103 Agency's (ESA's) Envisat, which provided nearly 10 years of measurements from July 2002 to April
104 2012. MIPAS spectral measurements cover the wavelength range from 4.15 to 14.6 microns. The
105 vertical coverage of MIPAS' nominal measurement mode during the so-called 'optimized resolution
106 phase' from January 2005 to April 2012 was 7–72 km. The field of view of MIPAS was about 3 km × 30
107 km (vertically × horizontally) at the tangent point. The extent of the measurement volume along the line
108 of sight was about 300 km, and the horizontal distance between two adjacent limb scans was about 500
109 km. On each day, ~14 orbits with ~90 profiles per orbit were measured. The vertical sampling was 1.5
110 km in the UTLS and 3 km above the UTLS. In 2010 and 2011, MIPAS measured for 4 days in nominal
111 mode followed alternately by one day in middle atmosphere mode or upper atmosphere mode. In this
112 study, we focussed on measurements in the nominal mode.

113 For the aerosol **detections**, we used the MIPAS altitude-resolved aerosol-cloud-index (ACI) products as
114 introduced by Griessbach et al. (2016) to compare with the MPTRAC simulations and analyze the
115 poleward transport of the Merapi volcanic plume. Small ACI values indicate large aerosol extinction
116 coefficients and vice versa. For instance, MIPAS data points with $ACI < 7$ can cover infrared extinction
117 coefficients larger than $1 \times 10^{-4} \text{ km}^{-1}$, which corresponds to $3 \times 10^{-4} \text{ km}^{-1}$ in the visible wavelength
118 range (Griessbach et al. 2016). Larger ACI values will show aerosol load with even smaller extinction
119 coefficients. As ice clouds usually have extinction coefficients larger than $1 \times 10^{-4} \text{ km}^{-1}$, we applied a
120 brightness-temperature-correlation method, that serves as an ice cloud filter, to all MIPAS spectra with
121 $ACI < 7$ (Griessbach et al., 2016) to remove the ice clouds from the data set. The resulting aerosol
122 product is **2e** sensitive to different types of aerosol, in particular, volcanic ash, sulfate aerosol, mineral
123 dust, as well as non-ice PSCs.

 Number: 1 Author: Subject: Highlight Date: 5/31/2018 9:09:48 PM
detection,

 Author: Administrator Subject: Sticky Note Date: 6/2/2018 4:22:18 PM
fixed

 Number: 2 Author: Subject: Highlight Date: 5/31/2018 9:11:38 PM
delete

 Author: Administrator Subject: Sticky Note Date: 6/2/2018 4:22:51 PM
fixed

124 **2.2 AIRS**

125 AIRS (Aumann et al., 2003) is an infrared nadir sounder with across-track scanning capabilities aboard
126 the National Aeronautics and Space Administration's (NASA's) Aqua satellite. Aqua was launched in
127 2002 and operates in a nearly polar Sun-synchronous orbit at about 710 km with a period of 98 min.
128 AIRS provides nearly continuous measurement coverage with 14.5 orbits per day and with a swath width
129 of 1780 km it covers the globe almost twice a day. The AIRS footprint size is 13.5 km × 13.5 km at nadir
130 and 41 km × 21.4 km for the outermost scan angles respectively. The along-track distance between two
131 adjacent scans is 18 km. The AIRS observations provide good horizontal resolution and make it ideal for
132 observing the fine filamentary structures of volcanic SO₂ plumes.


133 In this study, we use an optimized SO₂ index (SI, unit: K) to estimate the amount of SO₂ injected into the
134 atmosphere by the Merapi eruption 2010. The SI is defined as the brightness temperature differences in
135 the 7.3 μm SO₂ waveband.


$$136 \quad SI = BT \left(1412.87 \text{ cm}^{-1} \right) - BT \left(1371.52 \text{ cm}^{-1} \right), \quad (1)$$


137 where BT is the brightness temperature measured at wavenumber ν . This SI is more sensitive to low
138 concentrations and performs better on suppressing background interfering signals than the SI provided in
139 the AIRS operational data products. It is an improvement of the SI definition given by Hoffmann et al.
140 (2014) by means of a better choice of the background channel (selecting 1412.87 cm⁻¹ rather than
141 1407.2 cm⁻¹). The SI increases with increasing SO₂ column density and it is most sensitive to SO₂ at
142 altitudes above 3-5 km. SO₂ injections into the lower troposphere are usually not detectable in the infrared
143 spectral region because the atmosphere gets opaque due to the water vapor continuum. A detection
144 threshold of 1 K was used in this study to identify the Merapi SO₂ injections. AIRS detected the Merapi
145 SO₂ cloud from 3 November to 15 November 2010.

146 **2.3 MPTRAC model and reconstruction of the volcanic SO₂ injection time series of the Merapi**
147 **eruption**

148 In this study, we used the highly scalable MPTRAC model to investigate the volcanic eruption event. In
149 the **MPTRAC** model, air parcel trajectories are calculated based on numerical integration using wind
150 fields from global meteorological **analyses** (Hoffmann et al., 2016; Rößler et al., 2017). Diffusion is
151 modeled by uncorrelated Gaussian random displacements of the air parcels with zero mean and standard
152 deviations $\sigma_x = \sqrt{D_x \Delta t}$ (horizontally) and $\sigma_z = \sqrt{D_z \Delta t}$ (vertically). D_x and D_z are the horizontal
153 and vertical diffusivities respectively, and Δt is the time step for the trajectory calculations. For the

 Number: 1 Author: Subject: Highlight Date: 5/31/2018 9:16:28 PM
MPTRAC

 Author: Administrator Subject: Sticky Note Date: 6/2/2018 4:22:57 PM
fixed


 Number: 2 Author: Subject: Highlight Date: 5/31/2018 9:29:44 PM
specify which ones

 Author: Administrator Subject: Sticky Note Date: 8/27/2018 1:59:44 AM

The MPTRAC model can be driven with reanalyses, i.e., ERA-Interim, Modern-Era Retrospective Analysis for Research and Applications (MERRA), and National Centers for Environmental Prediction (NCEP)/National Center for Atmospheric Research (NCAR) etc. In a previous study about the impact of reanalyses on the simulation results of the MPTRAC model (Hoffmann et al., 2016), it shows that the ERA-interim data can ensure the performance of MPTRAC with a reasonable computing time. So in this study, our calculations are based on ERA-interim data, which is mentioned in the last paragraph of Sect. 2.3. Explanations are added here in the revised manuscript.




154 Merapi simulation, D_x and D_z were set to $50 \text{ m}^2 \text{ s}^{-1}$ and $0 \text{ m}^2 \text{ s}^{-1}$ in the troposphere and $0 \text{ m}^2 \text{ s}^{-1}$ and 0.1
155 $\text{m}^2 \text{ s}^{-1}$ in the stratosphere, respectively. In addition, sub-grid scale wind fluctuations, which are
156 particularly important for long-range simulations, are simulated by a Markov model (Stohl et al., 2005;
157 Hoffmann et al., 2016). Loss processes of chemical species, SO_2 in our case, are simulated based on an
158 exponential decay of the mass assigned to each air parcel. In the stratosphere a constant half lifetime of
159 7 days was assumed for SO_2 . Considering that the Merapi eruption occurred in the humid tropics, with
160 high concentration of hydroxyl radical, a ¹half lifetime of 2.5 days was assumed for the troposphere.
161 To estimate the time- and altitude-resolved SO_2 injections, we follow the approach of Hoffmann et al.
162 (2016) and Wu et al. (2017) and use backward trajectories calculated with the MPTRAC model together
163 with AIRS SO_2 measurements. Observations from 3 to 7 November 2010 were used for estimating the
164 SO_2 injection during the explosive eruption. Since the AIRS measurements do not provide altitude
165 information, we established a column of air parcels at each AIRS SO_2 detection. The vertical range of
166 the column was set to 0–25 km, covering the possible vertical dispersion range of the SO_2 plume in the
167 first few days. The AIRS footprint size varies between 14 and 41 km, hence in the horizontal direction,
168 we chose an average of 30 km as the full width at half maximum (²FWHM) for the Gaussian scatter of
169 the air parcels. In our simulation, a fixed total number of 100,000 air parcels was assigned to all air
170 columns and the number of air parcels in each column was scaled linearly proportional to the SO_2 index.
171 Then backward trajectories were calculated for all air parcels, and trajectories that were at least 2 days
172 but no more than 5 days long and that passed the volcano domain were recorded as emissions of Merapi.
173 The volcano domain was defined by means of a search radius of 75 km around the location of the
174 Merapi and 0–20 km in the vertical direction, covering all possible injection heights. Sensitivity
175 experiments have been conducted to optimize these pre-assigned parameters to obtain the best
176 simulation results. Our estimates of the Merapi SO_2 injection are shown in Sect. 3.
177 Starting with the reconstructed altitude-resolved SO_2 injection time series, the transport of the Merapi
178 plume is simulated for 6 months, covering the time period from the initial eruption on 26 October 2010
179 to 30 April 2011. The trajectory calculations are driven by the ERA–Interim data (Dee et al., 2011)
180 interpolated on a $1^\circ \times 1^\circ$ horizontal grid on 60 model levels with the vertical range extending from the
181 surface to 0.1 hPa. The ERA–Interim data are provided at 00, 06, 12 and 18 UTC. Outputs of model
182 simulations are given every 3 hours at 00, 03, 06, 09, 12, 15, 18 and 21 UTC. The impact of different
183 meteorological ³analysis on MPTRAC simulations was assessed by Hoffmann et al. (2016, 2017). In
184 both studies the ERA–Interim data showed good performance.


 Number: 1 Author: Subject: Highlight Date: 5/31/2018 9:54:50 PM
what about removal by precipitation?


 Author: Administrator Subject: Sticky Note Date: 6/3/2018 1:29:19 PM

Precipitation is a very important way of removal of SO₂, but the time life of SO₂ in the case of precipitation which could be very short is very difficult to define in the model we use. We can only roughly estimate the life of SO₂ based on some parameters with a clear climatological trend, for example, the humidity and the concentration of oxidant. And we also compare the SO₂ column density from our model results with AIRS SO₂ observations, and in this way, we can adjust the life time of SO₂ set up in our model to get a better agreement with the observations. This approach can not guarantee an accurate simulation of SO₂ in the troposphere, but fortunately, the SO₂ in lower troposphere and sulfate aerosol converted from these SO₂ are not the interests in our study. We only focus on the SO₂ injected into the upper troposphere and stratosphere.
Thank you for pointing this out. We added more detailed description of our model set-up in Sect. 2.3 in the revised manuscript.

 Number: 2 Author: Subject: Highlight Date: 5/31/2018 9:55:18 PM
delete

 Author: Administrator Subject: Sticky Note Date: 6/3/2018 12:05:54 PM
fixed

 Number: 3 Author: Subject: Highlight Date: 5/31/2018 9:58:02 PM
analyses

 Author: Administrator Subject: Sticky Note Date: 6/2/2018 5:01:21 PM
fixed



185 3 Results


186 Figure 1 displays the time-latitude section of MIPAS aerosol detections with median ACI value in each
187 bin smaller than 7 and within the vertical range of 13 and 20 km, covering the tropical tropopause layer
188 (TTL) and the extratropical lowermost stratosphere (LMS). The MIPAS data captured all the major
189 events that contributed to the aerosol load in the UTLS, i.e., moderate volcanic eruptions from 2002 to
190 2012 and one large bushfire in 2009, as well as the subsequent dispersion and change of aerosol load
191 over time. Particularly, after the Merapi eruption in 2010, marked by the red triangle in Fig. 1, the
192 MIPAS data show an obvious poleward transport of aerosol from the tropics to Antarctica.

193 3.1 Merapi eruption and SO₂ injection time series


194 According to the chronology of the Merapi eruption (Suroño et al., 2012), the explosive eruption first
195 occurred between 10:00 and 12:00 UTC on 26 October and this eruption generated a plume that reached
196 12 km altitude. A period of relative small explosive eruptions continued from 26 October to 31 October.
197 During the initial period of the dome growth (1–3 November), the level of SO₂ degassing was relatively
198 low compared with the SO₂ degassing before 1 November. On 3 November, the eruptive intensity
199 increased again accompanied by much stronger degassing and a series of explosions. The intermittent
200 explosive eruptions occurred during 4–5 November with the climactic eruption on 4 November,
201 producing an ash column that reached up to 17 km altitude. From 6 November, explosive activity
202 decreased slowly and the degassing declined.

203 Figure 2 shows the time- and altitude-resolved SO₂ injections of the Merapi eruption retrieved using the
204 AIRS SO₂ index data and the backward-trajectory approach. It successfully reproduced the chronology
205 of the Merapi eruption as outlined by Suroño et al. (2012). Significant SO₂ was injected into altitudes
206 below 8 km during the initial explosive eruptions on 26–30 October. Starting from 30 October the
207 plume reached up to 12 km. During 1–3 November the SO₂ injections into altitudes below 12 km
208 continued but the mass was less than in the initial phase. On 3 November the intensity increased again
209 and peaked in the climactic explosive eruptions of 4–5 November. Before 3 November the
210 reconstruction indicates a minor fraction of SO₂ right above the tropopause.


211 To study the long-range transport of the Merapi plume, we initialized 100,000 air parcels at the SO₂
212 injection time series shown in Fig. 2 with a SO₂ mass of 0.44 Tg as provided in Suroño et al. (2012) and
213 calculated forward trajectories for 6 months. Here, we only considered the plume in the upper
214 troposphere and stratosphere where the lifetime of both SO₂ and sulfate aerosol is longer than that in the
215 lower troposphere. Further, the SO₂ was all converted into sulfate aerosol within a few weeks (von

 Number: 1 Author: Subject: Highlight Date: 5/31/2018 10:05:50 PM

Not seen in Fig. 2. Why?

 Author: Administrator Subject: Sticky Note Date: 6/3/2018 5:38:49 PM

In the study of Surono et al., 2012, it was claimed that between 10:00 UTC and 12:00 UTC on 26 October, there was an ash plume that reached 12 km altitude and released SO₂ emissions, but they did not give the amount or the altitude of the SO₂ injection. But it is clear that this period of time was the initial explosive phase, when only a small amount of SO₂ was injected, about two orders of magnitude smaller than it was on 3 or 4 November (Surono et al., 2012). In our Fig. 2, there was a small amount of SO₂ around 10-13 km on 26 October. Although its time of presence was a little earlier than 12:00 UTC 26 October, it would not bring notable error to the simulation later in this study.

 Number: 2 Author: Subject: Highlight Date: 5/31/2018 10:07:07 PM

Also not seen in Fig. 2, particularly the 17 km signal.

 Author: Administrator Subject: Sticky Note Date: 6/3/2018 4:01:59 PM


There is SO₂ injection up to around 17 km on 4 November shown in Fig. 2.





216 Glasow et al., 2009; we could also see it in the AIRS SO₂ and MIPAS aerosol data), and we assumed
217 that the sulfate aerosol converted from SO₂ remains collocated with the SO₂ plume, i.e., the
218 sedimentation of small sulfate aerosol particles was negligible for the timescale considered.
219 Figure 3 shows the evolution of the simulated Merapi plume and compares the plume altitudes to the
220 aerosol top altitudes measured by MIPAS between 7 and 23 November. Immediately after the eruption,
221 the majority of the plume moved towards the southwest and was entrained by the anticyclonic
222 circulation of the tropical cyclone Anggrek (not shown). After ¹the Anggrek weakened and dissipated,
223 the majority of the plume parcels ²upper troposphere moved eastward and those in the lower
224 stratosphere ³moved westward. In general, the altitudes of the simulated plume are comparable to the
225 MIPAS observations. The remaining discrepancies of air parcel altitudes being higher than the altitudes
226 of MIPAS aerosol detections can be attributed to the fact that the MIPAS tends to underestimate aerosol
227 top cloud altitudes, which is about 0.9 km in case of low extinction aerosol layers and can reach down
228 to -4.5 km in case of broken cloud conditions (Höpfner et al., 2009).


229 3.2 Meteorological background conditions after the Merapi eruption


230 The Merapi eruption in October 2010 occurred during the seasonal transition from austral spring to
231 summer when the polar vortex typically weakens and the ozone hole shrinks. As depicted in Fig. 4, the
232 meteorological conditions at the polar lower stratosphere (150hPa, ~12km) after the eruption deviated
233 from the climatological mean. The minimum temperature south of 50°S (Fig. 4a) was much lower than
234 the climatological mean during mid-November to mid-December but still higher than the low
235 temperature necessary for existence of PSCs. The polar mean temperature in Fig. 4b, defined as the
236 temperature averaged over latitudes south of 60°S, stayed lower than the climatological mean from
237 November 2010 until February 2011. Corresponding to the low temperatures, the average zonal wind
238 speed at 60°S (Fig. 4c) was significantly larger than the climatological mean value from November
239 2010 to mid-January 2011. The eddy heat flux in Fig. 4d is the product of meridional wind departures
240 and temperature departures from the respective zonal mean values. A more negative value of eddy heat
241 flux indicates that wave systems are propagating into the stratosphere and are warming the polar region.
242 There is a strong anticorrelation between temperature and the 45-day average of the eddy heat flux
243 lagged prior to the temperature. Comparing with the climatological mean state, the polar vortex was
244 more disturbed during mid-July to end of August. But from mid-October to late November, the heat
245 flux was much smaller than the long-term average, which meant a reduction in dynamical disturbances
246 of the polar vortex as the QBO changed into a strong westerly phase. Considering the temperature, the


 Number: 1 Author: Subject: Highlight Date: 5/31/2018 10:10:09 PM
delete

 Author: Administrator Subject: Sticky Note Date: 6/2/2018 5:04:42 PM
fixed

 Number: 2 Author: Subject: Highlight Date: 5/31/2018 10:10:44 PM
in the upper

 Author: Administrator Subject: Sticky Note Date: 6/2/2018 5:04:47 PM
fixed

 Number: 3 Author: Subject: Highlight Date: 5/31/2018 10:17:34 PM
This is an easterly phase of the QBO, not westerly as stated in the abstract. If the wind was westerly (Fig. 4f), how could the plume have moved westward?

 Author: Administrator Subject: Sticky Note Date: 6/3/2018 12:06:54 PM
Please refer to the reply for details.




247 subpolar wind speed and the heat flux, the polar vortex was colder and stronger in November and
248 December 2010 compared with the same time in other years. ¹The study of Klekociuk et al. (2011) also
249 confirmed that the polar vortex area was consistently larger than the climatological mean particularly
250 during November and December (see their Fig. 9). Consistent with the strength of the polar vortex, in
251 November and December 2010 the ozone hole area in Fig. 4e, defined as the region of ozone values
252 below 220 Dobson Units (DU) located south of 40°S, was larger than the climatological mean.
253 Meanwhile, the low polar mean temperature and stable polar vortex resulted in a long-lasting ozone
254 hole, which disappeared in the last week of December. The polar vortex broke down by mid-January
255 2011 when subpolar wind speed decreased below 15 m/s (Fig. 4c).


256 The poleward transport from the tropics to the polar region is known to be modulated by the phase of
257 the ²quasi-biennial oscillation (QBO) and the state of the polar vortex itself: Fig. 4f shows that just before
258 the Merapi eruption in 2010, the QBO switched from easterly phase to westerly phase. The westerly
259 phase of the QBO promotes meridional transport from the tropics to subtropics, especially into the
260 winter hemisphere (O'Sullivan and Dunkerton, 1997; Shuckburgh et al., 2001; Jäger, 2005). However, it
261 also results in zonal wind acceleration at the high latitudes (Watson and Gray, 2014; Holton and Tan,
262 1980) and a less dynamically disturbed polar vortex (Anstey and Shepherd, 2014; Baldwin and
263 Dunkerton, 1999), which will make it less possible for air parcels to penetrate the polar vortex.


264 3.3 Lagrangian simulation and satellite observation of poleward transport of the Merapi plume


265 The early plume evolution until about one month after the initial eruption is shown on the maps in Fig.
266 3 together with MIPAS observations of volcanic aerosol (only aerosol detections with $ACI < 7$ are
267 shown). Within about one month after the initial eruption, the plume was nearly entirely transported
268 around the globe in the tropics, moving west at altitudes of about 17 km. The lower part of the plume,
269 below about 17 km was transported south-eastward and reached latitudes south of 30°S by
270 mid-November. The simulated long-term transport of the Merapi plume is illustrated in Fig. 5, showing
271 the relative number of air parcels reaching a latitude-altitude bin every half a month. To verify the
272 model results, the poleward transport of aerosols as detected by MIPAS is shown in Fig. 6. For
273 comparison, only simulation results above the minimum altitude of MIPAS aerosol detections in Fig. 6
274 are shown in Fig. 5. In this study, we only focus on aerosol distributions in the upper troposphere and
275 stratosphere, where sulfate aerosol has a longer lifetime and potential climate impacts.

276 During the first month after the eruption (Figs. 5a–b), the majority of the plume was transported
277 southward roughly along the isentropic surfaces. The most significant pathway is above the core of the

 Number: 1 Author: Subject: Highlight Date: 5/31/2018 10:19:52 PM
delete

 Author: Administrator Subject: Sticky Note Date: 6/2/2018 5:17:14 PM
fixed

 Number: 2 Author: Subject: Highlight Date: 5/31/2018 10:20:57 PM
define once when first used, and then just use acronym.


 Author: Administrator Subject: Sticky Note Date: 6/2/2018 5:17:29 PM
fixed





278 subtropical jet in the ¹southern hemisphere. However, because of the transport barrier of the polar jet
279 during austral spring, the plume was confined to the north of 60°S. In December 2010 (Figs. 5c–d), a
280 larger fraction of the plume was transported southward above the subtropical jet core, and deep into the
281 polar region south of 60°S as the polar jet broke up. Till the end of January 2011, the majority of the
282 plume had entered the mid- and high latitudes in the ²southern hemisphere, whereas only a very small
283 proportion of the plume was transported north of 30°N. Substantial quasi-horizontal poleward transport
284 from the TTL towards the LMS in Antarctica was found from November 2010 to February 2011 (Figs.
285 5a–h), approximately between 350 and 480 K (~10–20 km). From March to April 2011 (Figs. 5i–l), the
286 proportion of the plume that went across 60°S stopped increasing and the maxima of the plume
287 descended from 380 to 350 K. During this transport towards Antarctica, a secondary upward transport
288 split from the plume, which was particularly observable from January 2011 till the end of the simulation
289 in April 2011 (Figs. 5e–l). This slow upward transport was mainly located around 15°S above the
290 tropopause and can be attributed to the upward branch of the BDC.


291 The poleward transport in the MPTRAC simulations was confirmed by MIPAS aerosol detections.
292 MIPAS ACI zonal median values are shown in Fig. 6 for all MIPAS measurements after filtering out
293 ice clouds. Small ACI values indicate a large aerosol load and large ACI values indicate clear air. As
294 seen in Fig. 6, the locally confined aerosol plume from the Merapi eruption did not dominate the zonal
295 median during the first half month after the eruption (Fig. 6a), but became evident between 350 and 380
296 K around the latitude of 7.5°S by the end of November (Fig. 6b) as the plume was transported around
297 the globe in the tropics. As shown in the MPTRAC simulations, the transport towards the northern mid-
298 and high latitudes was suppressed by the strong subtropical jets. The transport of the volcanic plume
299 towards Antarctica in the UTLS region was observed from December 2010 to February 2011 (Figs. 6c–
300 h) consistent with the simulations. The MIPAS aerosol data also demonstrated the upward transport
301 from the tropical upper troposphere to the stratosphere, which was observed after late January 2010.
302 The aerosol transported upward had increased the aerosol load in the tropical stratosphere reservoir
303 compared to the aerosol load before the Merapi eruption.


304 Fig. 6 verified aerosol transport from the tropics to Antarctica and upward into the tropical stratosphere.
305 However, before the eruption of Merapi, the aerosol load in the tropical stratosphere was already
306 elevated by several small and moderate-size volcanic eruptions, namely the Sarychev Peak (12 ³Jun
307 2009), Nyamuragira (20 Jan 2010), Soufriere Hills (11 Feb 2010) and Pacaya (28 May 2010). In order
308 to infer the increase of the aerosol load due to the eruption of Merapi from the MIPAS data, we
309 calculated the median ACI between 1–4 November 2010 when there was no aerosol from the Merapi

 Number: 1 Author: Subject: Highlight Date: 5/31/2018 10:29:33 PM
Southern Hemisphere

 Author: Administrator Subject: Sticky Note Date: 6/3/2018 1:30:14 PM
fixed

 Number: 2 Author: Subject: Highlight Date: 5/31/2018 10:29:57 PM
southern hemisphere

 Author: Administrator Subject: Sticky Note Date: 6/2/2018 5:17:34 PM
fixed

 Number: 3 Author: Subject: Highlight Date: 5/31/2018 10:33:06 PM
June


 Author: Administrator Subject: Sticky Note Date: 6/2/2018 5:17:48 PM
fixed





310 eruption, to define the “background” aerosol load and then remove this “background” from the median
311 ACI in Fig. 6. The results shown in Fig.7 demonstrate the change of median ACIs in the tropics and
312 southern hemisphere corresponding to the same time period as Fig. 6, with positive/negative values
313 indicating an increase/decrease of aerosol load. No significant change was observed during the first half
314 month after the eruption due to the zonal averaging degrading the aerosol signal (Fig. 7a). The largest
315 increase first appeared in the upper troposphere directly above Mount Merapi (Fig. 7b) and then moved
316 quasi-horizontally southward into the UTLS region to ~40°S (Figs. 7c–f), consistent with what Figs. 5
317 and 6 showed. A relatively small but still significant increase of aerosol south of 60°S in the tropopause
318 region was found from January 2011 (Fig. 7e) and it lasted until mid- April 2011 (Fig. 7j). Six months
319 after the eruption, the aerosol levels were still slightly elevated in the tropical upper troposphere above
320 350 K. There should have been a decrease of the aerosol load in the tropical stratosphere because of
321 sedimentation and poleward transport of aerosol if there were no aerosol from the Merapi eruption. But
322 the upward transport of the Merapi aerosol ¹compensated the loss.


323 **3.4 Efficiency of quasi-horizontal transport from the tropics to Antarctica**

324 As the results of the Lagrangian transport simulations with the MPTRAC model were comparable to the
325 MIPAS observations (Sect. 3.3), it was possible not only to demonstrate the transport pathways but also
326 to estimate the efficiency of the transport. The MPTRAC simulations and the MIPAS observations have
327 demonstrated transport on the “surf zone” that reaches from the subtropics to high latitudes (Holton et
328 al., 1995), where air masses are affected by both fast meridional transport and the slow BDC. Our data
329 show that quasi-horizontal mixing in the lower extratropical stratosphere between 350 and 480 K is the
330 main transport pathway for the volcanic aerosol. Figure 8 illustrates how the volcanic plume between
331 350 and 480 K approached Antarctica over time. Gray dashed and solid lines mark potential ²vortices
332 (PV) contours with the largest PV gradients on the 350 and 480 K isentropic surfaces. These
333 dynamically relevant PV contours represent horizontal transport barriers for air masses on the respective
334 isentropic surface. On isentropic surfaces below 380 K, the contours of maximum PV gradients
335 represent the dynamical discontinuity near the core of the subtropical jet stream and thus represent a
336 transport barrier between the tropics and midlatitudes (Haynes and Shuckburgh, 2000; Kunz et al.,
337 2011a,b). Isentropic transport of air masses across these boundaries indicates exchange between the
338 tropics and extratropics due to Rossby wave breaking. On isentropic surfaces above 400 K, the contours
339 of maximum PV gradients represent a boundary in the lower stratosphere, in particular, due to the polar
340 vortices in winter (Kunz et al., 2015). For comparison we have also shown contour lines of ozone

 Number: 1 Author: Subject: Highlight Date: 5/31/2018 10:35:30 PM
compensated for

 Author: Administrator Subject: Sticky Note Date: 6/2/2018 5:18:32 PM
fixed

 Number: 2 Author: Subject: Highlight Date: 5/31/2018 10:39:24 PM
vorticity

 Author: Administrator Subject: Sticky Note Date: 6/2/2018 5:23:25 PM
fixed



341 column density of 220 DU (black isolines in Fig. 8), indicating the location and size of the ozone hole.
342 The PV boundary on 480 K is in most cases collocated with the area of the ozone hole, showing that
343 both quantities provide a consistent representation of the area of the polar vortex.
344 The Merapi volcanic plume first reached the 350 K transport boundary in mid-November and went
345 close to the 480 K transport boundary in December. The long-lasting polar vortex prevented the
346 volcanic plume from crossing the transport boundary in the beginning of December, but from
347 mid-December, the polar vortex became more disturbed and displaced from the south pole, together
348 with a shrinking ozone hole. As mentioned in Sect.3.2, the ozone hole broke up at the end of December
349 2010 and the polar vortex broke down by mid-January 2011.
350 The fractions of the volcanic plume that crossed the individual transport boundaries or the latitude of
351 60°S on each isentropic surface are shown in Fig. 9. In both cases, the proportion increased from
352 November 2010 to January 2011. In November and December 2010 the largest plume transport across
353 the transport boundaries occurred between the 360 and 430 K isentropic surface (Fig. 9a), with a peak at
354 380–390 K. In January and February 2011 the peak was slightly elevated to 390–400 K. In November
355 2010, the volcanic plume did not cross the 480 K transport boundary of the polar vortex at high altitudes,
356 especially above about 450 K. The high-latitude fraction kept increasing from December 2010 to
357 February 2011 as the weakening of the polar vortex made the transport boundary more permeable. In
358 March and April 2011, the total proportion decreased and the peak descended to 370 K in March and
359 further to 360 K in April. The proportion of the volcanic plume south of 60°S (Fig. 9b) increased
360 slightly from November to December 2010, and then increased significantly from December 2010 to
361 January and February 2011 at all altitudes as the polar vortex displaced and broke down. Finally, the
362 transport to south of 60°S started to decrease in March 2011. From November 2010 to February 2011
363 the peak was around 370–400 K, but in March and April 2011 the peak resided around 350–370 K.
364 Figure 10 summarizes the poleward transport of the volcanic plume between 350 and 480 K. The
365 zonally resolved fractions derived from the Lagrangian MPTRAC simulations and the fraction of air
366 parcels south of 60°S are shown in Fig. 10a. Figure 10b demonstrates the increasing and decreasing
367 aerosol load in this vertical range for MIPAS aerosol detections relative to 1–4 November median (see
368 Sect.3.3). The poleward transport trend in Fig. 10a is comparable to the poleward migration of the
369 enhanced aerosol in Fig. 10b. The simulations show that the plume reached 60°S by the end of
370 November 2010. Correspondingly, the aerosol load south of 60°S was elevated when the volcanic
371 plume was transported there. The percentage fluctuated, but increased until the end of February 2011,
372 with a maximum percentage of about 4%. A steep increase occurred from mid-December 2010 to end of

This page contains no comments




373 January 2011, following the displacement and breakdown of the polar vortex. The elevated aerosol load
374 south of 60°S decreased from March 2011, because the plume descended to altitudes below 350 K as
375 shown by Fig. 9b. Overall, enhanced aerosol due to Merapi eruption was observed mostly in the
376 subtropics and midlatitudes, but the aerosol load in the south polar region was also significantly
377 elevated for three months from December 2010 to February 2011.

378 4 Discussion


379 The results presented in Sect. 3 show that the meridional transport of the Merapi volcanic plume to
380 Antarctica mostly occurred between the isentropic surfaces of 350 and 480 K (about 10 to 20 km),
381 covering the TTL and the lower stratosphere at mid- and high latitudes. For this long-range transport on
382 timescales of a few months, fast isentropic transport associated with quasi-horizontal mixing was found
383 to be the most efficient pathway. The phase of QBO, ¹subtropical Rossby wave breaking and the strength
384 and stability of the polar vortex all have an impact on the transport efficiency. The Merapi eruption
385 occurred in austral spring and fast poleward transport was facilitated by the weakening subtropical jet
386 and active Rossby wave breaking events. The westerly QBO enhanced transport and mixing in the
387 subtropics with implications on the position of the subtropical barrier (Shuckburgh et al., 2001; Palazzi et
388 al., 2011). The QBO also modulated the ability of upward propagating planetary waves to influence the
389 strength of the polar vortex. Although the polar vortex was relatively stable when the Merapi eruption
390 occurred, after the volcanic plume reached the south polar region, the polar vortex was displaced from
391 the south pole and distorted because more wave systems propagated into the polar stratosphere and
392 warmed the polar region, so that the volcanic plume could be transported from the tropics deep into
393 Antarctica under all these favourable conditions.


394 The phase of the QBO influences the amount of volcanic emissions transported out of tropics, while the
395 heating effect of a large amount of sulfur injected by volcanic eruptions can change the pattern of the
396 QBO (Niemeier and Schmidt, 2017). With increasing emission rates the velocity of the equatorial jet
397 streams increases and less sulfate is transported out of the tropics. The amount of SO₂ injected during
398 the Merapi eruption 2010 was 0.44 Tg, far less than the ²TgS/yr required to shut down or reverse the
399 QBO pattern (Niemeier and Schmidt, 2017), so that the westerly phase of the QBO that promote
400 meridional transport was under minor influence of the heating effect of sulfur in this case.

401 Based on the simulations in Sect. 3.4, up to ~4% of air parcels composed of SO₂ and sulfate aerosol
402 were transported from the TTL to the lower stratosphere in the south polar region till the end of

 Number: 1 Author: Subject: Highlight Date: 6/3/2018 12:08:16 PM
not discussed or plotted above. If you are going to claim this, you have to show evidence.

 Author: Administrator Subject: Sticky Note Date: 6/3/2018 12:08:12 PM
Please refer to the reply for details.

 Number: 2 Author: Subject: Highlight Date: 5/31/2018 10:51:57 PM
That is a continuous emission. It cannot be compared to a one time emission.


 Author: Administrator Subject: Sticky Note Date: 8/28/2018 3:47:40 PM
We rephrase this sentence: The amount of SO₂ injected during the Merapi eruption 2010 was only 0.44 Tg, so that the westerly phase of the QBO that promotes meridional transport was under minor influence of the heating effect of sulfur in this case.
This sentence has been removed from the revised manuscript.




403 February 2011, which means the Merapi eruption contributed about 8800 tons of sulfur to the polar
404 lower stratosphere within 4 months after the eruption, assuming that the sulfate aerosol converted from
405 SO₂ remained in the plume. In the lower stratosphere, the atmosphere is relatively dry and clean
406 compared with the lower troposphere, so the sulfate aerosols may have a smaller chance to interact with
407 clouds or to be washed out. In fact, in the polar lower stratosphere usually sedimentation and downward
408 transport by the BDC are the main removal processes. Clouds and washout processes usually cannot be
409 expected in the lower stratosphere. However, the amount of sulfate aerosols in the plume could also be
410 affected by other mechanisms that speed up the loss of sulfur, for example, coagulation in the volcanic
411 plume, the absorption of sulfur onto fine ash particles ¹c. But for a moderate eruption, such as the
412 Merapi eruption, ²sulphuric particle growth may not be as significant as it is in a large volcanic eruption,
413 so the scavenging efficiency of sulfur will be low.


414 Besides, a kinematic trajectory model like MPTRAC, in which reanalysis vertical wind is used as
415 vertical velocity, typically shows higher vertical dispersion in the equatorial lower stratosphere
416 compared with a diabatic trajectory model (Schoeberl et al., 2003; Wohltmann and Rex, 2008; Liu et al.,
417 2010; Ploeger et al., 2010, 2011). However, the ERA–Interim reanalysis data used in this study to drive
418 the model may constrain the vertical dispersion much better than older reanalyses (Liu et al., 2010;
419 Hoffmann et al., 2017). The meridional transport in this study was mainly quasi-horizontal transport in
420 the mid- and high latitude UTLS region, so the effect of the vertical speed scheme is limited.
421 Meanwhile, the MIPAS aerosol detections confirmed the MPTRAC simulations, so our results can be
422 considered as a representative value.

423 The aerosol transported to the polar lower stratosphere will finally descend with the downward flow in
424 the polar region to lower altitudes, and have a chance to become a nonlocal source of sulfur for
425 Antarctica by dry and wet deposition, following the general precipitation patterns. Quantifying the
426 sulfur deposition flux onto Antarctica is beyond the scope of this study, though. Model results of
427 Solomon et al. (2016) suggest that the Merapi eruption made a small but significant contribution to
428 ozone depletion over Antarctica in the vertical range of 200–100 hPa (~10–14 km). This altitude range
429 is in agreement with our results, where we found transport into the Antarctic stratosphere between 10
430 and 20 km. When the volcanic plume was transported to Antarctica in December 2010, the polar
431 synoptic temperature at these low height levels was already too high for the formation of PSCs. The
432 additional ozone depletion found by Solomon et al. (2016) together with the fact that sulfate aerosol was
433 transported from the Merapi into the Antarctic stratosphere between November and February where no
434 PSCs are present during polar summer, may support the study which suggested that significant ozone


 Number: 1 Author: Subject: Highlight Date: 5/31/2018 10:53:04 PM

DELETE. You can't use this with "for example," and anyway it has no information content.

 Author: Administrator Subject: Sticky Note Date: 6/2/2018 5:23:57 PM
fixed

 Number: 2 Author: Subject: Highlight Date: 5/31/2018 10:53:40 PM

sulfuric [stick to the standard spelling]

 Author: Administrator Subject: Sticky Note Date: 6/2/2018 5:26:46 PM
fixed



435 depletion can also occur on cold binary aerosol (Drdla and Müller, 2012). The Merapi eruption in 2010
436 could be an interesting case study for more sophisticated geophysical models to study the aftermath of
437 volcanic eruptions on polar processes.

438 **5 Summary and conclusion**

439 In this study, we analyzed the poleward transport pathway and the transport efficiency of volcanic
440 aerosol released by the Merapi eruption in October 2010 from tropics to the Antarctic lower
441 stratosphere. The analysis was based on AIRS SO₂ measurements, MIPAS sulfate aerosol detections
442 and MPTRAC transport simulations. First, we estimated altitude-resolved SO₂ injection time series
443 during the explosive eruption period using AIRS data together with a backward trajectory approach.
444 Second, the long-range transport of the volcanic plume from the initial eruption to 30 April 2010 was
445 simulated based on the derived SO₂ injection time series. Then the evolution and the poleward
446 migration of the volcanic plume was analyzed and validated with MIPAS aerosol measurements.

447 Results of this study suggest that the volcanic plume from the Merapi eruption was transported from the
448 tropics to south of 60°S within a time scale of one month. Later on a significant fraction of the volcanic
449 plume crossed 60°S, even further to Antarctica until the end of February 2011. As a result, the aerosol
450 load in the Antarctic lower stratosphere was significantly elevated for 3 months from December 2010 to
451 February 2011. From March 2011, the aerosol transported to the polar lower stratosphere descended
452 with the downward flow of the Brewer-Dobson circulation to lower altitudes. This relatively fast
453 meridional transport and the distribution of volcanic aerosol was mainly carried out by quasi-horizontal
454 mixing from the TTL to the extratropical lower stratosphere, which in turn was facilitated by the
455 weakening of the subtropical jet in the seasonal transition from austral spring to summer. Based on the
456 simulations, the most efficient pathway for this quasi-horizontal mixing occurred between isentropic
457 surfaces of 360 to 430 K. The polar vortex in late austral spring 2010 was relatively strong compared to
458 the climatological mean state. However, when the plume went to the south polar region, the polar vortex
459 was displaced off the south pole, so that the volcanic plume was able to enter to the south pole without
460 even penetrating the polar vortex.

461 Overall, after the Merapi eruption, the largest increase of aerosol load occurred in the southern
462 hemisphere midlatitudes and a relatively small but significant fraction of the volcanic plume (4%) was
463 further transported to the Antarctic lower stratosphere within 4 months after the eruption. This
464 contributed 8800 tons of sulfur to the Antarctic stratosphere, which indicates that long-range transport

This page contains no comments



465 under favorable meteorological conditions enables tropical volcanic eruptions to be an important remote
466 source of sulfur to Antarctica.

467 *Code and data availability.* AIRS data are distributed by the NASA Goddard Earth Sciences Data
468 Information and Services Center. The SO₂ index data used in this study (Hoffmann et al., 2014) are
469 available for download at <https://datapub.fz-juelich.de/slcs/airs/volcanoes/> (last access: 17 December
470 2017). Envisat MIPAS Level-1B data are distributed by the European Space Agency. The ERA–Interim
471 reanalysis data (Dee et al., 2011) were obtained from the European Centre for Medium-Range Weather
472 Forecasts. The code of the Massive-Parallel Trajectory Calculations (MPTRAC) model is available
473 under the terms and conditions of the GNU General Public License, Version 3 from the repository at
474 <https://github.com/slcs-jsc/mptrac> (last access: 31 December 2017).

475

476 *Competing interests.* The authors declare that they have no conflict of interest.

477

478 *Acknowledgments.* This work was supported by National Natural Science Foundation of China under
479 grant no. 41605023 and International Postdoctoral Exchange Fellowship Program 2015 under grant no.
480 20151006.

481 Reference

- 482 Anstey, J. A., and Shepherd, T. G.: High-latitude influence of the quasi-biennial oscillation, Q. J. R.
483 Meteorol. Soc., 140, 1-21, doi: 10.1002/qj.2132, 2014.
- 484 Aquila, V., C. I. Garfinkel, P. A. Newman, L. D. Oman, and D. W. Waugh, Modifications of the
485 quasi-biennial oscillation by a geoengineering perturbation of the stratospheric aerosol layer,
486 Geophys. Res. Lett., 41, 1738-1744, doi: 10.1002/2013GL058818, 2014.
- 487 Aumann, H. H., Chahine, M. T., Gautier, C., Goldberg, M. D., Kalnay, E., McMillin, L. M., Revercomb,
488 H., Rosenkranz, P. W., Smith, W. L., Staelin, D. H., Strow, L. L., and Susskind, J.: AIRS/AMSU/HSB
489 on the Aqua mission: design, science objectives, data products, and processing systems, IEEE Trans.
490 Geosci. Remote Sens., 41, 253-264, doi: 10.1109/TGRS.2002.808356, 2003.
- 491 Baldwin, M. P., and Dunkerton, T. J.: Propagation of the Arctic Oscillation from the stratosphere to the
492 troposphere, J. Geophys. Res. Atmos., 104, 30937-30946, doi: 10.1029/1999JD900445, 1999.
- 493 Dee, D. P., Uppala, S. M., Simmons, A. J., Berrisford, P., Poli, P., Kobayashi, S., Andrae, U.,
494 Balmaseda, M. A., Balsamo, G., Bauer, P., Bechtold, P., Beljaars, A. C. M., van de Berg, L., Bidlot,
495 J., Bormann, N., Delsol, C., Dragani, R., Fuentes, M., Geer, A. J., Haimberger, L., Healy, S. B.,
496 Hersbach, H., Holm, E. V., Isaksen, L., Kallberg, P., Kohler, M., Matricardi, M., McNally, A. P.,
497 Monge-Sanz, B. M., Morcrette, J. J., Park, B. K., Peubey, C., de Rosnay, P., Tavolato, C., Thepaut, J.
498 N., and Vitart, F.: The ERA-Interim reanalysis: configuration and performance of the data
499 assimilation system, Q. J. R. Meteorol. Soc., 137, 553-597, doi: 10.1002/qj.828, 2011.
- 500 Drdla, K., and Müller, R.: Temperature thresholds for chlorine activation and ozone loss in the polar
501 stratosphere, Ann. Geophys., 30, 1055-1073, doi: 10.5194/angeo-30-1055-2012, 2012.

This page contains no comments



- 502 Fischer, H., Birk, M., Blom, C., Carli, B., Carlotti, M., von Clarmann, T., Delbouille, L., Dudhia, A.,
503 Ehhalt, D., Endemann, M., Flaud, J. M., Gessner, R., Kleinert, A., Koopman, R., Langen, J.,
504 López-Puertas, M., Mosner, P., Nett, H., Oelhaf, H., Perron, G., Remedios, J., Ridolfi, M., Stiller, G.,
505 and Zander, R.: MIPAS: an instrument for atmospheric and climate research, *Atmos. Chem. Phys.*, 8,
506 2151-2188, doi: 10.5194/acp-8-2151-2008, 2008.
- 507 Gao, C., Oman, L., Robock, A., and Stenchikov, G. L.: Atmospheric volcanic loading derived from
508 bipolar ice cores: Accounting for the spatial distribution of volcanic deposition, *J. Geophys. Res.*
509 *Atmos.*, 112, D09109, doi: 10.1029/2006JD007461, 2007.
- 510 Griessbach, S., Hoffmann, L., Spang, R., von Hobe, M., Müller, R., and Riese, M.: Infrared limb emission
511 measurements of aerosol in the troposphere and stratosphere, *Atmos. Meas. Tech.*, 9, 4399-4423,
512 doi:10.5194/amt-9-4399-2016, 2016.
- 513 Günther, A., Höpfner, M., Sinnhuber, B. M., Griessbach, S., Deshler, T., von Clarmann, T., and Stiller,
514 G.: MIPAS observations of volcanic sulphate aerosol and sulphur dioxide in the stratosphere, *Atmos.*
515 *Chem. Phys. Discuss.*, 2017, 1-32, doi: 10.5194/acp-2017-538, 2017.
- 516 Haynes, P., and Shuckburgh, E.: Effective diffusivity as a diagnostic of atmospheric transport: 2.
517 Troposphere and lower stratosphere, *J. Geophys. Res. Atmos.*, 105, 22795-22810, doi:
518 10.1029/2000JD900092, 2000.
- 519 Heng, Y., Hoffmann, L., Griessbach, S., Röbber, T., and Stein, O.: Inverse transport modeling of volcanic
520 sulfur dioxide emissions using large-scale simulations, *Geosci. Model Dev.*, 9, 1627-1645,
521 doi:10.5194/gmd-9-1627-2016, 2016.
- 522 Hoffmann, L., Griessbach, S., and Meyer, C. I.: Volcanic emissions from AIRS observations: detection
523 methods, case study, and statistical analysis, in: *Remote Sensing of Clouds and the Atmosphere XIX*
524 *and Optics in Atmospheric Propagation and Adaptive Systems XVII*, edited by: Comeron, A.,
525 Kassianov, E. I., Schafer, K., Picard, R. H., Stein, K., and Gonglewski, J. D., *Proceedings of SPIE*,
526 *Spie-Int Soc Optical Engineering*, Bellingham, doi: 92421410.1117/12.2066326, 2014.
- 527 Hoffmann, L., Hertzog, A., Röbber, T., Stein, O., and Wu, X.: Intercomparison of meteorological
528 analyses and trajectories in the Antarctic lower stratosphere with Concordiasi superpressure balloon
529 observations, *Atmos. Chem. Phys.*, 17, 8045-8061, doi: 10.5194/acp-17-8045-2017, 2017.
- 530 Hoffmann, L., Röbber, T., Griessbach, S., Heng, Y., and Stein, O.: Lagrangian transport simulations of
531 volcanic sulfur dioxide emissions: Impact of meteorological data products, *J. Geophys. Res. Atmos.*,
532 121, 4651-4673, doi: 10.1002/2015JD023749, 2016.
- 533 Hofmann, D. J., Rosen, J. M., and Gringel, W.: Delayed production of sulfuric acid condensation nuclei
534 in the polar stratosphere from El Chichon volcanic vapors, *Journal of Geophysical Research:*
535 *Atmospheres*, 90, 2341-2354, doi:10.1029/JD090iD01p02341, 1985.
- 536 Hofmann, D. J., Rosen, J. M., and Harder, J. W.: Aerosol measurements in the winter/spring Antarctic
537 stratosphere: 1. Correlative measurements with ozone, *Journal of Geophysical Research:*
538 *Atmospheres*, 93, 665-676, doi:10.1029/JD093iD01p00665, 1988.
- 539 Holton, J. R., Haynes, P. H., McIntyre, M. E., Douglass, A. R., Rood, R. B., and Pfister, L.:
540 Stratosphere-troposphere exchange, *Reviews of Geophysics*, 33, 403-439, doi: 10.1029/95RG02097,
541 1995.
- 542 Holton, J. R., and Tan, H. C.: The Influence of the Equatorial Quasi-Biennial Oscillation on the Global
543 Circulation at 50 mb, *J. Atmos. Sci.*, 37, 2200-2208, doi:
544 10.1175/1520-0469(1980)037<2200:tioteq>2.0.co;2, 1980.
- 545 Höpfner, M., Pitts, M. C., and Poole, L. R.: Comparison between CALIPSO and MIPAS observations
546 of polar stratospheric clouds, *Journal of Geophysical Research: Atmospheres*, 114,
547 doi:10.1029/2009JD012114, 2009.

This page contains no comments



- 548 Ivy, D. J., Solomon, S., Kinnison, D., Mills, M. J., Schmidt, A., and Neely, R. R.: The influence of the
549 Calbuco eruption on the 2015 Antarctic ozone hole in a fully coupled chemistry-climate model,
550 *Geophys. Res. Lett.*, 44, 2556-2561, doi: 10.1002/2016GL071925, 2017.
- 551 Jäger, H.: Long-term record of lidar observations of the stratospheric aerosol layer at
552 Garmisch-Partenkirchen, *J. Geophys. Res. Atmos.*, 110, D08106, doi: 10.1029/2004JD005506, 2005.
- 553 Jäger, H., and Wege, K.: Stratospheric ozone depletion at northern midlatitudes after major volcanic
554 eruptions, *J. Atmos. Chem.*, 10, 273-287, doi: 10.1007/bf00053863, 1990.
- 555 Khaykin, S. M., Godin-Beekmann, S., Keckhut, P., Hauchecorne, A., Jumelet, J., Vernier, J. P.,
556 Bourassa, A., Degenstein, D. A., Rieger, L. A., Bingen, C., Vanhellefont, F., Robert, C., DeLand,
557 M., and Bhartia, P. K.: Variability and evolution of the midlatitude stratospheric aerosol budget from
558 22 years of ground-based lidar and satellite observations, *Atmos. Chem. Phys.*, 17, 1829-1845, doi:
559 10.5194/acp-17-1829-2017, 2017.
- 560 Klekociuk, A., Tully, M., Alexander, S., Dargaville, R., Deschamps, L., Fraser, P., Gies, H., Henderson,
561 S., Javorniczky, J., and Krummel, P.: The Antarctic ozone hole during 2010, *Aust. Meteorol. Ocean.
562 Journal.*, 61, 253, 2011.
- 563 Kravitz, B., and Robock, A.: Climate effects of high-latitude volcanic eruptions: Role of the time of
564 year, *J. Geophys. Res. Atmos.*, 116, D01105, 10.1029/2010JD014448, 2011.
- 565 Kunz, A., Konopka, P., Müller, R., and Pan, L. L.: Dynamical tropopause based on isentropic potential
566 vorticity gradients, *J. Geophys. Res. Atmos.*, 116, D01110, doi: 10.1029/2010JD014343, 2011a.
- 567 Kunz, A., Pan, L. L., Konopka, P., Kinnison, D. E., and Tilmes, S.: Chemical and dynamical
568 discontinuity at the extratropical tropopause based on START08 and WACCM analyses, *J. Geophys.
569 Res. Atmos.*, 116, D24302, doi: 10.1029/2011JD016686, 2011b.
- 570 Kunz, A., Sprenger, M., and Wernli, H.: Climatology of potential vorticity streamers and associated
571 isentropic transport pathways across PV gradient barriers, *J. Geophys. Res. Atmos.*, 120, 3802-3821,
572 doi: 10.1002/2014jd022615, 2015.
- 573 Liu, Y. S., Fueglistaler, S., and Haynes, P. H.: Advection-condensation paradigm for stratospheric water
574 vapor, *J. Geophys. Res. Atmos.*, 115, D24307, doi: 10.1029/2010JD014352, 2010.
- 575 Mazzera, D. M., Lowenthal, D. H., Chow, J. C., and Watson, J. G.: Sources of PM10 and sulfate aerosol
576 at McMurdo station, Antarctica, *Chemosphere*, 45, 347-356, doi:
577 [https://doi.org/10.1016/S0045-6535\(00\)00591-9](https://doi.org/10.1016/S0045-6535(00)00591-9), 2001.
- 578 Niemeier, U., and Schmidt, H.: Changing transport processes in the stratosphere by radiative heating of
579 sulfate aerosols, *Atmos. Chem. Phys.*, 17, 14871-14886, doi: 10.5194/acp-17-14871-2017, 2017.
- 580 Olsen, M. A., Douglass, A. R., Schoeberl, M. R., Rodriguez, J. M., and Yoshida, Y.: Interannual
581 variability of ozone in the winter lower stratosphere and the relationship to lamina and irreversible
582 transport, *J. Geophys. Res.-Atmos.*, 115, 10.1029/2009jd013004, 2010.
- 583 O'Sullivan, D., and Dunkerton, T. J.: The influence of the quasi-biennial oscillation on global
584 constituent distributions, *J. Geophys. Res. Atmos.*, 102, 21731-21743, doi: 10.1029/97JD01689,
585 1997.
- 586 Palazzi, E., Fierli, F., Stiller, G. P., and Urban, J.: Probability density functions of long-lived tracer
587 observations from satellite in the subtropical barrier region: data intercomparison, *Atmos. Chem.
588 Phys.*, 11, 10579-10598, doi: 10.5194/acp-11-10579-2011, 2011.
- 589 Pallister, J. S., Schneider, D. J., Griswold, J. P., Keeler, R. H., Burton, W. C., Noyles, C., Newhall, C.
590 G., and Ratdomopurbo, A.: Merapi 2010 eruption—Chronology and extrusion rates monitored with
591 satellite radar and used in eruption forecasting, *J. Volcanol. Geotherm. Res.*, 261, 144-152, doi:
592 <http://dx.doi.org/10.1016/j.jvolgeores.2012.07.012>, 2013.

This page contains no comments



- 593 Pausata, F. S. R., Chafik, L., Caballero, R., and Battisti, D. S.: Impacts of high-latitude volcanic
594 eruptions on ENSO and Asian monsoon, *Proceedings of the National Academy of Sciences*, 112,
595 13784-13788, doi: 10.1073/pnas.1509153112, 2015.
- 596 Ploeger, F., Konopka, P., Gunther, G., Grooss, J. U., and Muller, R.: Impact of the vertical velocity
597 scheme on modeling transport in the tropical tropopause layer, *J. Geophys. Res. Atmos.*, 115, 14, doi:
598 10.1029/2009jd012023, 2010.
- 599 Ploeger, F., Fueglistaler, S., Grooss, J. U., Gunther, G., Konopka, P., Liu, Y. S., Muller, R., Ravegnani,
600 F., Schiller, C., Ulanovski, A., and Riese, M.: Insight from ozone and water vapour on transport in
601 the tropical tropopause layer (TTL), *Atmos. Chem. Phys.*, 11, 407-419, doi:
602 10.5194/acp-11-407-2011, 2011.
- 603 Rößler, T., Stein, O., Heng, Y., and Hoffmann, L.: Regional and seasonal truncation errors of trajectory
604 calculations using ECMWF high-resolution operational analyses and forecasts, *Geosci. Model Dev.*
605 *Discuss.*, 2017, 1-27, doi: 10.5194/gmd-2016-314, 2017.
- 606 Sand, M., Samset, B. H., Balkanski, Y., Bauer, S., Bellouin, N., Berntsen, T. K., Bian, H., Chin, M.,
607 Diehl, T., Easter, R., Ghan, S. J., Iversen, T., Kirkevåg, A., Lamarque, J. F., Lin, G., Liu, X., Luo, G.,
608 Myhre, G., Noije, T. V., Penner, J. E., Schulz, M., Seland, Ø., Skeie, R. B., Stier, P., Takemura, T.,
609 Tsigaridis, K., Yu, F., Zhang, K., and Zhang, H.: Aerosols at the poles: an AeroCom Phase II
610 multi-model evaluation, *Atmos. Chem. Phys.*, 17, 12197-12218, doi: 10.5194/acp-17-12197-2017,
611 2017.
- 612 Schoeberl, M. R., Douglass, A. R., Zhu, Z. X., and Pawson, S.: A comparison of the lower stratospheric
613 age spectra derived from a general circulation model and two data assimilation systems, *J. Geophys.*
614 *Res. Atmos.*, 108, 16, doi: 10.1029/2002jd002652, 2003.
- 615 Shuckburgh, E., Norton, W., Iwi, A., and Haynes, P.: Influence of the quasi-biennial oscillation on
616 isentropic transport and mixing in the tropics and subtropics, *J. Geophys. Res. Atmos.*, 106,
617 14327-14337, doi: 10.1029/2000JD900664, 2001.
- 618 Sigl, M., Winstrup, M., McConnell, J. R., Welten, K. C., Plunkett, G., Ludlow, F., Buntgen, U., Caffee,
619 M., Chellman, N., Dahl-Jensen, D., Fischer, H., Kipfstuhl, S., Kostick, C., Maselli, O. J., Mekhaldi,
620 F., Mulvaney, R., Muscheler, R., Pasteris, D. R., Pilcher, J. R., Salzer, M., Schupbach, S., Steffensen,
621 J. P., Vinther, B. M., and Woodruff, T. E.: Timing and climate forcing of volcanic eruptions for the
622 past 2,500 years, *Nature*, 523, 543-549, doi:
623 10.1038/nature14565 [http://www.nature.com/nature/journal/v523/n7562/abs/nature14565.html#suppl](http://www.nature.com/nature/journal/v523/n7562/abs/nature14565.html#supplementary-information)
624 [ementary-information](http://www.nature.com/nature/journal/v523/n7562/abs/nature14565.html#supplementary-information), 2015.
- 625 Solomon, S.: Stratospheric ozone depletion: A review of concepts and history, *Reviews of Geophysics*,
626 37, 275-316, doi: 10.1029/1999RG900008, 1999.
- 627 Solomon, S., Daniel, J. S., Neely, R. R., Vernier, J.-P., Dutton, E. G., and Thomason, L. W.: The
628 Persistently Variable “Background” Stratospheric Aerosol Layer and Global Climate Change,
629 *Science*, 333, 866-870, doi: 10.1126/science.1206027, 2011.
- 630 Solomon, S., Ivy, D. J., Kinnison, D., Mills, M. J., Neely, R. R., and Schmidt, A.: Emergence of healing
631 in the Antarctic ozone layer, *Science*, doi: 10.1126/science.aae0061, 2016.
- 632 Solomon, S., Sanders, R. W., Garcia, R. R., and Keys, J. G.: Increased chlorine dioxide over Antarctica
633 caused by volcanic aerosols from Mount-Pinatubo, *Nature*, 363, 245-248, doi:
634 <https://doi.org/10.1038/363245a0>, 1993.
- 635 Stohl, A., Forster, C., Frank, A., Seibert, P., and Wotawa, G.: Technical note: The Lagrangian particle
636 dispersion model FLEXPART version 6.2, *Atmos. Chem. Phys.*, 5, 2461-2474,
637 doi:10.5194/acp-5-2461-2005, 2005.
- 638 Stone, K. A., Solomon, S., Kinnison, D. E., Pitts, M. C., Poole, L. R., Mills, M. J., Schmidt, A., Neely,
639 R. R., Ivy, D., Schwartz, M. J., Vernier, J.-P., Johnson, B. J., Tully, M. B., Klekociuk, A. R.,

This page contains no comments



- 640 König-Langlo, G., and Hagiya, S.: Observing the Impact of Calbuco Volcanic Aerosols on South
641 Polar Ozone Depletion in 2015, *J. Geophys. Res. Atmos.*, 122, 11,862-811,879, doi:
642 10.1002/2017JD026987, 2017.
- 643 Surono, Jousset, P., Pallister, J., Boichu, M., Buongiorno, M. F., Budisantoso, A., Costa, F., Andreastuti,
644 S., Prata, F., Schneider, D., Clarisse, L., Humaida, H., Sumarti, S., Bignami, C., Griswold, J., Carn,
645 S., Oppenheimer, C., and Lavigne, F.: The 2010 explosive eruption of Java's Merapi volcano—A
646 '100-year' event, *J. Volcanol. Geotherm. Res.*, 241, 121-135, doi:
647 <http://dx.doi.org/10.1016/j.jvolgeores.2012.06.018>, 2012.
- 648 Tilmes, S., Muller, R., and Salawitch, R.: The sensitivity of polar ozone depletion to proposed
649 geoengineering schemes, *Science*, 320, 1201-1204, doi: 10.1126/science.1153966, 2008.
- 650 Vernier, J. P., Thomason, L. W., Pommereau, J. P., Bourassa, A., Pelon, J., Garnier, A., Hauchecorne,
651 A., Blanot, L., Trepte, C., Degenstein, D., and Vargas, F.: Major influence of tropical volcanic
652 eruptions on the stratospheric aerosol layer during the last decade, *Geophys. Res. Lett.*, 38, L12807,
653 10.1029/2011GL047563, 2011.
- 654 Vogel, B., Pan, L. L., Konopka, P., Gunther, G., Muller, R., Hall, W., Campos, T., Pollack, I.,
655 Weinheimer, A., Wei, J., Atlas, E. L., and Bowman, K. P.: Transport pathways and signatures of
656 mixing in the extratropical tropopause region derived from Lagrangian model simulations, *J.*
657 *Geophys. Res.-Atmos.*, 116, 16, doi: 10.1029/2010jd014876, 2011.
- 658 von Glasow, R., Bobrowski, N., and Kern, C.: The effects of volcanic eruptions on atmospheric
659 chemistry, *Chem. Geol.*, 263, 131-142, doi: <http://dx.doi.org/10.1016/j.chemgeo.2008.08.020>, 2009.
- 660 Watson, P. A. G., and Gray, L. J.: How Does the Quasi-Biennial Oscillation Affect the Stratospheric
661 Polar Vortex?, *J. Atmos. Sci.*, 71, 391-409, doi: 10.1175/jas-d-13-096.1, 2014.
- 662 Wohltmann, I., and Rex, M.: Improvement of vertical and residual velocities in pressure or hybrid
663 sigma-pressure coordinates in analysis data in the stratosphere, *Atmos. Chem. Phys.*, 8, 265-272, doi:
664 10.5194/acp-8-265-2008, 2008.
- 665 Wu, X., Griessbach, S., and Hoffmann, L.: Equatorward dispersion of a high-latitude volcanic plume
666 and its relation to the Asian summer monsoon: a case study of the Sarychev eruption in 2009, *Atmos.*
667 *Chem. Phys.*, 17, 13439-13455, doi: 10.5194/acp-17-13439-2017, 2017.
- 668 Zuev, V. V., Zueva, N. E., Savelieva, E. S., and Gerasimov, V. V.: The Antarctic ozone depletion
669 caused by Erebus volcano gas emissions, *Atmos. Environ.*, 122, 393-399, doi:
670 <https://doi.org/10.1016/j.atmosenv.2015.10.005>, 2015.

This page contains no comments

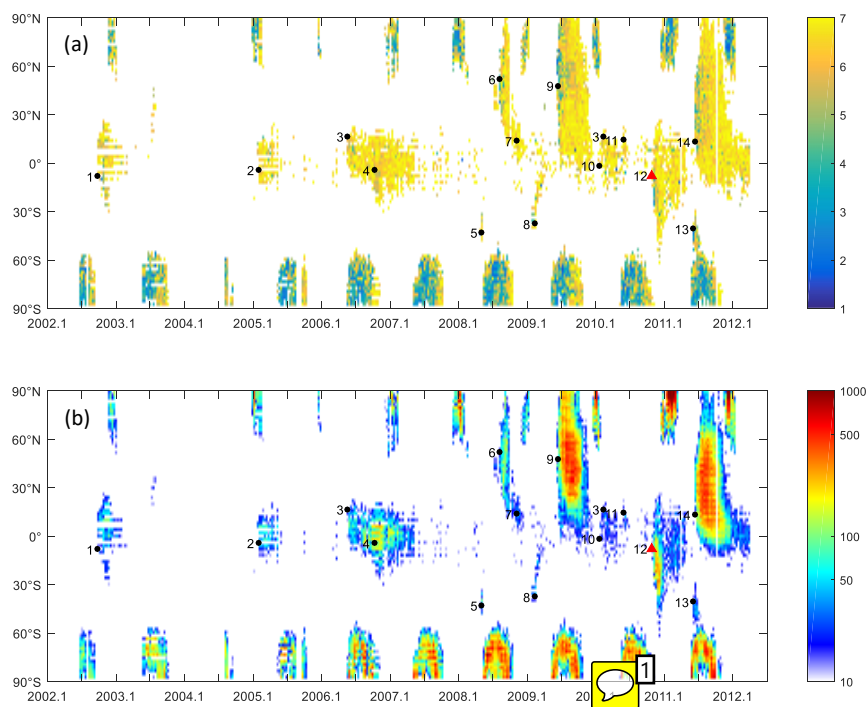



Figure 1: (a) Median value of ACI ($ACI < 7$) and (b) number of MIPAS aerosol detections between 13 and 20 km (bin size 10 days and 2° in latitude). The red triangle indicates the eruption of Mount Merapi. The black dots indicate 1 Raung, 2 Manam, 3 Soufriere Hills, 4 Tavurvur (Rabaul), 5 Chaitín, 6 Kasatochi, 7 Dalaffilla, 8 Australian bushfire, 9 Sarychev Peak, 10 Nyamuragira, 11 Pacaya, 12 Mount Merapi, 13 Puyehue-Cordón Caulle, 14 Nabro.

 Number: 1 Author: Subject: Sticky Note Date: 5/31/2018 10:04:22 PM
Explain label. Does 2010.1 mean January 2010?

 Author: Administrator Subject: Sticky Note Date: 6/3/2018 3:02:31 PM
Yes, 2010.1 means January 2010. But we realize it is not necessary to include the '.1' in the tick labels, and it brought confusion too. So we replaced the '2010.1' with '2010' in the revised manuscript.

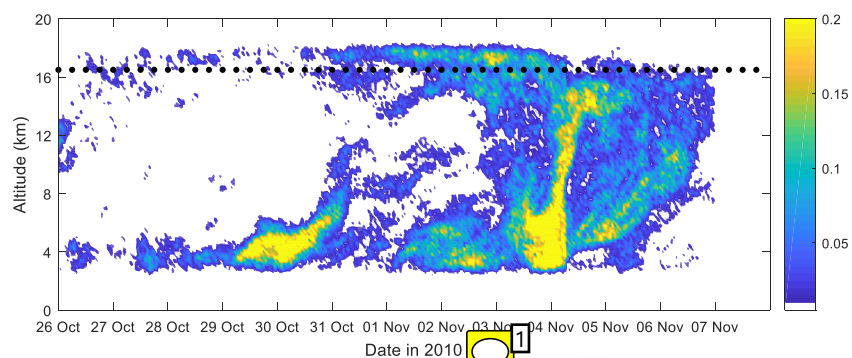


Figure 2: Merapi SO_2 emission time series (unit: $\text{kg m}^{-2} \text{s}^{-1}$) derived from AIRS measurements using a backward trajectory approach (see text for details). The emission data are binned every 1 h and 0.2 km. Gray dots denote the height of the thermal tropopause (based on the ERA–Interim reanalysis).

Number: 1 Author: Subject: Sticky Note Date: 5/31/2018 10:01:31 PM

What time of the day are the tick marks? OOO?

Author: Administrator Subject: Sticky Note Date: 6/3/2018 12:17:21 PM

The tick marks show 0 UTC on each day. We add a one sentence in the figure caption to make it clear.

Number: 2 Author: Subject: Highlight Date: 5/31/2018 10:05:33 PM

Explain these units. How does length unit work?

Author: Administrator Subject: Sticky Note Date: 8/28/2018 3:57:24 PM

In our study, we considered the SO₂ within a radius of 75 km to the location of volcano as the SO₂ injected by the volcanic eruption. So the unit kg m⁻¹ s⁻¹ can be simply converted to kg m⁻³ s⁻¹ by dividing the area. However, in the real case, the SO₂ emission is not evenly distributed in this circular area, so we prefer to use the exact longitude, latitude, altitude of the SO₂ to initialize the trajectories. In Fig. 2, we decide to group the SO₂ emission only by time and altitude instead of showing the area-averaged value.

The choice of radius is verified by carrying out sensitivity simulation experiments and comparing the SO₂ simulations with AIRS SO₂ observations, which is not shown in the paper. If the radius is too large, it will include SO₂ that was not necessarily injected by the volcanic eruption, and the simulated SO₂ plume will be too dispersive compared with observations. But if the radius is too small, the injected SO₂ will be underestimated. 75 km is considered as the best choice of radius for the Merapi case.

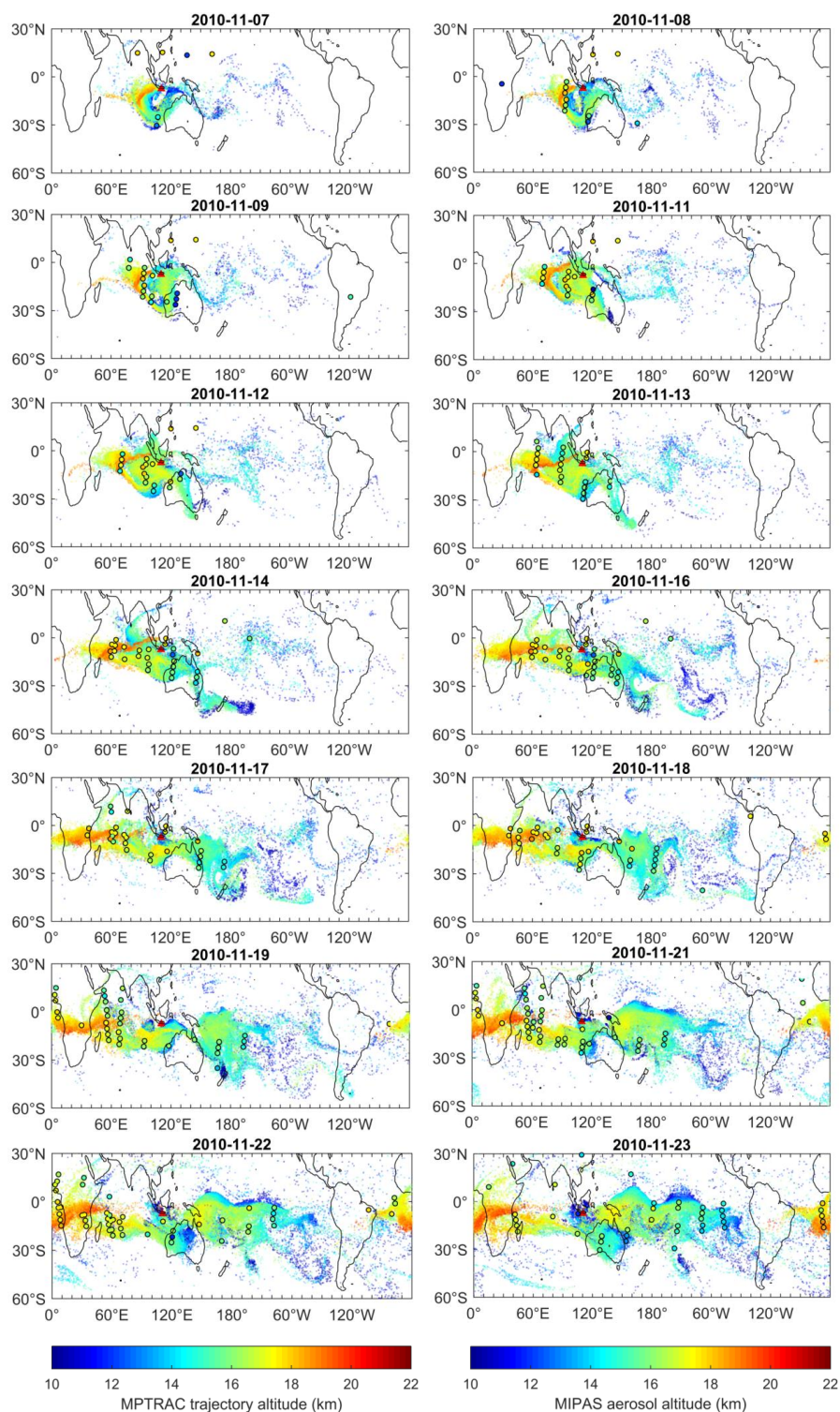


Figure 3: Distribution of the volcanic plume (showing only air parcels higher than 10 km, shading) from MPTRAC simulations (shown for 00:00UTC on selected days) and MIPAS aerosol detections ($ACI < 7$) within ± 6 h (color-filled circles). The altitudes of all

This page contains no comments



air parcels, regardless of their SO_2 values, are shown. The red triangle denotes the location of Mount Merapi.

This page contains no comments

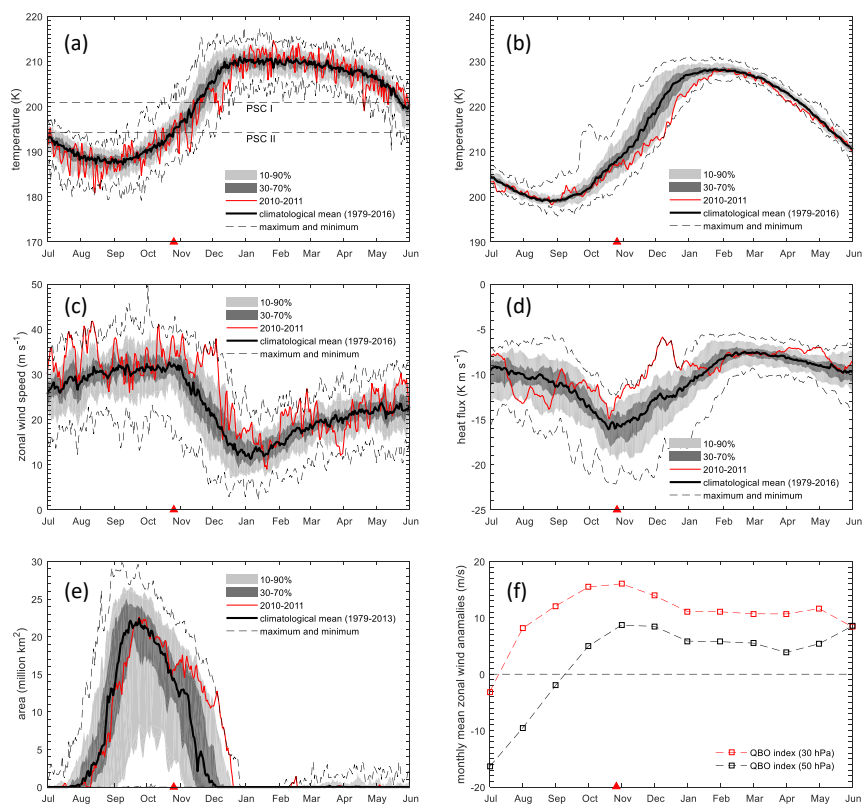







Figure 4: (a) Minimum temperature south of 50°S at 150 hPa; (b) temperature averaged over the polar cap for latitudes south of 60°S at 150 hPa; (c) zonal wind speed at 60°S at 150 hPa; (d) eddy heat flux averaged between 45°S and 75°S for the 45-day period prior to the date indicated at 150 hPa; (e) ozone hole area from July 2010 to May 2011; (f) **1**monthly mean zonal wind anomalies at 30 and 50 hPa. Temperatures for PSC existence in (a) are determined by assuming a nitric acid concentration of 6 ppbv and a water vapor concentration of 4.5 ppmv. (a)–(e) are based on **2**IERRA2 data and (f) is based on **3**CEP/NCAR reanalysis. The ozone hole area in (e) is determined from **4**MI ozone satellite measurements. The red triangles indicate the time of the Merapi eruption.


 Number: 1 Author: Subject: Highlight Date: 5/31/2018 10:18:02 PM
Where?


 Author: Administrator Subject: Sticky Note Date: 6/3/2018 2:51:26 PM
fixed.


 Number: 2 Author: Subject: Highlight Date: 5/31/2018 10:18:22 PM
reference?

 Author: Administrator Subject: Sticky Note Date: 6/3/2018 2:51:32 PM
fixed

 Number: 3 Author: Subject: Highlight Date: 5/31/2018 10:18:29 PM
reference?

 Author: Administrator Subject: Sticky Note Date: 6/3/2018 2:51:37 PM
fixed

 Number: 4 Author: Subject: Highlight Date: 5/31/2018 10:18:41 PM
reference?

 Author: Administrator Subject: Sticky Note Date: 6/3/2018 2:51:44 PM
fixed

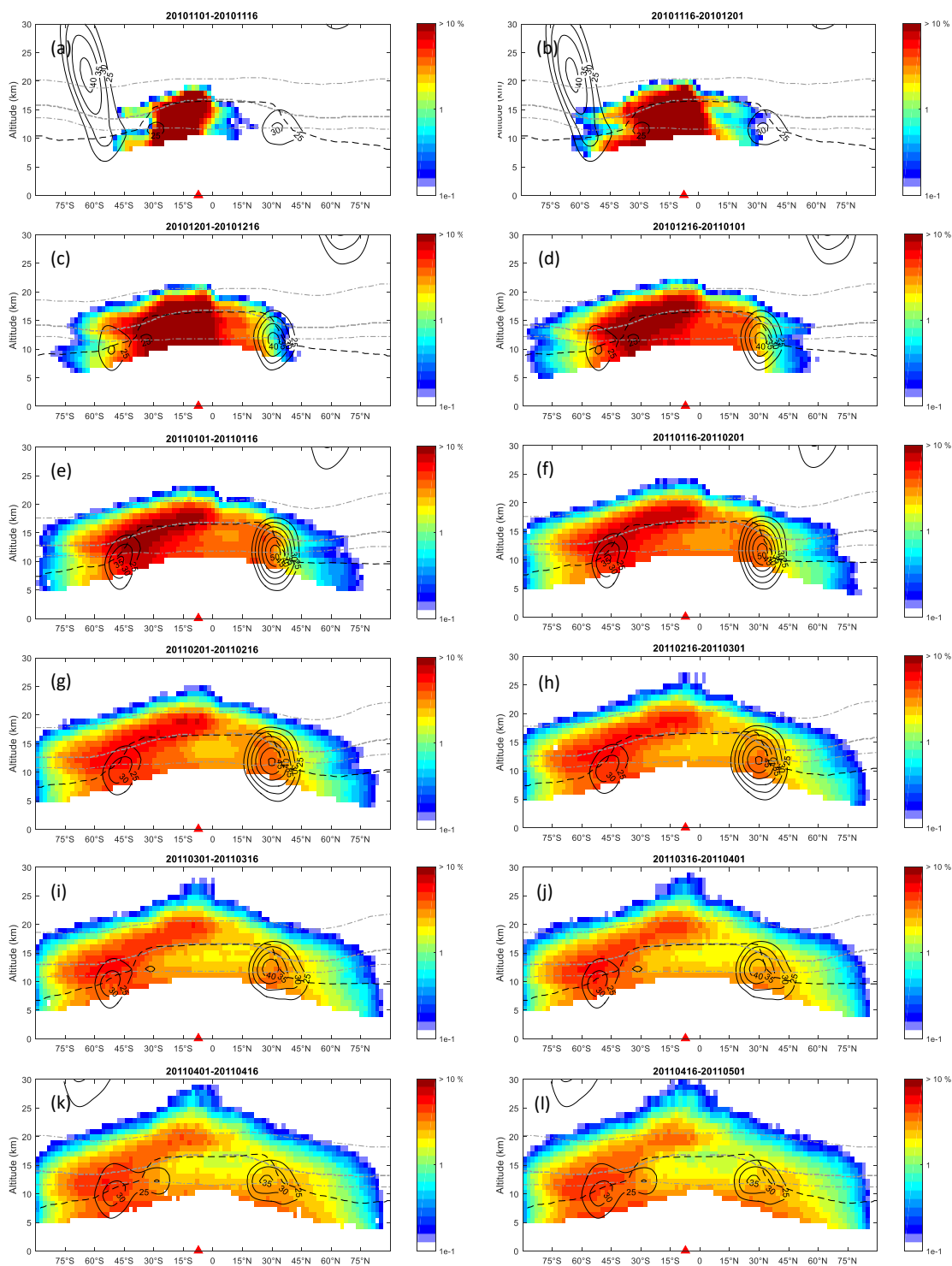


Figure 5: Percentage (%) of air parcels in proportion to the total number of air parcels from MPTRAC simulations, overlapped with monthly mean zonal winds (black contours), the thermal tropopause (black dashed line), the 380 K potential temperature isoline (thick gray dashed line) and 350 and 480 K potential temperature isolines (thin gray dashed lines). Results

This page contains no comments



are binned every 2° in latitude and 1 km in altitude. The red triangle denotes the latitude of the Merapi. Please see title of each figure for the time period covered.

This page contains no comments

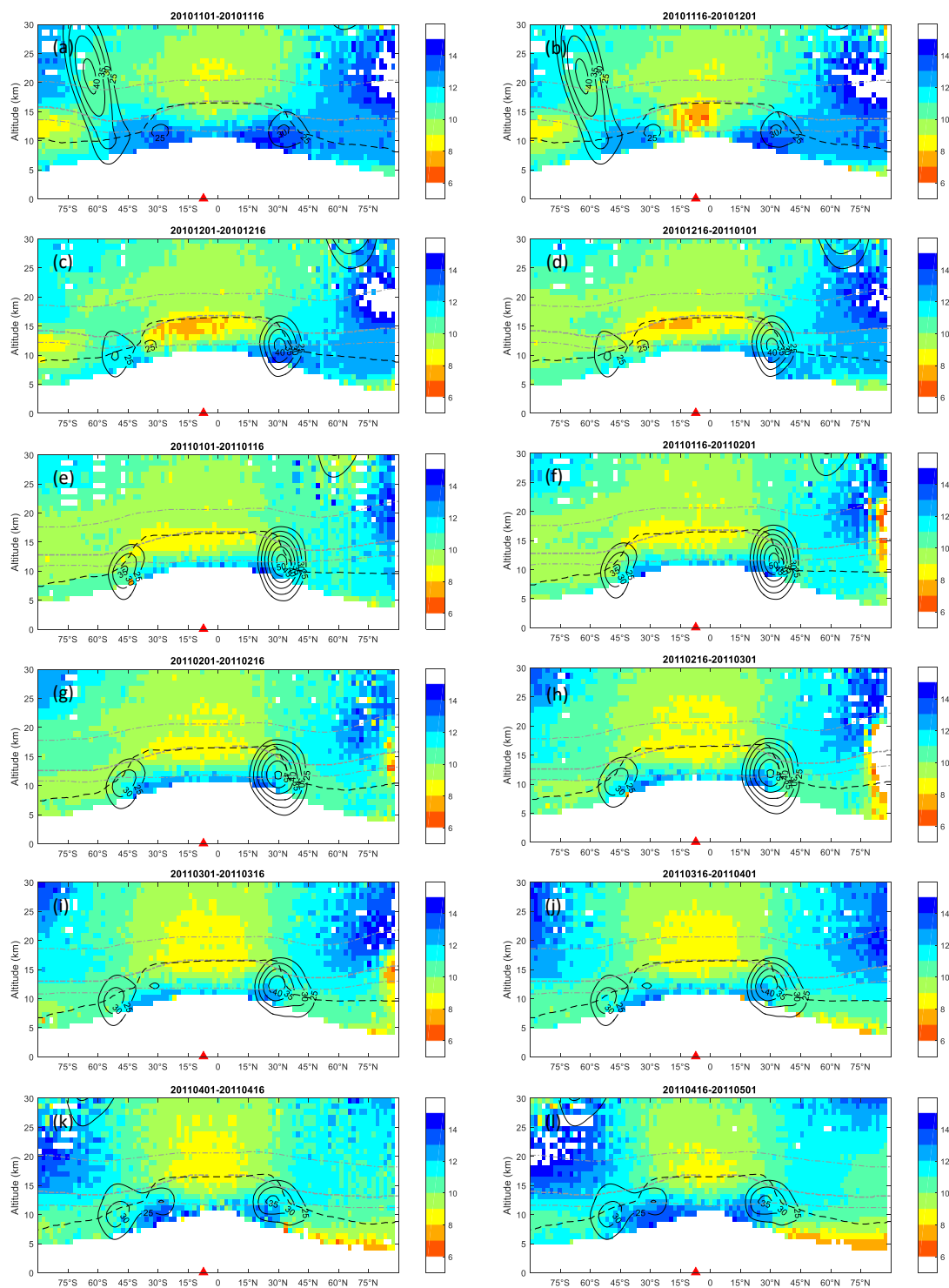


Figure 6: Median value of ACI of MIPAS aerosol detections (ice clouds filtered out), overlapped with monthly mean zonal winds (black contours), the thermal tropopause (black dashed line), the 380 K potential temperature isoline (thick gray dashed line) and 350 and 480 K potential temperature isolines (thin gray dashed lines). Results are binned

This page contains no comments



every 2° in latitude and 1 km in altitude. Only median ACI values of 5–15 are shown. The red triangle denotes the latitude of the Merapi. Please see title of each figure for the time period covered.

This page contains no comments

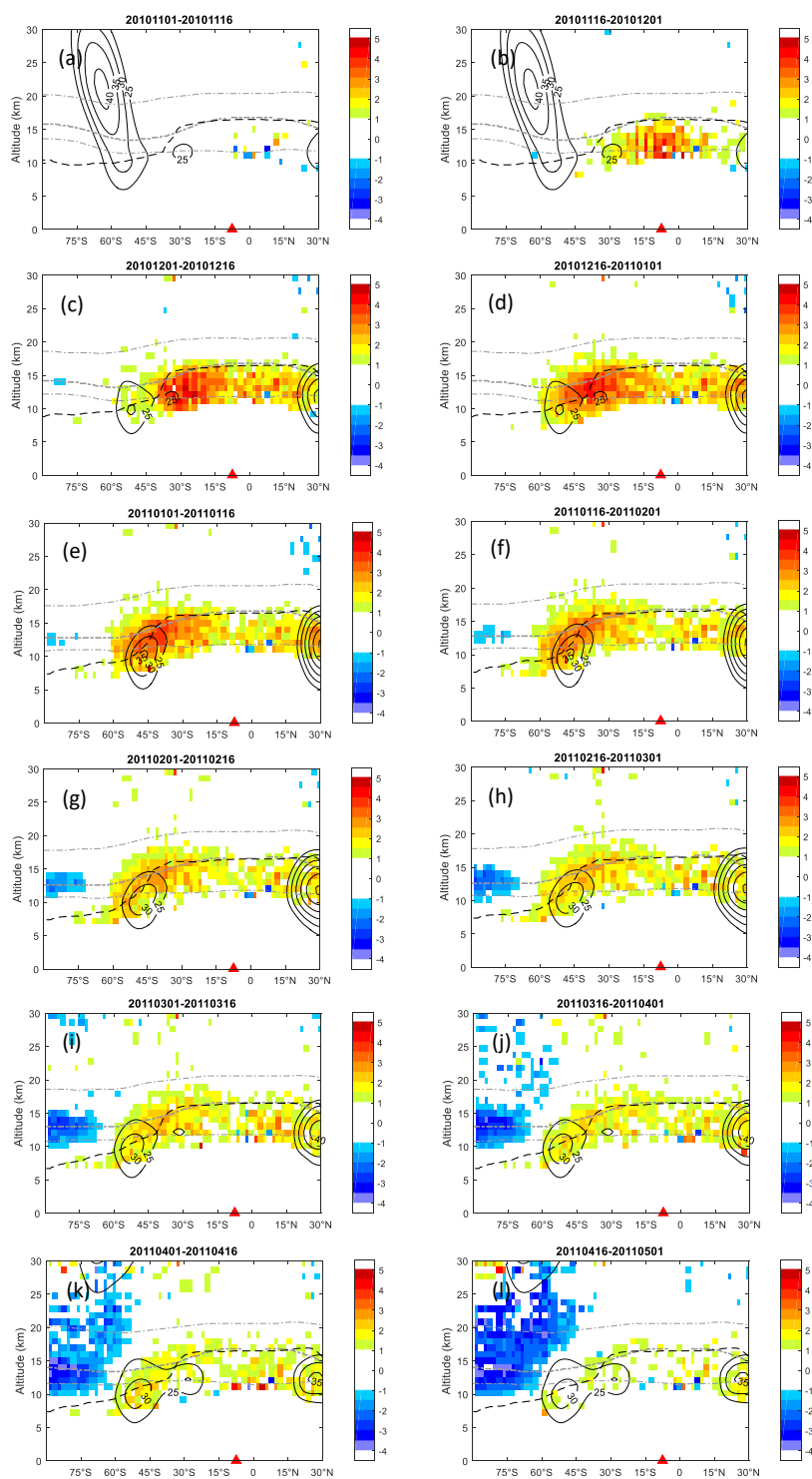




Figure 7: **Change of aerosol load** after the eruption of Merapi in 2010, overlapped with monthly mean zonal winds (black contours), the thermal tropopause (black dashed line), the 380 K potential temperature isotherm (thick gray dashed line) and 350 and 480 K potential temperature isotherms (thin gray dashed lines). Results are binned every 2° in

 Number: 1 Author: Subject: Highlight Date: 5/31/2018 10:34:38 PM
What are the units? Are negative a higher load?

 Author: Administrator Subject: Sticky Note Date: 8/28/2018 4:01:31 PM
It is explained in the main texts that the ACI is a unitless value. We edited the explanation to make it clearer and repeated the explanation in the figure caption in the revised manuscript. Please also pay attention that in the revised manuscript, we choose a volcanically quiescent year as the 'reference state' and regenerate this figure. Now is the new Fig. 6 in the revised manuscript.



latitude and 1 km in altitude. The red triangle denotes the latitude of the Merapi. Please see title of each figure for the time period covered.

This page contains no comments

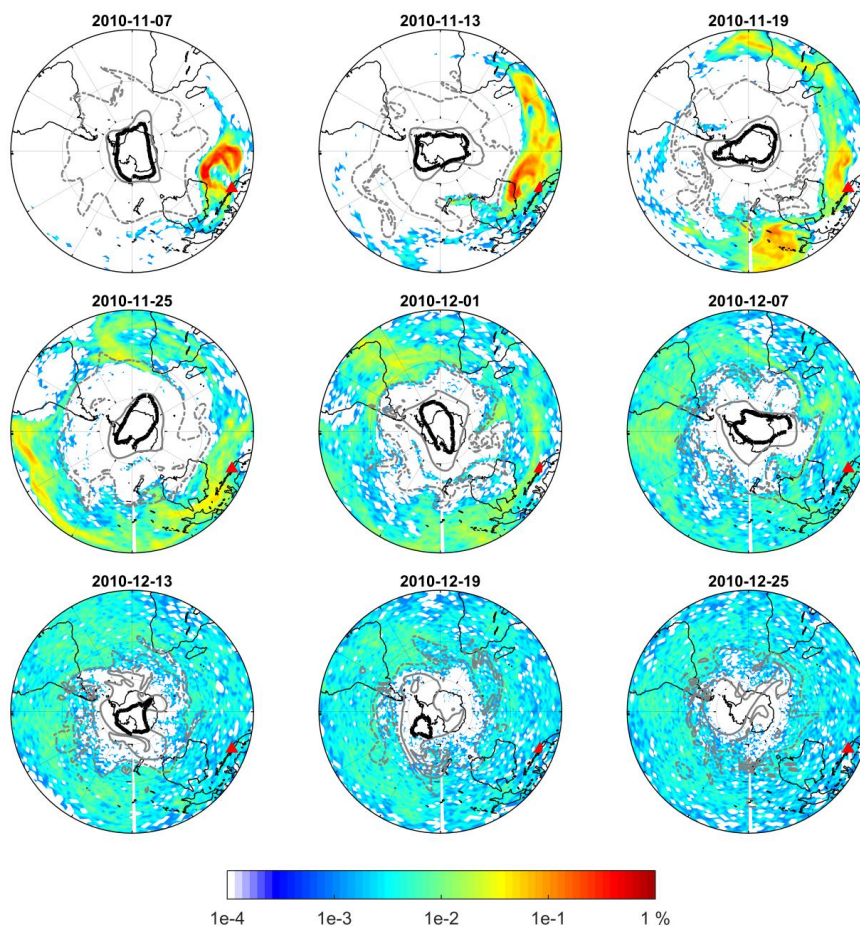





Figure 8: Percentage (%) of air parcels between the isentropic surfaces of 350 and 480 K in proportion to the total number of air parcels initialized in the Lagrangian transport simulation, at 12:00 UTC on selected dates. Results are binned every 2° in longitude and 1° in latitude. The black contour indicates OMI daily mean ozone column density of 20 DU . 2 V contours marked with gray dashed and solid lines show transport boundaries on the 350 and 480 K isentropic surfaces respectively (Kunz et al., 2015). The red triangle denotes the location of Mount Merapi

 Number: 1 Author: Subject: Highlight Date: 5/31/2018 10:41:02 PM

Is it higher or lower inside the contour?

 Author: Administrator Subject: Sticky Note Date: 6/3/2018 12:44:37 PM

220 DU contour is the boundary of the Antarctic ozone hole. The ozone column density is lower inside of the contour than outside of the contour.

 Number: 2 Author: Subject: Highlight Date: 5/31/2018 10:40:05 PM

explain the units, and why these units correspond to transport boundaries.

 Author: Administrator Subject: Sticky Note Date: 6/3/2018 12:47:11 PM

It is described in Sect. 3.4. We explain it with further details in the revised manuscript.

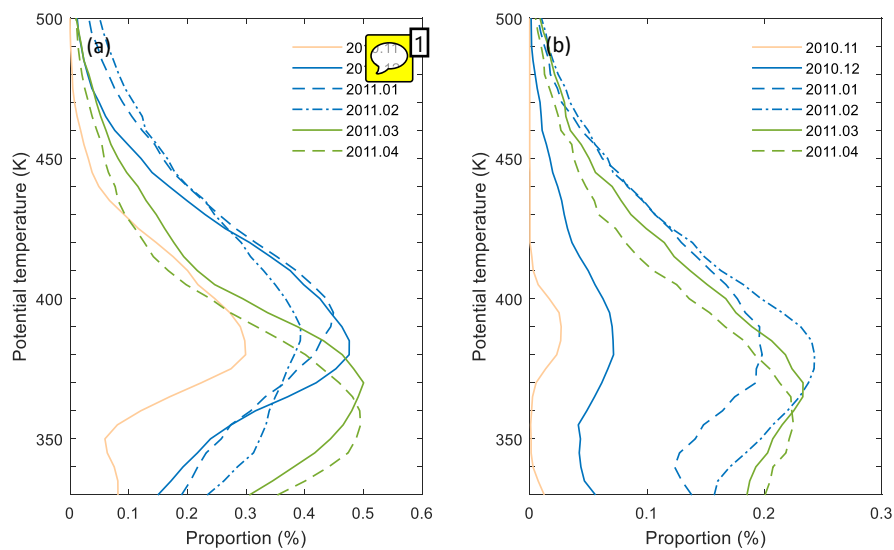



Figure 9: (a) Proportion (%) of the air parcels poleward of the PV-based transport boundaries at the end of each month; (b) proportion (%) of the air parcels south of 60°S.

 Number: 1 Author: Subject: Sticky Note Date: 5/31/2018 10:42:15 PM

What does this notation mean?

 Author: Administrator Subject: Sticky Note Date: 6/3/2018 1:12:07 PM

It indicates the year and month. For example, 2010.11 indicates November 2011. To avoid the ambiguity, we replace it with Nov 2011 in the revised paper.

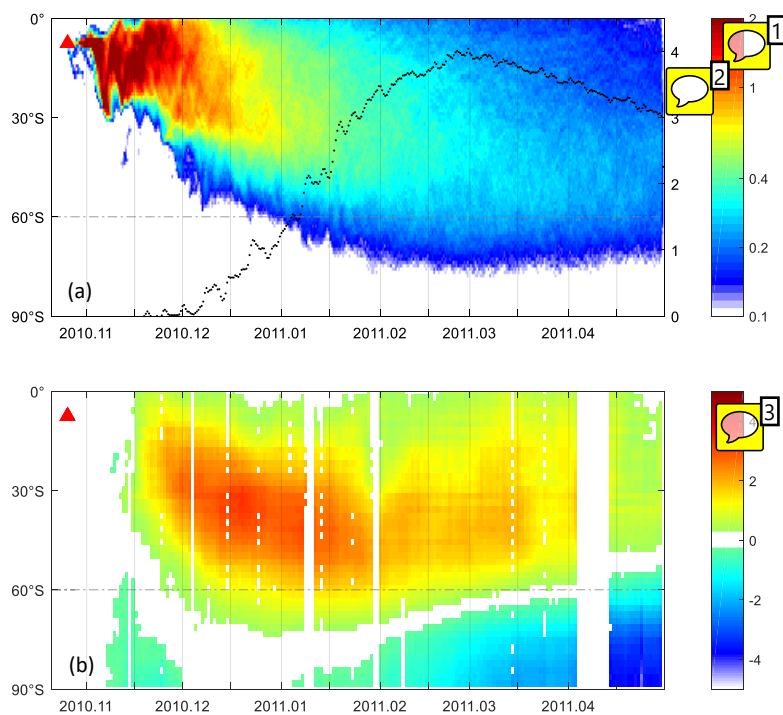






Figure 10: (a) Percentage (%) of air parcels between 350 and 480 K from MPTRAC simulations (shading, only percentages larger than 0.1% are shown; bin size: 12h and 1° in latitude), overlapped with proportion (%) of air parcels south of 60°S (black dots); (b) Change of measured aerosol load between 350 and 480 K. **positive/negative values indicate increase/decrease** of aerosol (bin size: 24h and 1° in latitude). The red triangle denotes the time and latitude of the Merapi eruption


 Number: 1 Author: Subject: Sticky Note Date: 5/31/2018 10:46:31 PM
color scale needs label of variable and units.


 Author: Administrator Subject: Sticky Note Date: 6/2/2018 5:53:27 PM
fixed

 Number: 2 Author: Subject: Sticky Note Date: 5/31/2018 10:46:07 PM
axis needs label of variable and units.

 Author: Administrator Subject: Sticky Note Date: 6/2/2018 5:56:00 PM
fixed

 Number: 3 Author: Subject: Sticky Note Date: 5/31/2018 10:48:52 PM
color scale needs label of variable and units.

 Author: Administrator Subject: Sticky Note Date: 6/2/2018 5:56:06 PM
fixed

 Number: 4 Author: Subject: Highlight Date: 6/2/2018 5:36:42 PM
DON'T USE THIS CONFUSING CONSTRUCTION. WRITE IT OUT: Positive values indicate increase and negative values indicate decrease

 Author: Administrator Subject: Sticky Note Date: 6/2/2018 5:36:19 PM
fixed

1 Long-range transport of volcanic aerosol from the 2010 Merapi 2 tropical eruption to Antarctica

3 Xue Wu^{1,2}, Sabine Griessbach¹, Lars Hoffmann¹

4 ¹Jülich Supercomputing Centre, Forschungszentrum Jülich, Jülich, Germany

5 ²Key Laboratory of Middle Atmosphere and Global Environment Observation, Institute of Atmospheric
6 Physics, Chinese Academy of Sciences, Beijing, China

7 *Correspondence to:* Xue Wu (xu.wu@fz-juelich.de)

8 Abstract

9 Volcanic sulfate aerosol is an important source of sulfur for Antarctica where other local sources of
10 sulfur are rare. Mid- and high latitude volcanic eruptions can directly influence the aerosol budget of the
11 polar stratosphere. However, tropical eruptions can also enhance polar aerosol load following
12 long-range transport. In the present work, we analyze the volcanic plume of a tropical eruption, Mount
13 Merapi in October 2010, and investigate the transport pathway of the volcanic aerosol from the tropical
14 tropopause layer (TTL) to the lower stratosphere over Antarctica. We use the Lagrangian particle
15 dispersion model Massive-Parallel Trajectory Calculations (MPTRAC) and Atmospheric Infrared
16 Sounder (AIRS) SO₂ measurements to reconstruct the altitude-resolved SO₂ injection time series during
17 the explosive eruption period and simulate the transport of the volcanic plume using the MPTRAC
18 model. AIRS SO₂ and aerosol measurements, the aerosol-cloud-index values provided by Michelson
19 Interferometer for Passive Atmospheric Sounding (MIPAS) are used to verify and complement the
20 simulations. We investigate the pathway and transport efficiency of the volcanic aerosol from the
21 tropical tropopause layer (TTL) to the lower stratosphere over Antarctica. We first estimated the time-
22 and height-resolved SO₂ injection time series over Mount Merapi during the explosive eruption using
23 the AIRS SO₂ observations and a backward trajectory approach. Then the SO₂ injections were are
24 tracked for up to 6 months using the MPTRAC model. The Lagrangian transport simulation of the
25 volcanic plume iswas compared withto MIPAS aerosol measurements and showsed good agreement.
26 Both of the simulations and the observations presented in this study suggest that aerosols of the volcanic
27 plume volcanic plumes from the Merapi eruption were transported to the south of 60 °S one month after
28 the eruption and even further to Antarctica in the following months. This relatively fast meridional
29 transport of volcanic aerosol was mainly driven by quasi-horizontal mixing from the TTL to the
30 extratropical lower stratosphere and the most of the quasi-horizontal mixing occurred between the
31 isentropic surfaces of 360 to 430 K., which was facilitated by the weakening of the subtropical jet

32 ~~during the seasonal transition from austral spring to summer and linked to the westerly phase of the~~
33 ~~quasi-biennial oscillation (QBO).~~ When the plume went to Southern Hemisphere high latitudes, the
34 polar vortex was displaced from the ~~south pole~~South Pole, so that the volcanic plume was carried to the
35 ~~south pole~~South Pole without penetrating the polar vortex. ~~Based on the model results, the most~~
36 ~~efficient pathway for the quasi-horizontal mixing was in between the isentropic surfaces of 360 and 430~~
37 ~~K.~~ Although only 4% of the ~~sulfur injected by the Merapi eruption~~initial SO₂ load was transported into
38 the lower stratosphere south of 60 °S, the Merapi eruption contributed up to 8800 tons of sulfur to the
39 Antarctic lower stratosphere. This indicates that the long-range transport under favorable
40 meteorological conditions enables a moderate tropical volcanic eruptions to be an important remote
41 source of sulfur for the Antarctic stratosphere.

42 **1 Introduction**

43 Over the past two decades, multiple volcanic eruptions injected sulfur into the upper troposphere and
44 lower stratosphere, which has been the dominant source of the stratospheric sulfate aerosol load
45 (Vernier et al., 2011), preventing the background level from other sources ever being seen (Solomon et
46 al., 2011). Stratospheric sulfate aerosol mainly reflects solar radiation and absorbs infrared radiation,
47 causing cooling of the troposphere and heating of the stratosphere. ~~It contributes to the largest~~
48 ~~uncertainties to estimates and interpretations of the Earth's changing energy budget (Boucher et al.,~~
49 ~~2013).~~~~by modulating the stratospheric and tropospheric temperature it has an impact on stratospheric~~
50 ~~dynamics, e. g. it can lead to dramatic phase changes of the quasi-biennial oscillation (Aquila et al.,~~
51 ~~2014) and alter the spatiotemporal characteristics of the El Niño–Southern Oscillation (ENSO) on both~~
52 ~~short (few years) and long (decades) timescales (Pausata et al., 2015).~~Stratospheric sulfate aerosol also
53 has an impact on chemical processes in the lower stratosphere (Jäger and Wege, 1990; Solomon et al.,
54 1993), in particular on polar ozone depletion (e.g. McCormick et al., 1982; Solomon et al., 1986, 1999,
55 2016; Portmann et al., 1996; Tilmes et al., 2008; Drdla and Müller, 2012; ~~Solomon et al., 2016~~). The
56 presence of H₂SO₄ in the polar stratosphere in combination with cold temperatures facilitates the
57 formation of polar stratospheric clouds (PSCs), which increase heterogeneous ozone depletion
58 chemistry (Solomon et al., 1999; Zuev et al., 2015). Recent healing of Antarctic ozone depletion was
59 constantly disturbed by moderate volcanic eruptions (Solomon et al., 2016). Mid- and high latitude
60 explosive volcanic eruptions may directly influence the polar stratosphere and may have an effect on
61 ozone depletion in the next austral spring. For example, the aerosol plume from the Calbuco eruption in

62 | 2015, including various volcanic gases, penetrated the polar vortex and caused an Antarctic ozone hole
63 | with the largest daily averaged size on record in October 2015 (Solomon et al., 2016; Ivy et al., 2017;
64 | Stone et al., 2017).

65 | Usually, Antarctica is relatively free of local aerosol sources, but ~~aerosols~~aerosol from low latitudes can
66 | reach Antarctica through long-range transport (Sand et al., 2017). ~~Some~~ Most of the sulfate found in ~~the~~
67 | ice cores can be attributed to volcanic eruptions (Mazzera et al., 2001; Gao et al., 2007; Sigl et al., 2015).
68 | Measurements of enhanced aerosol in the lower Antarctic stratosphere right above the tropopause were
69 | made in October/November 1983, 1984 and 1985. These enhanced aerosol number concentrations were
70 | attributed to aerosol transported to Antarctica from the eruption of the tropical volcano El Chichón
71 | ~~Chichon~~ in 1982 (Hofman and Rosen, 1985; Hofmann et al., 1988). ~~Tropical volcanic eruptions can also~~
72 | ~~enhance polar aerosols by long range transport.~~ Model results indicated that numerous moderate
73 | eruptions affected ozone distributions over Antarctica, including the Merapi tropical eruption in October
74 | 2010 (Solomon et al., 2016). However, due to the limit of spatial and temporal resolution of satellite
75 | data and in-situ observations, it is difficult to investigate transport process as well as the influence of the
76 | location of the eruption, the plume height and the background meteorological conditions. Thus the
77 | transport mechanism is not well represented in present global climate models and the uncertainties of
78 | the modeled AOD in polar regions are large (Sand et al., 2017).

79 | ~~The~~ Mount Merapi (7.5 °S, 110.4 °E, elevation: 2930 m) is an active stratovolcano located in Central
80 | Java, Indonesia. Merapi has a long record of eruptive activities. The most recent large eruption with a
81 | volcanic explosivity index (~~VEI~~) of 4 occurred between 26 October and 7 November 2010 (Pallister et
82 | al., 2013), with SO₂ emission rates being a few orders of magnitude higher than previous eruptions.
83 | Following the Merapi eruption in 2010, evidence of poleward transport of sulfate aerosol towards the
84 | Southern Hemisphere high latitudes was found in time series of aerosol measurements by the Michelson
85 | Interferometer for Passive Atmospheric Sounding (MIPAS) (Günther et al., 2018) and Cloud-Aerosol
86 | Lidar with Orthogonal Polarization (CALIOP) (Khaykin et al., 2017; Friberg et al., 2018) .

87 | There are three main ways for transport out of the tropical tropopause layer (TTL): the deep and shallow
88 | branches of the Brewer-Dobson circulation (BDC) and horizontal mixing (Vogel et al., 2011). There is
89 | considerable year-to-year seasonal variability in the amount of irreversible transport from the tropics to
90 | high latitudes, which is related to the phase of the quasi-biennial oscillation (QBO) and the state of the
91 | polar vortex (Olsen et al., 2010). The BDC plays a large role in determining the distributions of many
92 | constituents in the extratropical lower stratosphere. The faster quasi-horizontal transport between the
93 | tropics and polar regions also significantly contributes to determining these distributions. The efficiency

94 of transporting constituents quasi-horizontally depends on wave breaking patterns and varies with the
95 time of the year ([Toohey et al., 2011](#)~~[Kravitz and Robock, 2011](#)~~; Wu et al., 2017). Better knowledge of
96 the transport pathways and an accurate representation of volcanic sulfur injections into the upper
97 troposphere and lower stratosphere (UTLS) are key elements for estimating the global stratospheric
98 aerosol budget, the cooling effects and the ozone loss linked to volcanic activity.

99 The aim of the present study is to— [reveal the transport process and the influence of meteorological](#)
100 [conditions by combining satellite observations with model simulations in a case study.](#) We investigate
101 the quasi-horizontal transport by tracing the volcanic plume of the Merapi eruption from the tropics to
102 Antarctica and quantifying its contribution to the sulfur load in the Antarctic lower stratosphere. In Sect.
103 2, the new Atmospheric Infrared Sounder (AIRS) SO₂ measurements ([Hoffmann et al., 2014](#)), the
104 MIPAS aerosol measurements ([Griessbach et al., 2016](#)) and the method for reconstructing the SO₂
105 injection time series of the Merapi eruption are introduced. In Sect. 3 the results are presented: first, the
106 reconstructed time series of the Merapi eruption is discussed; second, the dispersion of the Merapi
107 plume is investigated using long Lagrangian forward trajectories initialized with the reconstructed SO₂
108 time series; third, the simulation results are compared with MIPAS aerosol measurements and the plume
109 dispersion is investigated using MIPAS aerosol detections. In Sect.4 the results are discussed and the
110 conclusions are given in Sect. 5.

111 **2 Satellite data, model and method**

112 **2.1 MIPAS ~~instrument and~~ aerosol measurements**

113 MIPAS ([Fischer et al., 2008](#)) is an infrared limb emission spectrometer aboard the European Space
114 Agency's (ESA's) Envisat, which provided nearly 10 years of measurements from July 2002 to April
115 2012. MIPAS spectral measurements cover the wavelength range from 4.15 to 14.6 microns. The
116 vertical coverage of MIPAS nominal measurement mode during the optimized resolution phase from
117 January 2005 to April 2012 was 7–72 km. The field of view of MIPAS was about 3 km×30 km
118 (vertically×horizontally) at the tangent point. The extent of the measurement volume along the line of
119 sight was about 300 km, and the horizontal distance between two adjacent limb scans was about 500 km.

120 On each day, ~14 orbits with ~90 profiles per orbit were measured. [From January 2005 to April 2012,](#)
121 [the vertical sampling grid spacing between the tangent altitudes was 1.5 km in the UTLS and 3 km at](#)
122 [altitudes above](#)~~The vertical sampling was 1.5 km in the UTLS and 3 km above the UTLS.~~ In 2010 and
123 2011, MIPAS measured for 4 days in nominal mode followed alternately by one day in middle

124 atmosphere mode or upper atmosphere mode. In this study, we focussed on measurements in the
125 nominal mode.

126 For the aerosol detections, we used the MIPAS altitude-resolved aerosol-cloud-index (ACI) as
127 introduced by Griessbach et al. (2016) to compare with the MPTRAC-model simulations and to analyze
128 the poleward transport of the Merapi volcanic plume.

129 ACI is the maximum value of the cloud index (CI) and aerosol index (AI):

$$ACI = \max(CI; AI), \quad (1)$$

130 The CI is an established method to detect clouds and aerosol with MIPAS. The CI is the ratio between
131 the mean radiances around the 792 cm⁻¹, where a CO₂ line is located and the atmospheric window
132 region around 833 cm⁻¹ (Spang et al., 2001):

$$CI = \frac{\bar{I}_1([788.25, 796.25 \text{ cm}^{-1}])}{\bar{I}_2([832.31, 834.37 \text{ cm}^{-1}])}, \quad (2)$$

133 where \bar{I}_1 and \bar{I}_2 are the mean radiances of each window. The AI is defined as the ratio between the mean
134 radiance around the 792 cm⁻¹ CO₂ band and the atmospheric window region between 960 and 961 cm⁻¹:

$$AI = \frac{\bar{I}_1([788.25, 796.25 \text{ cm}^{-1}])}{\bar{I}_3([960.00, 961.00 \text{ cm}^{-1}])}, \quad (3)$$

135 where \bar{I}_1 and \bar{I}_3 are the mean radiance of each window.

136 The ACI is a continuous unitless value. Small ACI values indicate a high cloud or aerosol particle load
137 and large values indicate a smaller cloud or aerosol particle load. For the CI, Sembhi et al. (2012)
138 defined a set of variable (latitude, altitude and season) thresholds to discriminate between clear and
139 cloudy air. The most advanced set of altitude and latitude dependent thresholds allows for the detection
140 of aerosol and clouds with infrared extinction coefficients larger than 10⁻⁵ km⁻¹. For the ACI, a
141 comparable sensitivity is achieved when using a fixed threshold value of 7 (Griessbach et al. 2016).
142 Variations in the background aerosol are also visible with larger ACI values.

143 To remove ice clouds and volcanic ash from the MIPAS aerosol measurements, we first separated the
144 data into clear air (ACI>7) and cloudy air (ACI<=7). Then we applied the ice cloud filter (Griessbach et
145 al., 2016) and the volcanic ash and mineral dust filter (Griessbach et al., 2014) to the cloudy part and
146 removed all ice or ash detections. However, since the ice and ash cloud filters are not sensitive to
147 non-ice PSCs, the resulting aerosol retrieval results still contain non-ice PSCs (supercooled ternary
148 solutions and nitric acid trihydrate). We keep the non-ice PSCs in the MIPAS retrieval results in this
149 study to show the temporal and spatial extent of the PSCs, when and where the identification of
150 volcanic is not possible.

~~Small ACI values indicate large aerosol extinction coefficients and vice versa. As ice clouds usually have extinction coefficients larger than $1 \times 10^{-4} \text{ km}^{-1}$, we applied a brightness temperature correlation method, that serves as an ice cloud filter, to all MIPAS spectra with $\text{ACI} < 7$ (Griessbach et al., 2016) to remove the ice clouds from the data set. The resulting aerosol product is be sensitive to different types of aerosol, in particular, volcanic ash, sulfate aerosol, mineral dust, as well as non-ice PSCs.~~

2.2 AIRS

AIRS (Aumann et al., 2003) is an infrared nadir sounder with across-track scanning capabilities aboard the National Aeronautics and Space Administration's (NASA's) Aqua satellite. Aqua was launched in 2002 and operates in a nearly polar Sun-synchronous orbit at about 710 km with a period of 98 min. AIRS provides nearly continuous measurement coverage with 14.5 orbits per day and with a swath width of 1780 km it covers the globe almost twice a day. The AIRS footprint size is $13.5 \text{ km} \times 13.5 \text{ km}$ at nadir and $41 \text{ km} \times 21.4 \text{ km}$ for the outermost scan angles respectively. The along-track distance between two adjacent scans is 18 km. The AIRS measurements provide good horizontal resolution and make it ideal for observing the fine filamentary structures of volcanic SO_2 plumes.

In this study, we use an optimized SO_2 index (SI, unit: K) to estimate the amount of SO_2 injected into the atmosphere by the Merapi eruption [in](#) 2010. The SI is defined as the brightness temperature differences in the $7.3 \text{ }\mu\text{m}$ SO_2 waveband.

$$\text{SI} = \text{BT} \left(1412.87 \text{ cm}^{-1} \right) - \text{BT} \left(1371.52 \text{ cm}^{-1} \right), \quad (1)$$

where BT is the brightness temperature measured at wavenumber ν . This SI is more sensitive to low concentrations and performs better on suppressing background interfering signals than the SI provided in the AIRS operational data products. It is an improvement of the SI definition given by Hoffmann et al. (2014) by means of a better choice of the background channel (selecting 1412.87 cm^{-1} rather than 1407.2 cm^{-1}). The SI increases with increasing SO_2 column density and it is most sensitive to SO_2 at altitudes above 3-5 km. SO_2 injections into the lower troposphere are usually not detectable in the infrared spectral region because the atmosphere gets opaque due to the water vapor continuum. A detection threshold of 1 K was used in this study to identify the Merapi SO_2 injections. AIRS detected the Merapi SO_2 cloud from 3 November to 15 November 2010.

2.3 MPTRAC model and reconstruction of the volcanic SO₂ injection time series of the Merapi eruption

In this study, we use the highly scalable [Massive-Parallel Trajectory Calculations \(MPTRAC\)](#) ~~MPTRAC model~~ to investigate the volcanic eruption event. In the MPTRAC model, air parcel trajectories are calculated based on numerical integration using wind fields from global meteorological reanalyses (Hoffmann et al., 2016; Röβler et al., 2018). [The MPTRAC model can be driven by reanalyses, e.g., ERA-Interim, Modern-Era Retrospective Analysis for Research and Applications \(MERRA\) and National Centers for Environmental Prediction \(NCEP\)/National Center for Atmospheric Research \(NCAR\).](#) Hoffmann et al. (2016) showed that ERA-interim data provides the best trade-off between accuracy and computing time. So in this study, our calculations are based on [ERA-interim data](#).

Diffusion is modeled by uncorrelated Gaussian random displacements of the air parcels with zero mean and standard deviations $\sigma_x = \sqrt{D_x \Delta t}$ (horizontally) and $\sigma_z = \sqrt{D_z \Delta t}$ (vertically). D_x and D_z are the horizontal and vertical diffusivities respectively, and Δt is the time step for the trajectory calculations. For the Merapi simulation, D_x and D_z were set to $50 \text{ m}^2 \text{ s}^{-1}$ and $0 \text{ m}^2 \text{ s}^{-1}$ in the troposphere and $0 \text{ m}^2 \text{ s}^{-1}$ and $0.1 \text{ m}^2 \text{ s}^{-1}$ in the stratosphere, respectively. In addition, sub-grid scale wind fluctuations, which are particularly important for long-range simulations, are simulated by a Markov model (Stohl et al., 2005; Hoffmann et al., 2016). Loss processes of chemical species, SO₂ in our case, are simulated based on an exponential decay of the mass assigned to each air parcel. In the stratosphere, a constant half lifetime of 7 days was assumed for SO₂. Considering that the Merapi eruption occurred in the humid tropics with a high concentration of hydroxyl radical, a half lifetime of 2.5 days was assumed for the troposphere.

To estimate the time- and altitude-resolved SO₂ injections, we follow the approach of Hoffmann et al. (2016) and Wu et al. (2017) and use backward trajectories calculated with the MPTRAC model together with AIRS SO₂ measurements. Measurements from 3 to 7 November 2010 were used to estimate the SO₂ injection during the explosive eruption. Since the AIRS measurements do not provide altitude information, we established a column of air parcels at each AIRS SO₂ detection. The vertical range of the column was set to 0–25 km, covering the possible vertical dispersion range of the SO₂ plume in the first few days. The AIRS footprint size varies between 14 and 41 km, hence in the horizontal direction, we chose an average of 30 km as the full width at half maximum (~~FWHM~~) for the Gaussian scatter of the air parcels. In our simulations, a fixed total number of 100,000 air parcels was assigned to all air columns and the number of air parcels in each column was scaled linearly proportional to the SO₂ index.

209 Then backward trajectories were calculated for all air parcels, and trajectories that were at least 2 days
210 but no more than 5 days long and that passed the volcano domain were recorded as emissions of Merapi.
211 The volcano domain was defined by means of a search radius of 75 km around the location of the
212 Merapi and 0–20 km in the vertical direction, covering all possible injection heights. Sensitivity
213 experiments have been conducted to optimize these pre-assigned parameters to obtain the best
214 simulation results. Our estimates of the Merapi SO₂ injection are shown in Sect. 3.

215 Starting with the reconstructed altitude-resolved SO₂ injection time series, the transport of the Merapi
216 plume is simulated for 6 months. The trajectory calculations are driven by the ERA–Interim data (Dee
217 et al., 2011) interpolated on a 1° × 1° horizontal grid on 60 model levels with the vertical range
218 extending from the surface to 0.1 hPa. The ERA–Interim data are provided at 00, 06, 12 and 18 UTC.
219 Outputs of model simulations are given every 3 hours at 00, 03, 06, 09, 12, 15, 18 and 21 UTC. The
220 impact of different meteorological analyses on MPTRAC simulations was assessed by Hoffmann et al.
221 (2016, 2017). In both studies the ERA–Interim data showed good performance.

222 **3 Results**

223 **3.1 Meteorological background conditions in Antarctica**

224 The Merapi eruption in October 2010 occurred during the seasonal transition from austral spring to
225 summer when the polar vortex typically weakens and the ozone hole shrinks. The poleward transport
226 from the tropics to the polar region is known to be modulated by the phase of the QBO and the state of
227 the polar vortex. Just before the Merapi eruption in 2010, the QBO switched from the easterly phase to
228 the westerly phase. The westerly phase of the QBO promotes meridional transport from the tropics to
229 subtropics, especially into the winter hemisphere (O'Sullivan and Dunkerton, 1997; Shuckburgh et al.,
230 2001; Jäger, 2005). However, it also results in zonal wind acceleration at the high latitudes (Holton and
231 Tan, 1980; Watson and Gray, 2014) and a less dynamically disturbed polar vortex (Baldwin and
232 Dunkerton, 1999; Anstey and Shepherd, 2014), which will make it less possible for air parcels to
233 penetrate the polar vortex.

234 Figure 1 depicts the meteorological conditions at the polar lower stratosphere (150hPa, ~12km) after the
235 eruption. As depicted in Fig. 1, the meteorological conditions at the polar lower stratosphere (150hPa,
236 ~12km) after the eruption deviated from the climatological mean. The minimum temperature south of
237 50°S (Fig. 1a) was much lower than the climatological mean during mid-November to mid-December
238 but still higher than the low temperature necessary for the existence of PSCs. The polar mean

239 temperature in Fig. 1b, defined as the temperature averaged over latitudes south of 60 °S, stayed lower
240 than the climatological mean from November 2010 until February 2011. Corresponding to the low
241 temperatures, the average zonal wind speed at 60 °S (Fig. 1c) was significantly larger than the
242 climatological mean value from November 2010 to mid-January 2011. The eddy heat flux in Fig. 1d is
243 the product of meridional wind departures and temperature departures from the respective zonal mean
244 values. A more negative value of the eddy heat flux indicates that wave systems are propagating into the
245 stratosphere and are warming the polar region (Edmon et al., 1980; Newman and Nash, 2000). There is
246 a strong anticorrelation between temperature and the 45-day average of the eddy heat flux lagged prior
247 to the temperature. Compared with the climatological mean state, the polar vortex was more disturbed
248 during mid-July to end of August, but from mid-October to late November, the heat flux was much
249 smaller than the long-term average, which meant a reduction in dynamical disturbances. Considering
250 the temperature, the subpolar wind speed and the heat flux, the polar vortex was colder and stronger in
251 November and early December 2010 than it was at the same time in other years (see Fig. 1e). Consistent
252 with the large wind speed and low temperature, the polar vortex was stable after the Merapi eruption
253 until early December 2010. Afterwards, it shrunk abruptly and was destructed in by mid-January 2011.
254 In accordance with the strength of the polar vortex, in November and early December 2010 the ozone
255 hole area in Fig. 1f, defined as the region of ozone values below 220 Dobson Units (DU) located south
256 of 40 °S, was larger than the climatological mean. Meanwhile, the low polar mean temperature and
257 stable polar vortex resulted in a long-lasting ozone hole, which disappeared in the last week of
258 December. The polar vortex broke down by mid-January 2011 when the subpolar wind speed decreased
259 below 15 m/s (Fig. 1c).

~~260 The poleward transport from the tropics to the polar region is known to be modulated by the phase of
261 the quasi-biennial oscillation (QBO) and the state of the polar vortex itself. Fig. 4f shows that just before
262 the Merapi eruption in 2010, the QBO switched from easterly phase to westerly phase. The westerly
263 phase of the QBO promotes meridional transport from the tropics to subtropics, especially into the
264 winter hemisphere (O'Sullivan and Dunkerton, 1997; Shuckburgh et al., 2001; Jäger, 2005). However, it
265 also results in zonal wind acceleration at the high latitudes (Watson and Gray, 2014; Holton and Tan,
266 1980) and a less dynamically disturbed polar vortex (Anstey and Shepherd, 2014; Baldwin and
267 Dunkerton, 1999), which will make it less possible for air parcels to penetrate the polar vortex.~~

3.2 Merapi eruption and SO₂ injection time series

According to the chronology of the Merapi eruption that combined satellite observations from AIRS, the Infrared Atmospheric Sounding Interferometer (IASI), the Ozone Monitoring Instrument (OMI) and a limited number of Ground-based ultra-violet Differential Optical Absorption Spectroscopy (DOAS) measurements (Surono et al., 2012), the explosive eruption first occurred between 10:00 and 12:00 UTC on 26 October and this eruption generated aan ash plume that reached 12 km altitude. A period of relatively small explosive eruptions continued from 26 October to 31 October. ~~During the initial period of the dome growth (1–3 November), the level of SO₂ degassing was relatively low compared with the SO₂ degassing before 1 November.~~ On 3 November, the eruptive intensity increased again accompanied by much stronger degassing and a series of explosions. The intermittent explosive eruptions occurred during 4–5 November with the climactic eruption on 4 November, producing an ash column that reached up to 17 km altitude. From 6 November, explosive activity decreased slowly and the degassing declined.

Figure 2 shows the time- and altitude-resolved SO₂ injections of the Merapi eruption retrieved using the AIRS SO₂ index data and the backward-trajectory approach. It agrees well with the chronology of the Merapi eruption as outlined by Surono et al. (2012). SO₂ was injected into altitudes below 8 km during the initial explosive eruptions on 26–30 October. Starting from 31 October the plume reached up to 12 km. During 1–2 November the SO₂ injections into altitudes below 12 km continued but the mass was less than the mass at the initial phase. On 3 November the intensity increased again and peaked on 4 November. Before 3 November the reconstruction indicates a minor fraction of SO₂ right above the tropopause. The SO₂ above the tropopause is not reported in the study Surono et al. (2012), but is quite robust in our simulations. Further, CALIOP profiles from 27 October 2010 to 10 November 2010 show that some dust appeared at the height from about 14 to 18 km around Mount Merapi on 2, 3, 5 November 2010, and between 3 and 17 km on 6 November 2010. It could be a fraction of volcanic plume elevated by the updraft in the convection associated with the tropical storm Anggrek. The center of the tropical storm Anggrek was on the Indian ocean about 1000 km southwest of the Mount Merapi. The SO₂ mass above the tropopause is very small compared with the total SO₂ mass.

To study the long-range transport of the Merapi plume, we initialized 100,000 air parcels as the SO₂ injection time series shown in Fig. 2. A total SO₂ mass of 0.44 Tg is assigned to these air parcels as provided in Surono et al. (2012). Then the trajectories are calculated forward for 6 months. Here, we only considered the plume in the upper troposphere and stratosphere where the lifetime of both SO₂ and

299 sulfate aerosol is longer than their lifetime in the lower troposphere. Further, the SO₂ was converted into
300 sulfate aerosol within a few weeks (von Glasow et al., 2009; also confirmed by the AIRS SO₂ and
301 MIPAS aerosol data), and we assumed that the sulfate aerosol remained collocated with the SO₂ plume;
302 ~~i.e., the sedimentation of small sulfate aerosol particles was negligible for the timescale considered.~~
303 Figure 3 shows the evolution of the simulated Merapi plume and compares the plume altitudes to the
304 aerosol top altitudes measured by MIPAS between 7 and 23 November. Immediately after the eruption,
305 the majority of the plume moved towards the southwest and was entrained by the circulation of the
306 tropical storm Anggrek. After ~~the~~ Anggrek weakened and dissipated, the majority of the plume parcels
307 in the upper troposphere moved eastward and those in the lower stratosphere moved westward. In
308 general, the altitudes of the simulated plume agree with the MIPAS measurements. The remaining
309 discrepancies of air parcel altitudes being higher than the altitudes of MIPAS aerosol detections can be
310 attributed to the fact that the MIPAS tends to underestimate aerosol top cloud altitudes, which is about
311 0.9 km in case of low extinction aerosol layers and can reach down to 4.5 km in case of broken cloud
312 conditions (Höpfner et al., 2009).

313 **3.3 Lagrangian simulation and satellite observation of the transport of the Merapi plume**

314 The early plume evolution until about one month after the initial eruption is shown on the maps in Fig.
315 3 together with MIPAS measurements of volcanic aerosol (only aerosol detections with ACI<7 are
316 shown). Within about one month after the initial eruption, the plume is nearly entirely transported
317 around the globe in the tropics, moving west at altitudes of about 17 km. The lower part of the plume,
318 below about 17 km is transported south-eastward and reaches latitudes south of 30 °S by mid-November.
319 The simulated long-term transport of the Merapi plume is illustrated in Fig. 54, showing the proportion
320 of air parcels reaching a latitude-altitude bin every half a month. ~~To verify the model results, the~~
321 ~~poleward transport of aerosols as detected by MIPAS is shown in Fig. 6. For comparison, only~~
322 ~~simulation results above the minimum altitude of MIPAS aerosol detections in Fig. 6 are shown in Fig.~~
323 ~~5. In this study, we only focus on aerosol distributions in the upper troposphere and stratosphere, where~~
324 ~~sulfate aerosol has a longer lifetime and potential climate impacts.~~
325 The simulation results show that during the first month after the eruption (Fig. 45a–b), the majority of
326 the plume was transported southward roughly along the isentropic surfaces. The most significant
327 pathway is above the core of the subtropical jet in the Southern Hemisphere. However, because of the
328 transport barrier of the polar jet during austral spring, the plume was confined to the north of 60 °S. In
329 December 2010 (Fig. 45c–d), a larger fraction of the plume was transported southward above the

330 subtropical jet core and deep into the polar region south of 60°S as the polar jet broke down. ~~Until~~
331 the end of January 2011, the majority of the plume entered the mid- and high latitudes in the Southern
332 Hemisphere. Substantial quasi-horizontal poleward transport from the TTL towards the ~~extratropical~~
333 ~~lowermost stratosphere (LMS)~~LMS in Antarctica was found from November 2010 to February 2011
334 (Fig. ~~45a–h~~), approximately between 350 and 480 K (~10–20 km). In March 2011(Fig. ~~4i–j~~), the
335 proportion of the plume that went across 60°S stopped increasing and the maxima of the proportion
336 descended ~~below 380 K~~. ~~Besides this transport towards Antarctica, a slow upward transport could also~~
337 ~~be seen. The top of the simulated plume was below the 480 K isentropic surface at around 18 km in Fig.~~
338 ~~4a and then the top of the plume went up to 25 km five months later in Fig. 4j. This slow upward~~
339 ~~transport was mainly located in the tropics and can be attributed to the tropical upwelling.~~
340 ~~MIPAS aerosol detections (ACI values) are used to compare with the simulations.~~ Figure 5 displays
341 the time-latitude section of the median value of the MIPAS ACI within the vertical range of 12 and 18
342 km ~~from January 2005 to April 2012~~, covering the ~~tropical tropopause layer (TTL)~~TTL and the
343 ~~extratropical lowermost stratosphere (LMS)~~LMS. ~~Only ACI values from 4 to 8 are shown in Fig.5.~~ The
344 MIPAS data show all the key events that contributed to the aerosol load in the UTLS, i.e., moderate
345 volcanic eruptions from 2005 to 2012 and one large bushfire in 2009, as well as the subsequent
346 dispersion and change of aerosol load over time. ~~The poleward transport of aerosol from the Merapi~~
347 ~~eruption in 2010, marked by the red triangle in Fig. 5, caused the most long-lasting aerosol signals in~~
348 ~~the Southern Hemisphere mid- and high latitudes. The small ACI values in the winter months of both~~
349 ~~hemispheres are attributed to the non-ice PSCs.~~
350 ~~The poleward transport in the MPTRAC simulations was confirmed by MIPAS aerosol detections.~~
351 ~~MIPAS ACI zonal median values are shown in Fig. 6 for all MIPAS measurements after filtering out~~
352 ~~ice clouds. Small ACI values indicate a large aerosol load and large ACI values indicate clear air. As~~
353 ~~seen in Fig. 6, the locally confined aerosol plume from the Merapi eruption did not dominate the zonal~~
354 ~~median during the first half month after the eruption (Fig. 6a), but became evident between 350 and 380~~
355 ~~K around the latitude of 7.5°S by the end of November (Fig. 6b) as the plume was transported around~~
356 ~~the globe in the tropics. As shown in the MPTRAC simulations, the transport towards the northern mid-~~
357 ~~and high latitudes was suppressed by the strong subtropical jets. The transport of the volcanic plume~~
358 ~~towards Antarctica in the UTLS region was observed from December 2010 to February 2011 (Figs. 6c–~~
359 ~~h) consistent with the simulations. The MIPAS aerosol data also demonstrated the upward transport~~
360 ~~from the tropical upper troposphere to the stratosphere, which was observed after late January 2010.~~

361 The aerosol transported upward had increased the aerosol load in the tropical stratosphere reservoir
362 compared to the aerosol load before the Merapi eruption.

363 Fig. 6 verified aerosol transport from the tropics to Antarctica and upward into the tropical stratosphere.
364 However, before the eruption of Merapi, the aerosol load in the tropical stratosphere was already
365 elevated by several small and moderate size volcanic eruptions, namely the Sarychev Peak (12 Jun
366 2009), Nyamuragira (20 Jan 2010), Soufriere Hills (11 Feb 2010) and Pacaya (28 May 2010). In order
367 to infer the increase of the aerosol load due to the eruption of Merapi from the MIPAS data, we
368 calculated the median ACI in 1–4 November 2010 when there was no aerosol from the Merapi eruption,
369 to define the “background” aerosol load and then remove this “background” from the median ACI in
370 Fig. 6. The results shown in Fig.7 demonstrate the change of median ACIs in the tropics and southern
371 hemisphere corresponding to the same time period as Fig. 6 positive/negative values indicating an
372 increase/decrease of aerosol load. No significant change was observed during the first half month after
373 the eruption due to the zonal averaging degrading the aerosol signal (Fig. 7a). The largest increase first
374 appeared in the upper troposphere directly above Mount Merapi (Fig. 7b) and then moved
375 quasi horizontally southward into the UTLS region to ~40°S (Figs. 7c–f), consistent with what Figs. 5
376 and 6 showed. A relatively small but still significant increase of aerosol south of 60°S in the tropopause
377 region was found from January 2011 (Fig. 7e) and it lasted until mid-April 2011 (Fig. 7j). Six months
378 after the eruption, the aerosol levels were still slightly elevated in the tropical upper troposphere above
379 350 K. To show the change of aerosol load in the Southern Hemisphere due to the Merapi eruption, we
380 first removed the seasonal cycle from the MIPAS aerosol data. Therefore, we selected a time period
381 from November 2007 to March 2008 with no major SO₂ emission in the Southern Hemisphere UTLS
382 (as shown in Fig. 5) as a “reference state”. We calculated the biweekly median ACI between November
383 2010 and March 2011 and subtracted it from the biweekly ACI median of the “reference state”. The
384 results are shown in Fig. 6. Since in the MIPAS retrievals, small ACI values represent large aerosol
385 extinction coefficients and large ACI values represent small aerosol extinction coefficients, in Fig. 6 the
386 positive values indicate an increase of the aerosol load and negative values indicate a decrease of the
387 aerosol load. Reference time periods from November 2003 to March 2004 and November 2005 to
388 March 2006 were also tested and they all showed qualitatively comparable results.

389 In the first half of November, the zonal median (Fig. 6a) does not show a signal of the Merapi eruption,
390 because during the initial time period, the plume was confined to longitudes around the volcano (see Fig.
391 3), and the MIPAS tracks did not always sample the maximum concentration, so the median ACI values
392 are large (low concentration or clear air). In the second half of November, the plume was transported

zonally around the globe, and hence the largest aerosol increase appeared in the upper troposphere at the latitude of the Mount Merapi (Fig. 6b) and then moved quasi-horizontally southward into the UTLS region at ~30–40 °S (Figs. 6c–d), confirming the simulation result in Fig. 4c–d. The increase of the aerosol load south of 60 °S started to become prominent after December 2010, and the poleward movement is most obvious above the 350 K isentropic surface (Figs. 6e–h). The observations confirm the temporal and spatial characteristics of the poleward movement of the aerosol in the simulation in Fig. 4. Later in March 2011, the enhanced aerosol load in the tropics phased out and the aerosol load maxima descended to around the 350 K isentropic surface.

However, the background aerosol level in the tropical upper troposphere and stratosphere is constantly disturbed by tropical and extratropical volcanic eruptions. The reference time period we chose (November 2007 to March 2008) is relatively free of large aerosol sources in the Southern Hemisphere, but the aerosol load in the tropical stratosphere is already elevated by previous volcanic eruptions, e.g., Soufriere Hills (May 2006), Tavurvur (October 2006), Piton de la Fournaise (April 2007), Jebel at Tair (September 2007). So the change of the aerosol load in Fig.6 underestimates the increase of aerosol load in the tropical stratosphere after the Merapi eruption. The slow upward transport in the tropics shown in Fig. 4 is about 7 km in five months. It is not visible in Fig. 6, but time series of the MIPAS measurements in the tropical stratosphere reveals a similar upward transport trend (see Fig. A1 in the appendix).

3.4 Quasi-horizontal transport from the tropics to Antarctica

~~As the results of the Lagrangian transport simulations with the MPTRAC model were comparable to the MIPAS observations (Sect. 3.3), it was possible not only to demonstrate the transport pathways but also to estimate the efficiency of the transport.~~ The MPTRAC simulations and the MIPAS measurements show the transport ~~in~~ the “surf zone” that reaches from the subtropics to high latitudes (Holton et al., 1995), where air masses are affected by both fast meridional transport and the slow BDC. ~~The reconstructed emission time series in Fig. 2 and the MIPAS aerosol measurements in Figs. 3 and 6 show that the volcanic plume was injected into the TTL. Hence, the main transport pathway towards Antarctica is the quasi-horizontal mixing in the lower extratropical stratosphere between 350 and 480 K (see Fig. 4 and Fig. 6).~~ Figure 78 illustrates how the volcanic plume between 350 and 480 K approached Antarctica over time. ~~Kunz et al. (2015) derived a climatology of potential vorticity (PV) streamer boundaries on isentropic surfaces between 320 and 500K using ERA-Interim reanalyses for the time~~

424 period from 1979 to 2011. This boundary is derived from the maximum product of the meridional PV
425 gradient and zonal wind speed on isentropic surfaces, which identifies a PV contour that best represents
426 the dynamical discontinuity on each isentropic surface. It can be used as an isentropic transport barrier
427 and to determine the isentropic cross-barrier transport related to Rossby wave breaking (Haynes and
428 Shuckburgh, 2000; Kunz et al., 2011a,b). In Fig. 7, gray dashed and solid lines mark PV boundaries on
429 the 350 K isentropic surface. These dynamically relevant PV contours represent horizontal transport
430 barriers for air masses on the respective isentropic surface. On isentropic surfaces below 380 K, the PV
431 boundaries represent the dynamical discontinuity near the core of the subtropical jet stream, and thus
432 represent a transport barrier between the tropics and midlatitudes (Haynes and Shuckburgh, 2000; Kunz
433 et al., 2011a,b). Isentropic transport of air masses across these boundaries indicates exchange between
434 the tropics and extratropics due to Rossby wave breaking. On isentropic surfaces above 400 K, PV
435 boundaries represent a transport barrier in the lower stratosphere, in particular, due to the polar vortices
436 in winter (Kunz et al., 2015). For comparison, we also show the 220 DU contour lines of ozone column
437 density (black isolines in Fig. 78), obtained from OMI on satellite Aura, indicating the location
438 boundary and size of the ozone hole. The PV boundary on 480 K is in most cases collocated with the
439 area of the ozone hole, showing that both quantities provide a consistent representation of the area of
440 the polar vortex.

441 The Merapi volcanic plume first reached the 350 K transport barrier on the 350 K isentropic surface in
442 mid-November and went close to the 480 K transport barrier on the 480 K isentropic surface in
443 December. The long-lasting polar vortex prevented the volcanic plume from crossing the transport
444 barrier at 480 K in early December, but from mid-December, the polar vortex became more
445 disturbed and displaced from the south pole South Pole, resulting in a shrinking ozone hole. As
446 mentioned in Sect. 3.23.1, the ozone hole broke down at the end of December 2010 and the polar vortex
447 broke down by mid-January 2011.

448 The fraction of the volcanic plume that crosses the individual transport barrier or the latitude of 60 °S on
449 each isentropic surface are shown in Fig. 89. In both cases, the proportion increased from November
450 2010 to January 2011. In November and December 2010 the largest plume transport across the transport
451 barriers occurred between the 360 and 430 K isentropic surface (Fig. 89a), with a peak at 380–390 K. In
452 January and February 2011 the peak was slightly elevated to 390–400 K. In November 2010, the
453 volcanic plume did not cross the 480 K transport barrier of the polar vortex at high altitudes, especially
454 above about 450 K. The high-latitude fraction increased from December 2010 to February 2011 as the
455 weakening of the polar vortex made the transport barrier more permeable. In March and April 2011, the

456 total proportion decreased and the peak descended to 370 K in March and further to 360 K in April. The
457 proportion of the volcanic plume south of 60 °S (Fig. 89b) increased slightly from November to
458 December 2010, and then increased significantly from December 2010 to January and February 2011 at
459 all altitudes as the polar vortex displaced and broke down. Finally, the transport to the south of 60 °S
460 started to decrease in March 2011. From November 2010 to February 2011 the peak was around 370–
461 400 K, but in March and April 2011 the peak resided around 350–370 K.

462 Figure 9a10 summarizes the simulated poleward transport of the volcanic plume between the isentropic
463 surfaces of 350 and 480 K from November 2010 to March 2011 and the percentage of air parcels south
464 of 60 °S. The percentage was calculated by dividing the number of SO₂ parcels between 350 and 480 K
465 south of 60 °S by the total number of SO₂ parcels released for the forward trajectory simulation. Figure
466 9b demonstrates the change of aerosol load in the same vertical range for MIPAS aerosol detections. As
467 in Sect. 3.3, we calculated the median ACI between November 2010 and March 2011 and subtracted it
468 from the ACI median of the “reference state” between November 2007 and March 2008. The zonally
469 resolved fractions derived from the Lagrangian MPTRAC simulations and the fraction of air parcels
470 south of 60 °S are shown in Fig. 10a. Figure 10b demonstrates the increasing and decreasing aerosol
471 load in this vertical range for MIPAS aerosol detections relative to 1–4 November median (see Sect.3.3).
472 The poleward transport trend in Fig. 10a is comparable to the poleward migration of the enhanced
473 aerosol in Fig. 10b. The simulations show that the plume reached 60 °S in December 2010.
474 Correspondingly, the aerosol load south of 60 °S was elevated. The percentage fluctuated, but increased
475 until the end of February 2011, with a maximum percentage of about 4%. A steep increase occurred
476 from mid-December 2010 to end of January 2011, following the displacement and breakdown of the
477 polar vortex. The elevated aerosol load south of 60 °S decreased from March 2011, and part of the
478 plume descended to altitudes below 350 K as shown by Fig. 89b. The MIPAS aerosol measurements in
479 Fig. 9b where a positive ACI difference indicates an increase in the aerosol load, confirm the simulated
480 transport pattern in Fig. 9a. Overall, simulations and observations indicate the largest increase of the
481 aerosol load in the tropics and mid-latitudes, but also show a significant enhancement over the south
482 polar region after December 2010.

483 **4 Discussion**

484 The results presented in Sect. 3 show that the main transport pathway for the poleward transport of the
485 Merapi volcanic plume to Antarctica was between the isentropic surfaces of 350 and 480 K (about 10 to

20 km), covering the TTL and the lower stratosphere at mid- and high latitudes. For this long-range transport on timescales of a few months, fast isentropic transport associated with quasi-horizontal mixing ~~played the main role in transporting the volcanic aerosol from the TTL to the Antarctic lower stratosphere. was found to be the most efficient pathway. The phase of QBO, subtropical Rossby wave breaking and the strength and stability of the polar vortex all have an impact on the transport efficiency.~~ The Merapi eruption occurred in austral spring and fast poleward transport was facilitated by the weakening of the subtropical jet and active Rossby wave breaking events. ~~The westerly QBO enhanced transport and mixing in the subtropics with implications on the position of the subtropical barrier (Shuckburgh et al., 2001; Palazzi et al., 2011). The QBO also modulated the ability of upward propagating planetary waves to influence the strength of the polar vortex.~~ The polar vortex was relatively stable when the Merapi erupted, but by the time the volcanic plume reached the south polar region, the polar vortex was displaced from the ~~south pole~~South Pole and distorted because more wave systems propagated into the polar stratosphere and warmed the polar region, so that the volcanic plume was transported from the tropics deep into Antarctica.

~~The phase of the QBO influences the amount of volcanic emissions transported out of tropics, while the heating effect of a large amount of sulfur injected by volcanic eruptions can change the pattern of the QBO (Niemeier and Schmidt, 2017). With increasing emission rates the velocity of the equatorial jet streams increases and less sulfate is transported out of the tropics. The amount of SO₂ injected during the Merapi eruption 2010 was 0.44 Tg, far less than the 8 TgS/yr required to shut down or reverse the QBO pattern (Niemeier and Schmidt, 2017), so that the westerly phase of the QBO that promote meridional transport was under minor influence of the heating effect of sulfur in this case.~~

Based on the simulation results in Sect. 3.4, up to 4% of the volcanic plume air parcels was transported from the TTL to the lower stratosphere in the south polar region till the end of February 2011. Based on previous research on the Merapi case, we assigned a total mass of 0.44 Tg to all SO₂ parcel released, which means the Merapi eruption contributed about 8800 tons of sulfur to the polar lower stratosphere within 4 months after the eruption, assuming that the sulfate aerosol converted from the SO₂ remained in the plume. Although the MPTRAC model we used to simulate the 3D movement of air parcels in the volcanic plumes can estimate the conversion of SO₂ to sulfate aerosol during the transport process, however, it does not resolve the chemical processes of aerosol formation. Hence, the estimated 8800 tons of sulfur are the maximum value since processes as e.g. wet deposition remove sulfur from the atmosphere. But in the lower stratosphere, the atmosphere is relatively dry and clean compared with the lower troposphere, so the sulfate ~~aerosols~~aerosol has a lower possibility to interact with clouds or to be

518 washed out. In fact, in the polar lower stratosphere usually sedimentation and downward transport by the
519 BDC are the main removal processes. Clouds and washout processes usually cannot be expected in the
520 lower stratosphere. However, the amount of sulfate ~~aerosols~~aerosol in the plume could also be affected
521 by other mechanisms that speed up the loss of sulfur, for example, coagulation in the volcanic plume, or
522 the absorption of sulfur onto fine ash particles. But for the moderate eruption Merapi in 2010,
523 ~~sulfuric~~sulphuric particle growth may not be as significant as it is in a large volcanic eruption, so the
524 scavenging efficiency of sulfur will be low. So generally, our estimation may be larger than the actual
525 value, but this number may be considered as the upper limit of the contribution of the Merapi eruption.
526 Besides, a kinematic trajectory model like MPTRAC, in which reanalysis vertical wind is used as
527 vertical velocity, typically shows higher vertical dispersion in the equatorial lower stratosphere
528 compared with a diabatic trajectory model (Schoeberl et al., 2003; Wohltmann and Rex, 2008; Liu et al.,
529 2010; Ploeger et al., 2010, 2011). However, the ERA–Interim reanalysis data used in this study to drive
530 the model may constrain the vertical dispersion much better than older reanalyses (Liu et al., 2010;
531 Hoffmann et al., 2017). The meridional transport in this study was mainly quasi-horizontal transport in
532 the mid- and high latitude UTLS region, so the effect of the vertical speed scheme is limited.
533 The aerosol transported to the polar lower stratosphere will finally descend with the downward flow and
534 have a chance to become a nonlocal source of sulfur for Antarctica by dry and wet deposition, following
535 the general precipitation patterns. Quantifying the sulfur deposition flux onto Antarctica is beyond the
536 scope of this study, though. Model results of Solomon et al. (2016) suggest that the Merapi eruption
537 made a small but significant contribution to the ozone depletion over Antarctica in the vertical range of
538 100–200 hPa, roughly between 10 and 14 km. This altitude range is in agreement with our results,
539 where we found transport into the Antarctic stratosphere between 10 and 20 km. When the volcanic
540 plume was transported to Antarctica in December 2010, the polar synoptic temperature at these low
541 height levels was already too high for the formation of PSCs. The additional ozone depletion found by
542 Solomon et al. (2016) together with the fact that sulfate aerosol was transported from the Merapi into
543 the Antarctic stratosphere between November and February where no PSCs are present during polar
544 summer, may support the study that suggested that significant ozone depletion can also occur on cold
545 binary aerosol (Drdla and Müller, 2012). The Merapi eruption in 2010 could be an interesting case
546 study for more sophisticated geophysical models to study the aftermath of volcanic eruptions on polar
547 processes.

548 5 Summary and conclusion

549 In this study, we analyzed the poleward transport of volcanic aerosol released by the Merapi eruption in
550 2010 from the tropics to the Antarctic lower stratosphere. The analysis was based on AIRS SO₂
551 measurements, MIPAS sulfate aerosol detections and MPTRAC transport simulations. First, we
552 estimated altitude-resolved SO₂ injection time series during the explosive eruption period using AIRS
553 data together with a backward trajectory approach. Second, the long-range transport of the volcanic
554 plume from the initial eruption to April 2011 was simulated based on the derived SO₂ injection time
555 series. Then the evolution and the poleward migration of the volcanic plume were analyzed using the
556 forward trajectory simulations and MIPAS aerosol measurements. The simulations are compared with
557 and verified by the MIPAS aerosol measurements.

558 Results of this study suggest that the volcanic plume from the Merapi eruption was transported from the
559 tropics to the south of 60 °S within a time scale of one month. Later on, in the UTLS region a fraction of
560 the volcanic plume (~4%) crossed 60 °S, even further to Antarctica until the end of February 2011. As a
561 result, the aerosol load in the Antarctic lower stratosphere was significantly elevated. This relatively fast
562 meridional transport of volcanic aerosol was mainly carried out by quasi-horizontal mixing from the
563 TTL to the extratropical lower stratosphere. Based on the simulations, most of the quasi-horizontal
564 mixing occurred between the isentropic surfaces of 360 to 430 K. This transport was in turn facilitated
565 by the weakening of the subtropical jet and the breakdown of the polar vortex in the seasonal transition
566 from austral spring to summer. The polar vortex in late austral spring 2010 was relatively strong
567 compared to the climatological mean state. However, in December 2010 the polar vortex was displaced
568 off the South Pole and later on broke down when the plume went to the south polar region high latitudes,
569 so the volcanic plume did not penetrate the polar vortex but entered the South Pole with the breakdown
570 of the polar vortex.

571 Overall, after the Merapi eruption, the largest increase of aerosol load occurred in the Southern
572 Hemisphere midlatitudes and a relatively small but significant fraction of the volcanic plume (4%) was
573 further transported to the Antarctic lower stratosphere within 4 months after the eruption. As a
574 maximum estimation, it contributed up to 8800 tons of sulfur to the Antarctic stratosphere, which
575 indicates that long-range transport under favorable meteorological conditions can make moderate
576 tropical volcanic eruptions an important remote source of sulfur to Antarctica.

577

578 *Code and data availability.* AIRS data are distributed by the NASA Goddard Earth Sciences Data
579 Information and Services Center. The SO₂ index data used in this study (Hoffmann et al., 2014) are
580 available for download at <https://datapub.fz-juelich.de/slcs/airs/volcanoes/> (last access: 26 March 2018).
581 Envisat MIPAS Level-1B data are distributed by the European Space Agency. The ERA–Interim
582 reanalysis data (Dee et al., 2011) were obtained from the European Centre for Medium-Range Weather
583 Forecasts. The code of the Massive-Parallel Trajectory Calculations (MPTRAC) model is available
584 under the terms and conditions of the GNU General Public License, Version 3 from the repository at
585 <https://github.com/slcs-jsc/mptrac> (last access: 31 January 2018).

586

587 Appendix

588 Figure A1 shows the 9-day running median values of the MIPAS ACI between 10 °N and 10 °S. During
589 the time period of the reference state (November 2007 to March 2008), the aerosol load in the tropical
590 stratosphere from 20 to 25 km is elevated by a couple of previous volcanic eruptions. The aerosol load
591 at this vertical range after the Merapi eruption in 2010 is apparently smaller compared with the
592 reference state.

593 It should be noted that there are semiannual data oscillations in the MIPAS ACI aerosol detections. This
594 periodic pattern is caused by the aerosol index that uses the atmospheric window region between 960
595 and 961 cm⁻¹. Around this window region, there are CO₂ laser bands. Due to the semiannual
596 temperature changes at about 50 km (semiannual oscillation), the CO₂ radiance contribution to this
597 window region also oscillates. As this window is generally very clear of other trace gases, this
598 oscillation is not only visible at higher altitudes but also in the lower stratosphere, because the satellite
599 line of sight looks through the whole layer (Wu et al., 2017). But even though with the semiannual data
600 oscillations, the upward transport of the aerosol from the Merapi eruption in the tropical stratosphere is
601 still visible and the vertical speed is estimated to about 7–8 km in five months (November 2010 to
602 March 2011).

603

604 *Competing interests.* The authors declare that they have no conflict of interest.

605

606 *Acknowledgments.* This work was supported by National Natural Science Foundation of China under
607 grant no. 41605023, China Postdoctoral Science Foundation under grant no. 2018T110131 and
608 International Postdoctoral Exchange Fellowship Program 2015 under grant no. 20151006.

- 610 Anstey, J. A., and Shepherd, T. G.: High-latitude influence of the quasi-biennial oscillation, *Q. J. R.*
611 *Meteorol. Soc.*, 140, 1-21, doi: 10.1002/qj.2132, 2014.
- 612 ~~Aquila, V., C. I. Garfinkel, P. A. Newman, L. D. Oman, and D. W. Waugh, Modifications of the~~
613 ~~quasi-biennial oscillation by a geoengineering perturbation of the stratospheric aerosol layer,~~
614 ~~*Geophys. Res. Lett.*, 41, 1738-1744, doi: 10.1002/2013GL058818, 2014.~~
- 615 Aumann, H. H., Chahine, M. T., Gautier, C., Goldberg, M. D., Kalnay, E., McMillin, L. M., Revercomb,
616 H., Rosenkranz, P. W., Smith, W. L., Staelin, D. H., Strow, L. L., and Susskind, J.: AIRS/AMSU/HSB
617 on the Aqua mission: design, science objectives, data products, and processing systems, *IEEE Trans.*
618 *Geosci. Remote Sens.*, 41, 253-264, doi: 10.1109/TGRS.2002.808356, 2003.
- 619 Baldwin, M. P., and Dunkerton, T. J.: Propagation of the Arctic Oscillation from the stratosphere to the
620 troposphere, *J. Geophys. Res. Atmos.*, 104, 30937-30946, doi: 10.1029/1999JD900445, 1999.
- 621 Bosilovich, M., Akella, S., Coy, L., Cullather, R., Draper, C., Gelaro, R., Kovach, R., Liu, Q., Molod,
622 A., Norris, P., Wargan, K., Chao, W., Reichle, R., Takacs, L., Vikhliav, Y., Bloom, S., Collow, A.,
623 Firth, S., Labow, G., Partyka, G., Pawson, S., Reale, O., Schubert, S. D., and Suarez, M.: MERRA-2:
624 Initial evaluation of the climate, Tech. rep., NASA, series on Global Modeling and Data
625 Assimilation, NASA/TM-2015-104606, Vol. 43, 2015.
- 626 Dee, D. P., Uppala, S. M., Simmons, A. J., Berrisford, P., Poli, P., Kobayashi, S., Andrae, U.,
627 Balmaseda, M. A., Balsamo, G., Bauer, P., Bechtold, P., Beljaars, A. C. M., van de Berg, L., Bidlot,
628 J., Bormann, N., Delsol, C., Dragani, R., Fuentes, M., Geer, A. J., Haimberger, L., Healy, S. B.,
629 Hersbach, H., Holm, E. V., Isaksen, L., Kallberg, P., Kohler, M., Matricardi, M., McNally, A. P.,
630 Monge-Sanz, B. M., Morcrette, J. J., Park, B. K., Peubey, C., de Rosnay, P., Tavolato, C., Thepaut, J.
631 N., and Vitart, F.: The ERA-Interim reanalysis: configuration and performance of the data
632 assimilation system, *Q. J. R. Meteorol. Soc.*, 137, 553-597, doi: 10.1002/qj.828, 2011.
- 633 Drdla, K., and Müller, R.: Temperature thresholds for chlorine activation and ozone loss in the polar
634 stratosphere, *Ann. Geophys.*, 30, 1055-1073, doi: 10.5194/angeo-30-1055-2012, 2012.
- 635 Edmon, H. J. J., Hoskins, B. J., and McIntyre, M. E.: Eliassen-Palm Cross Sections for the Troposphere,
636 *J. Atmos. Sci.*, 37, 2600-2616, doi: 10.1175/1520-0469(1980)037<2600:epcsft>2.0.co;2, 1980.
- 637 Fischer, H., Birk, M., Blom, C., Carli, B., Carlotti, M., von Clarmann, T., Delbouille, L., Dudhia, A.,
638 Ehhalt, D., Endemann, M., Flaud, J. M., Gessner, R., Kleinert, A., Koopman, R., Langen, J.,
639 López-Puertas, M., Mosner, P., Nett, H., Oelhaf, H., Perron, G., Remedios, J., Ridolfi, M., Stiller, G.,
640 and Zander, R.: MIPAS: an instrument for atmospheric and climate research, *Atmos. Chem. Phys.*, 8,
641 2151-2188, doi: 10.5194/acp-8-2151-2008, 2008.
- 642 Friberg, J., Martinsson, B. G., Andersson, S. M., and Sandvik, O. S.: Volcanic impact on the climate –
643 the stratospheric aerosol load in the period 2006–2015, *Atmos. Chem. Phys.*, 18, 11149-11169, doi:
644 10.5194/acp-18-11149-2018, 2018.
- 645 Gao, C., Oman, L., Robock, A., and Stenchikov, G. L.: Atmospheric volcanic loading derived from
646 bipolar ice cores: Accounting for the spatial distribution of volcanic deposition, *J. Geophys. Res.*
647 *Atmos.*, 112, D09109, doi: 10.1029/2006JD007461, 2007.
- 648 Griessbach, S., L. Hoffmann, R. Spang and M. Riese: Volcanic ash detection with infrared limb
649 sounding: MIPAS observations and radiative transfer simulations, *Atmos. Meas. Tech.* 7,
650 1487-1507, doi: 10.5194/amt-7-1487-2014, 2014.
- 651
- 652 Griessbach, S., Hoffmann, L., Spang, R., von Hobe, M., Müller, R., and Riese, M.: Infrared limb
653 emission measurements of aerosol in the troposphere and stratosphere, *Atmos. Meas. Tech.*, 9,
654 4399-4423, doi:10.5194/amt-9-4399-2016, 2016.

655 Günther, A., Höpfner, M., Sinnhuber, B. M., Griessbach, S., Deshler, T., von Clarmann, T., and Stiller,
656 G.: MIPAS observations of volcanic sulphate aerosol and sulphur dioxide in the stratosphere, *Atmos.*
657 *Chem. Phys.*, 2017, 1-32, doi: 10.5194/acp-18-1217-2018, 2018.

658 Haynes, P., and Shuckburgh, E.: Effective diffusivity as a diagnostic of atmospheric transport: 2.
659 Troposphere and lower stratosphere, *J. Geophys. Res. Atmos.*, 105, 22795-22810, doi:
660 10.1029/2000JD900092, 2000.

661 Heng, Y., Hoffmann, L., Griessbach, S., Rößler, T., and Stein, O.: Inverse transport modeling of volcanic
662 sulfur dioxide emissions using large-scale simulations, *Geosci. Model Dev.*, 9, 1627-1645,
663 doi:10.5194/gmd-9-1627-2016, 2016.

664 Hoffmann, L., Griessbach, S., and Meyer, C. I.: Volcanic emissions from AIRS observations: detection
665 methods, case study, and statistical analysis, in: *Remote Sensing of Clouds and the Atmosphere XIX*
666 *and Optics in Atmospheric Propagation and Adaptive Systems XVII*, edited by: Comerón, A.,
667 Kassianov, E. I., Schafer, K., Picard, R. H., Stein, K., and Gonglewski, J. D., *Proceedings of SPIE*,
668 *Spie-Int Soc Optical Engineering*, Bellingham, doi: 92421410.1117/12.2066326, 2014.

669 Hoffmann, L., Hertzog, A., Rößler, T., Stein, O., and Wu, X.: Intercomparison of meteorological
670 analyses and trajectories in the Antarctic lower stratosphere with Concordiasi superpressure balloon
671 observations, *Atmos. Chem. Phys.*, 17, 8045-8061, doi: 10.5194/acp-17-8045-2017, 2017.

672 Hoffmann, L., Rößler, T., Griessbach, S., Heng, Y., and Stein, O.: Lagrangian transport simulations of
673 volcanic sulfur dioxide emissions: Impact of meteorological data products, *J. Geophys. Res. Atmos.*,
674 121, 4651-4673, doi: 10.1002/2015JD023749, 2016.

675 Hofmann, D. J., Rosen, J. M., and Gringel, W.: Delayed production of sulfuric acid condensation nuclei
676 in the polar stratosphere from El Chichon volcanic vapors, *J. Geophys. Res. Atmos.*, 90, 2341-2354,
677 doi:10.1029/JD090iD01p02341, 1985.

678 Hofmann, D. J., Rosen, J. M., and Harder, J. W.: Aerosol measurements in the winter/spring Antarctic
679 stratosphere: 1. Correlative measurements with ozone, *J. Geophys. Res. Atmos.*, 93, 665-676,
680 doi:10.1029/JD093iD01p00665, 1988.

681 Holton, J. R., Haynes, P. H., McIntyre, M. E., Douglass, A. R., Rood, R. B., and Pfister, L.:
682 Stratosphere-troposphere exchange, *Rev. Geophys.*, 33, 403-439, doi: 10.1029/95RG02097, 1995.

683 Holton, J. R., and Tan, H. C.: The Influence of the Equatorial Quasi-Biennial Oscillation on the Global
684 Circulation at 50 mb, *J. Atmos. Sci.*, 37, 2200-2208, doi:
685 10.1175/1520-0469(1980)037<2200:tioteq>2.0.co;2, 1980.

686 Höpfner, M., Pitts, M. C., and Poole, L. R.: Comparison between CALIPSO and MIPAS observations
687 of polar stratospheric clouds, *J. Geophys. Res. Atmos.*, 114, doi:10.1029/2009JD012114, 2009.

688 Ivy, D. J., Solomon, S., Kinnison, D., Mills, M. J., Schmidt, A., and Neely, R. R.: The influence of the
689 Calbuco eruption on the 2015 Antarctic ozone hole in a fully coupled chemistry-climate model,
690 *Geophys. Res. Lett.*, 44, 2556-2561, doi: 10.1002/2016GL071925, 2017.

691 Jäger, H.: Long-term record of lidar observations of the stratospheric aerosol layer at
692 Garmisch-Partenkirchen, *J. Geophys. Res. Atmos.*, 110, D08106, doi: 10.1029/2004JD005506, 2005.

693 Jäger, H., and Wege, K.: Stratospheric ozone depletion at northern midlatitudes after major volcanic
694 eruptions, *J. Atmos. Chem.*, 10, 273-287, doi: 10.1007/bf00053863, 1990.

695 [Kalnay, E., Kanamitsu, M., Kistler, R., Collins, W., Deaven, D., Gandin, L., Iredell, M., Saha, S., White,](#)
696 [G., Woollen, J., Zhu, Y., Chelliah, M., Ebisuzaki, W., Higgins, W., Janowiak, J., Mo, K. C.,](#)
697 [Ropelewski, C., Wang, J., Leetmaa, A., Reynolds, R., Jenne, R., and Joseph, D.: The NCEP/NCAR](#)
698 [40-Year Reanalysis Project, *Bull. Am. Meteorol. Soc.* 77, 437-472, doi:](#)
699 [10.1175/1520-0477\(1996\)077<0437:tnyrp>2.0.co;2, 1996.](#)

700 Khaykin, S. M., Godin-Beekmann, S., Keckhut, P., Hauchecorne, A., Jumelet, J., Vernier, J. P.,
701 Bourassa, A., Degenstein, D. A., Rieger, L. A., Bingen, C., Vanhellemont, F., Robert, C., DeLand,

702 M., and Bhartia, P. K.: Variability and evolution of the midlatitude stratospheric aerosol budget from
703 22 years of ground-based lidar and satellite observations, *Atmos. Chem. Phys.*, 17, 1829-1845, doi:
704 10.5194/acp-17-1829-2017, 2017.

705 ~~Kravitz, B., and Robock, A.: Climate effects of high-latitude volcanic eruptions: Role of the time of
706 year, *J. Geophys. Res. Atmos.*, 116, D01105, 10.1029/2010JD014448, 2011.~~

707 Kunz, A., Konopka, P., Müller, R., and Pan, L. L.: Dynamical tropopause based on isentropic potential
708 vorticity gradients, *J. Geophys. Res. Atmos.*, 116, D01110, doi: 10.1029/2010JD014343, 2011a.

709 Kunz, A., Pan, L. L., Konopka, P., Kinnison, D. E., and Tilmes, S.: Chemical and dynamical
710 discontinuity at the extratropical tropopause based on START08 and WACCM analyses, *J. Geophys.
711 Res. Atmos.*, 116, D24302, doi: 10.1029/2011JD016686, 2011b.

712 Kunz, A., Sprenger, M., and Wernli, H.: Climatology of potential vorticity streamers and associated
713 isentropic transport pathways across PV gradient barriers, *J. Geophys. Res. Atmos.*, 120, 3802-3821,
714 doi: 10.1002/2014jd022615, 2015.

715 ~~Levelt, P. F., Oord, G. H. J. v. d., Dobber, M. R., Malkki, A., Huib, V., Johan de, V., Stammes, P.,
716 Lundell, J. O. V., and Saari, H.: The ozone monitoring instrument, *IEEE Trans. Geosci. Remote
717 Sens.*, 44, 1093-1101, doi: 10.1109/TGRS.2006.872333, 2006.~~

718 Liu, Y. S., Fueglistaler, S., and Haynes, P. H.: Advection-condensation paradigm for stratospheric water
719 vapor, *J. Geophys. Res. Atmos.*, 115, D24307, doi: 10.1029/2010JD014352, 2010.

720 Mazzer, D. M., Lowenthal, D. H., Chow, J. C., and Watson, J. G.: Sources of PM10 and sulfate aerosol
721 at McMurdo station, Antarctica, *Chemosphere*, 45, 347-356, doi:
722 https://doi.org/10.1016/S0045-6535(00)00591-9, 2001.

723 ~~McCormick, M. P., Steele, H. M., Hamill, P., Chu, W. P., and Swissler, T. J.: Polar Stratospheric Cloud
724 Sightings by SAM II, *J. Atmos. Sci.*, 39, 1387-1397, doi:
725 10.1175/1520-0469(1982)039<1387:pscsbs>2.0.co;2, 1982.~~

726 ~~Newman, P. A., and Nash, E. R.: Quantifying the wave driving of the stratosphere, *J. Geophys. Res.
727 Atmos.*, 105, 12485-12497, doi: 10.1029/1999JD901191, 2000.~~

728 ~~Niemeier, U., and Schmidt, H.: Changing transport processes in the stratosphere by radiative heating of
729 sulfate aerosols, *Atmos. Chem. Phys.*, 17, 14871-14886, doi: 10.5194/acp-17-14871-2017, 2017.~~

730 Olsen, M. A., Douglass, A. R., Schoeberl, M. R., Rodriguez, J. M., and Yoshida, Y.: Interannual
731 variability of ozone in the winter lower stratosphere and the relationship to lamina and irreversible
732 transport, *J. Geophys. Res. Atmos.*, 115, 10.1029/2009jd013004, 2010.

733 O'Sullivan, D., and Dunkerton, T. J.: The influence of the quasi-biennial oscillation on global
734 constituent distributions, *J. Geophys. Res. Atmos.*, 102, 21731-21743, doi: 10.1029/97JD01689,
735 1997.

736 ~~Palazzi, E., Fierli, F., Stiller, G. P., and Urban, J.: Probability density functions of long-lived tracer
737 observations from satellite in the subtropical barrier region: data intercomparison, *Atmos. Chem.
738 Phys.*, 11, 10579-10598, doi: 10.5194/acp-11-10579-2011, 2011.~~

739 Pallister, J. S., Schneider, D. J., Griswold, J. P., Keeler, R. H., Burton, W. C., Noyles, C., Newhall, C.
740 G., and Ratdomopurbo, A.: Merapi 2010 eruption—Chronology and extrusion rates monitored with
741 satellite radar and used in eruption forecasting, *J. Volcanol. Geotherm. Res.*, 261, 144-152, doi:
742 http://dx.doi.org/10.1016/j.jvolgeores.2012.07.012, 2013.

743 ~~Pausata, F. S. R., Chafik, L., Caballero, R., and Battisti, D. S.: Impacts of high-latitude volcanic
744 eruptions on ENSO and Asian monsoon, *Proc. Natl. Acad. Sci. U.S.A.*, 112, 13784-13788, doi:
745 10.1073/pnas.1509153112, 2015.~~

746 Ploeger, F., Konopka, P., Gunther, G., Grooss, J. U., and Müller, R.: Impact of the vertical velocity
747 scheme on modeling transport in the tropical tropopause layer, *J. Geophys. Res. Atmos.*, 115, 14, doi:
748 10.1029/2009jd012023, 2010.

749 Ploeger, F., Fueglistaler, S., Grooss, J. U., Gunther, G., Konopka, P., Liu, Y. S., Muller, R., Ravegnani,
750 F., Schiller, C., Ulanovski, A., and Riese, M.: Insight from ozone and water vapour on transport in
751 the tropical tropopause layer (TTL), *Atmos. Chem. Phys.*, 11, 407-419, doi:
752 10.5194/acp-11-407-2011, 2011.

753 [Portmann, R. W., Solomon, S., Garcia, R. R., Thomason, L. W., Poole, L. R., and McCormick, M. P.:
754 Role of aerosol variations in anthropogenic ozone depletion in the polar regions, *J. Geophys. Res.*
755 *Atmos.*, doi: 10.1029/96JD02608, 1996.](#)

756 Röfler, T., Stein, O., Heng, Y., Baumeister, P., and Hoffmann, L.: Trajectory errors of different
757 numerical integration schemes diagnosed with the MPTRAC advection module driven by ECMWF
758 operational analyses, *Geosci. Model Dev.*, 11, 575-592, doi: 10.5194/gmd-11-575-2018, 2018.

759 Sand, M., Samset, B. H., Balkanski, Y., Bauer, S., Bellouin, N., Berntsen, T. K., Bian, H., Chin, M.,
760 Diehl, T., Easter, R., Ghan, S. J., Iversen, T., Kirkevåg, A., Lamarque, J. F., Lin, G., Liu, X., Luo, G.,
761 Myhre, G., Noije, T. V., Penner, J. E., Schulz, M., Seland, Ø., Skeie, R. B., Stier, P., Takemura, T.,
762 Tsigaridis, K., Yu, F., Zhang, K., and Zhang, H.: Aerosols at the poles: an AeroCom Phase II
763 multi-model evaluation, *Atmos. Chem. Phys.*, 17, 12197-12218, doi: 10.5194/acp-17-12197-2017,
764 2017.

765 Schoeberl, M. R., Douglass, A. R., Zhu, Z. X., and Pawson, S.: A comparison of the lower stratospheric
766 age spectra derived from a general circulation model and two data assimilation systems, *J. Geophys.*
767 *Res. Atmos.*, 108, 16, doi: 10.1029/2002jd002652, 2003.

768 [Sembhi, H., Remedios, J., Trent, T., Moore, D. P., Spang, R., Massie, S., and Vernier, J. P.: MIPAS
769 detection of cloud and aerosol particle occurrence in the UTLS with comparison to HIRDLS and
770 CALIOP, *Atmos. Meas. Tech.*, 5, 2537-2553, doi: 10.5194/amt-5-2537-2012, 2012.](#)

771 Shuckburgh, E., Norton, W., Iwi, A., and Haynes, P.: Influence of the quasi-biennial oscillation on
772 isentropic transport and mixing in the tropics and subtropics, *J. Geophys. Res. Atmos.*, 106,
773 14327-14337, doi: 10.1029/2000JD900664, 2001.

774 Sigl, M., Winstrup, M., McConnell, J. R., Welten, K. C., Plunkett, G., Ludlow, F., Buntgen, U., Caffee,
775 M., Chellman, N., Dahl-Jensen, D., Fischer, H., Kipfstuhl, S., Kostick, C., Maselli, O. J., Mekhaldi,
776 F., Mulvaney, R., Muscheler, R., Pasteris, D. R., Pilcher, J. R., Salzer, M., Schupbach, S., Steffensen,
777 J. P., Vinther, B. M., and Woodruff, T. E.: Timing and climate forcing of volcanic eruptions for the
778 past 2,500 years, *Nature*, 523, 543-549, doi:
779 10.1038/nature14565http://www.nature.com/nature/journal/v523/n7562/abs/nature14565.html#suppl
780 ementary-information, 2015.

781 Solomon, S.: Stratospheric ozone depletion: A review of concepts and history, *Rev. Geophys.*, 37,
782 275-316, doi: 10.1029/1999RG900008, 1999.

783 Solomon, S., Daniel, J. S., Neely, R. R., Vernier, J.-P., Dutton, E. G., and Thomason, L. W.: The
784 Persistently Variable “Background” Stratospheric Aerosol Layer and Global Climate Change,
785 *Science*, 333, 866-870, doi: 10.1126/science.1206027, 2011.

786 [Solomon, S., Garcia, R. R., Rowland, F. S., and Wuebbles, D. J.: On the depletion of Antarctic ozone,
787 *Nature*, 321, 755, doi: 10.1038/321755a0, 1986.](#)

788 Solomon, S., Ivy, D. J., Kinnison, D., Mills, M. J., Neely, R. R., and Schmidt, A.: Emergence of healing
789 in the Antarctic ozone layer, *Science*, doi: 10.1126/science.aae0061, 2016.

790 Solomon, S., Sanders, R. W., Garcia, R. R., and Keys, J. G.: Increased chlorine dioxide over Antarctica
791 caused by volcanic aerosols from Mount-Pinatubo, *Nature*, 363, 245-248, doi:
792 https://doi.org/10.1038/363245a0, 1993.

793 [Spang, R., Riese, M., and Offermann, D.: CRISTA-2 observations of the south polar vortex in winter
794 1997: A new dataset for polar process studies, *Geophys. Res. Lett.*, 28, 3159-3162, doi:
795 10.1029/2000GL012374, 2001.](#)

796 Stohl, A., Forster, C., Frank, A., Seibert, P., and Wotawa, G.: Technical note: The Lagrangian particle
797 dispersion model FLEXPART version 6.2, *Atmos. Chem. Phys.*, 5, 2461-2474,
798 doi:10.5194/acp-5-2461-2005, 2005.

799 Stone, K. A., Solomon, S., Kinnison, D. E., Pitts, M. C., Poole, L. R., Mills, M. J., Schmidt, A., Neely,
800 R. R., Ivy, D., Schwartz, M. J., Vernier, J.-P., Johnson, B. J., Tully, M. B., Klekociuk, A. R.,
801 König-Langlo, G., and Hagiya, S.: Observing the Impact of Calbuco Volcanic Aerosols on South
802 Polar Ozone Depletion in 2015, *J. Geophys. Res. Atmos.*, 122, 11,862-811,879, doi:
803 10.1002/2017JD026987, 2017.

804 Surono, Jousset, P., Pallister, J., Boichu, M., Buongiorno, M. F., Budisantoso, A., Costa, F., Andreastuti,
805 S., Prata, F., Schneider, D., Clarisse, L., Humaida, H., Sumarti, S., Bignami, C., Griswold, J., Carn,
806 S., Oppenheimer, C., and Lavigne, F.: The 2010 explosive eruption of Java's Merapi volcano—A
807 '100-year' event, *J. Volcanol. Geotherm. Res.*, 241, 121-135, doi:
808 <http://dx.doi.org/10.1016/j.jvolgeores.2012.06.018>, 2012.

809 Tilmes, S., Muller, R., and Salawitch, R.: The sensitivity of polar ozone depletion to proposed
810 geoengineering schemes, *Science*, 320, 1201-1204, doi: 10.1126/science.1153966, 2008.

811 [Toohey, M., Krüger, K., Niemeier, U., and Timmreck, C.: The influence of eruption season on the](#)
812 [global aerosol evolution and radiative impact of tropical volcanic eruptions, *Atmos. Chem. Phys.*, 11,](#)
813 [doi: 12351-12367, 10.5194/acp-11-12351-2011, 2011.](#)

814 Vernier, J. P., Thomason, L. W., Pommereau, J. P., Bourassa, A., Pelon, J., Garnier, A., Hauchecorne,
815 A., Blanot, L., Trepte, C., Degenstein, D., and Vargas, F.: Major influence of tropical volcanic
816 eruptions on the stratospheric aerosol layer during the last decade, *Geophys. Res. Lett.*, 38, L12807,
817 doi: 10.1029/2011GL047563, 2011.

818 Vogel, B., Pan, L. L., Konopka, P., Gunther, G., Muller, R., Hall, W., Campos, T., Pollack, I.,
819 Weinheimer, A., Wei, J., Atlas, E. L., and Bowman, K. P.: Transport pathways and signatures of
820 mixing in the extratropical tropopause region derived from Lagrangian model simulations, *J.*
821 *Geophys. Res. Atmos.*, 116, 16, doi: 10.1029/2010jd014876, 2011.

822 von Glasow, R., Bobrowski, N., and Kern, C.: The effects of volcanic eruptions on atmospheric
823 chemistry, *Chem. Geol.*, 263, 131-142, doi: <http://dx.doi.org/10.1016/j.chemgeo.2008.08.020>, 2009.

824 Watson, P. A. G., and Gray, L. J.: How Does the Quasi-Biennial Oscillation Affect the Stratospheric
825 Polar Vortex?, *J. Atmos. Sci.*, 71, 391-409, doi: 10.1175/jas-d-13-096.1, 2014.

826 Wohltmann, I., and Rex, M.: Improvement of vertical and residual velocities in pressure or hybrid
827 sigma-pressure coordinates in analysis data in the stratosphere, *Atmos. Chem. Phys.*, 8, 265-272, doi:
828 10.5194/acp-8-265-2008, 2008.

829 Wu, X., Griessbach, S., and Hoffmann, L.: Equatorward dispersion of a high-latitude volcanic plume
830 and its relation to the Asian summer monsoon: a case study of the Sarychev eruption in 2009, *Atmos.*
831 *Chem. Phys.*, 17, 13439-13455, doi: 10.5194/acp-17-13439-2017, 2017.

832 Zuev, V. V., Zueva, N. E., Savelieva, E. S., and Gerasimov, V. V.: The Antarctic ozone depletion
833 caused by Erebus volcano gas emissions, *Atmos. Environ.*, 122, 393-399, doi:
834 <https://doi.org/10.1016/j.atmosenv.2015.10.005>, 2015.

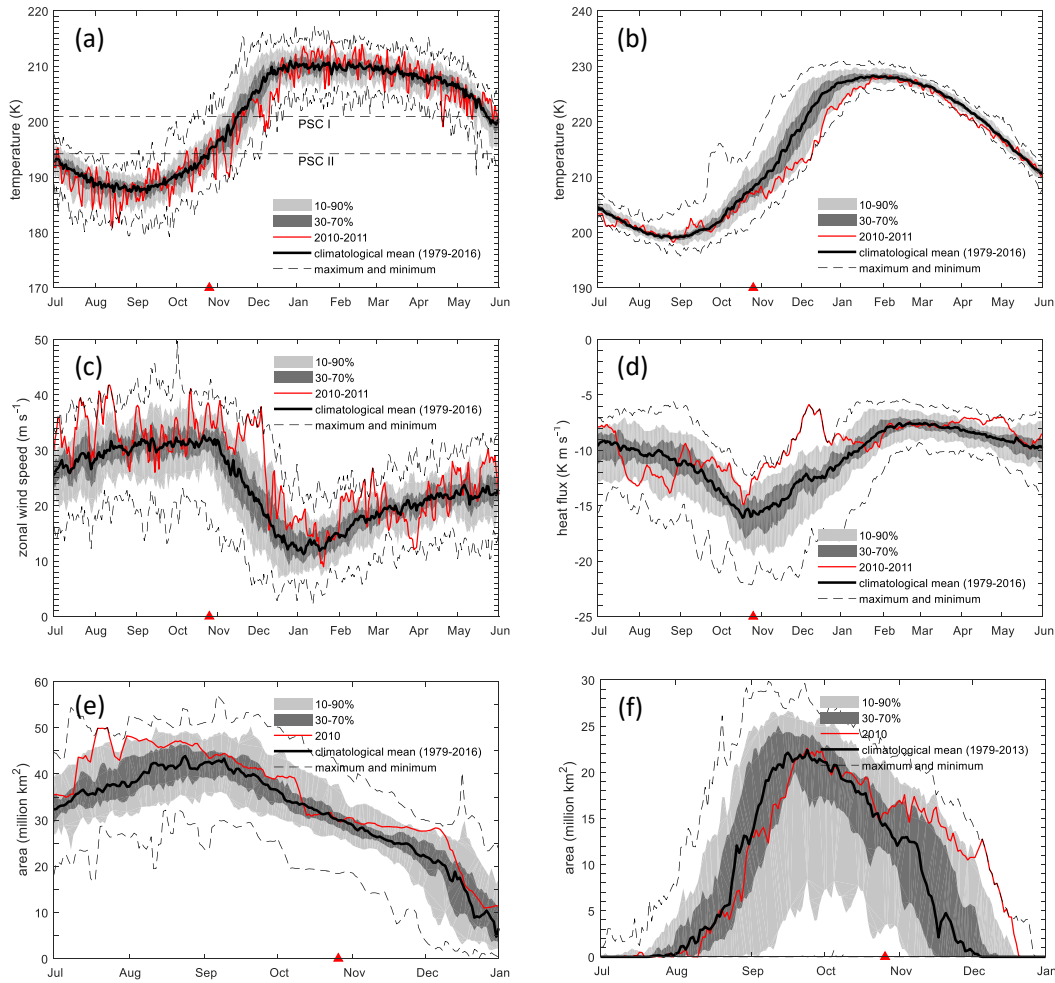


Figure 1: (a) Minimum temperature south of 50°S at 150 hPa; (b) temperature averaged over the polar cap for latitudes south of 60°S at 150 hPa; (c) zonal wind speed at 60°S at 150 hPa; (d) eddy heat flux averaged between 45°S and 75°S for the 45-day period prior to the date indicated at 150 hPa; (e) the area of the polar vortex for 1 July–31 December 2010 on the 460 K isentropic surface; (f) ozone hole area for 1 July 2010–31 December 2010. Temperatures for PSC existence in (a) are determined by assuming a nitric acid concentration of 6 ppbv and a water vapor concentration of 4.5 ppmv. (a)–(f) are based on [Modern-Era Retrospective analysis for Research and Applications reanalysis version 2](#) (MERRA2) data ([Bosilovich et al., 2015](#)). The ozone hole area in (f) is determined from OMI ozone satellite measurements ([Levelt et al., 2006](#)). The red triangles indicate the time of the Merapi eruption.

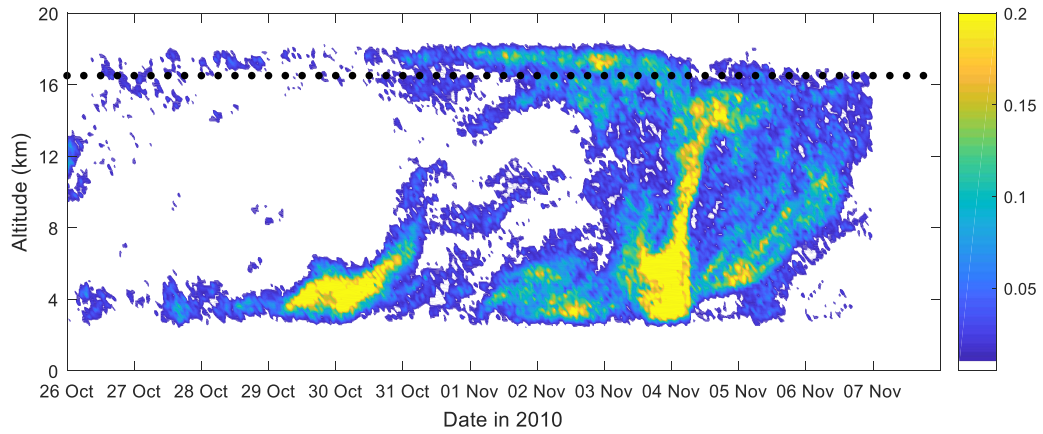


Figure 2: Merapi SO₂ emission time series (unit: kg m⁻¹ s⁻¹) derived from AIRS measurements using a backward trajectory approach (see text for details). The emission data are binned every 1 h and 0.2 km. The ticks for the horizontal axis mark 0 UTC on each day. Black dots denote the height of the thermal tropopause (based on the ERA–Interim reanalysis).

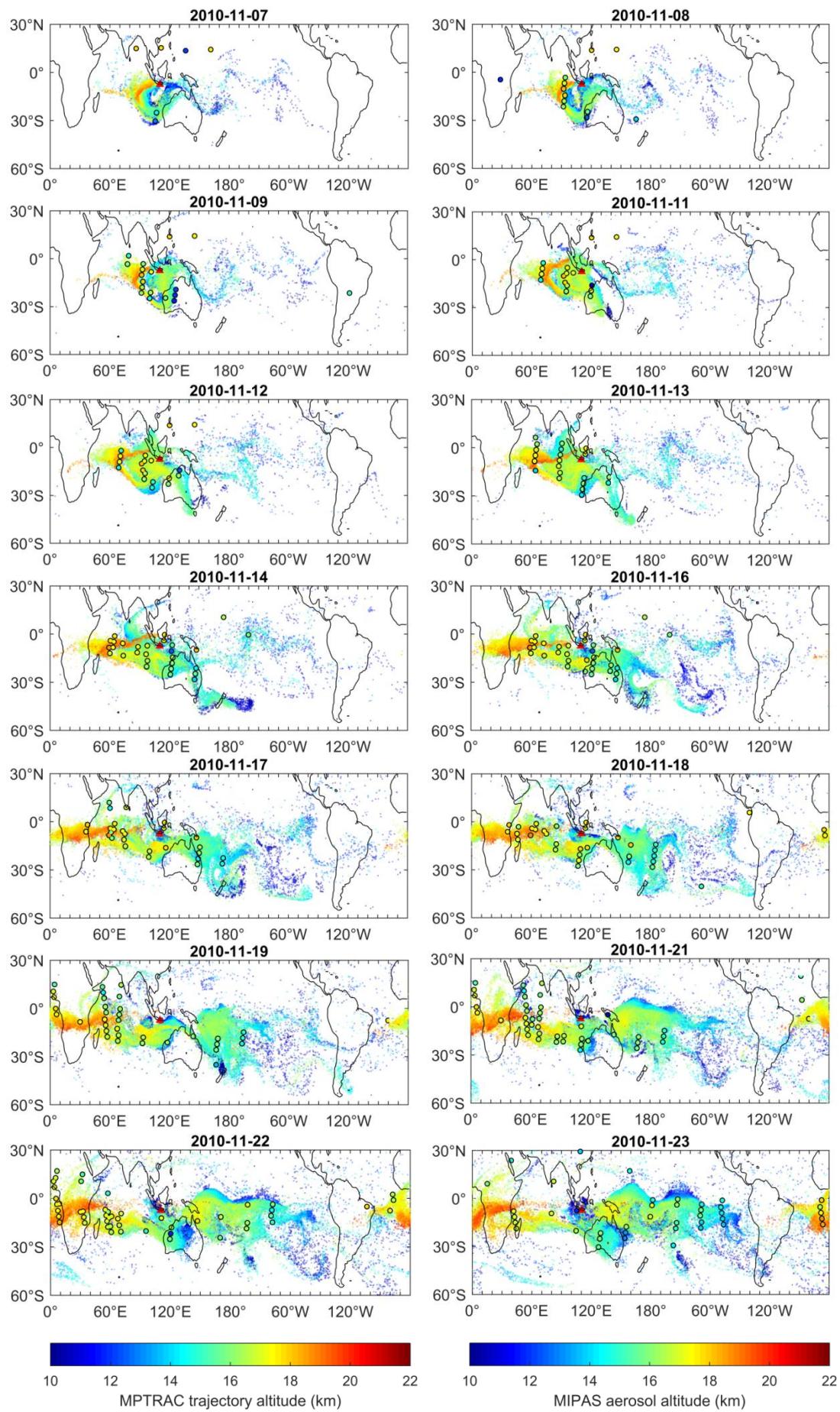


Figure 3: Distribution of the volcanic plume (showing only air parcels higher than 10 km, shading) from MPTRAC simulations (shown for 00:00UTC on selected days) and MIPAS aerosol detections ($ACI < 7$) within ± 6 h (color-filled circles). The altitudes of all

air parcels, regardless of their SO₂ values, are shown. The red triangle denotes the location of Mount Merapi.

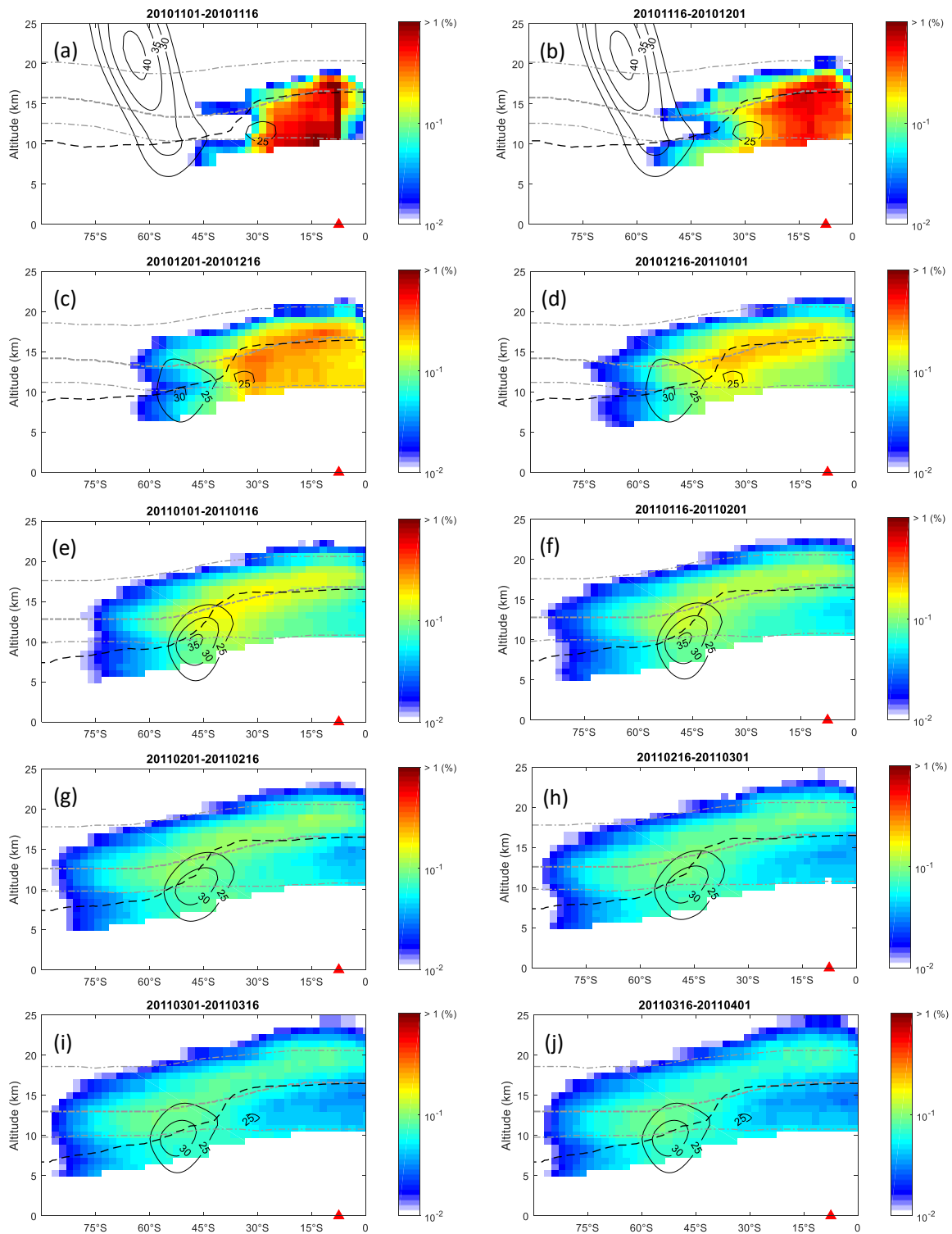


Figure 4: Percentage (%) of air parcels in proportion to the total number of air parcels released in the Lagrangian forward simulation, overlaid with monthly mean zonal winds (black contours), the thermal tropopause (black dashed line), the 380 K potential temperature isoline (thick gray dashed line) and 350 and 480 K potential temperature isolines (thin gray dashed lines). Results are binned every 2° in latitude and 1 km in altitude. The red triangle denotes the latitude of the Mount Merapi. Please see title of each figure for the time period covered.

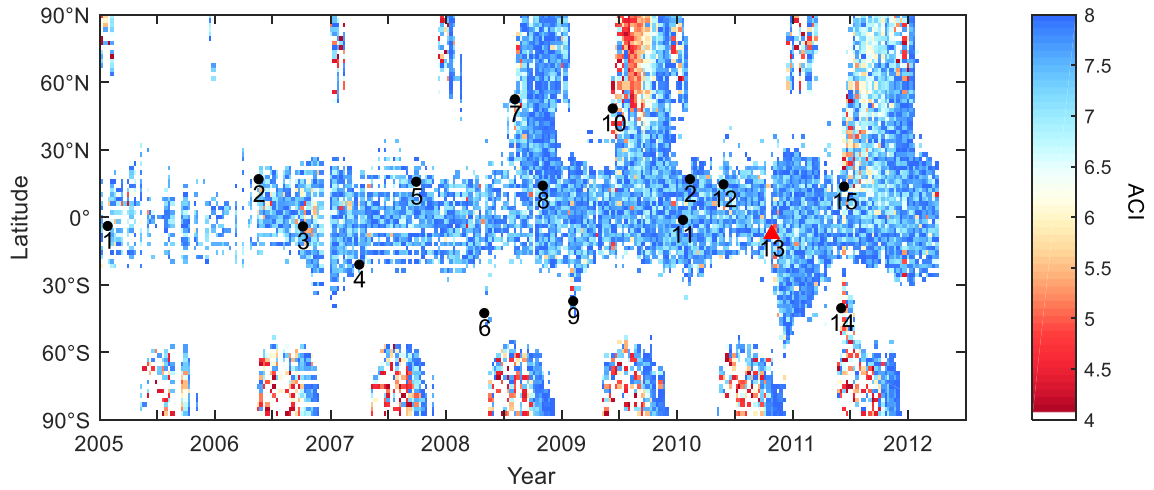


Figure 5: Median value of MIPAS ACI detections between 12–18 km (bin size: 10 days and 2° in latitude) from January 2005 to April 2012. Only ACI values from 4 to 8 are shown. The red triangle indicates the eruption of Mount Merapi (No. 13). The black filled circles indicate 1 Manam, 2 Soufriere Hills, 3 Tavurvur (Rabaul), 4 Piton de la Fournaise, 5 Jebel at Tair, 6 Chaitén, 7 Kasatochi, 8 Dalaffilla, 9 Australian bushfire, 10 Sarychev Peak, 11 Nyamuragira, 12 Pacaya, 14 Puyehue-Cordón Caulle, 15 Nabro.

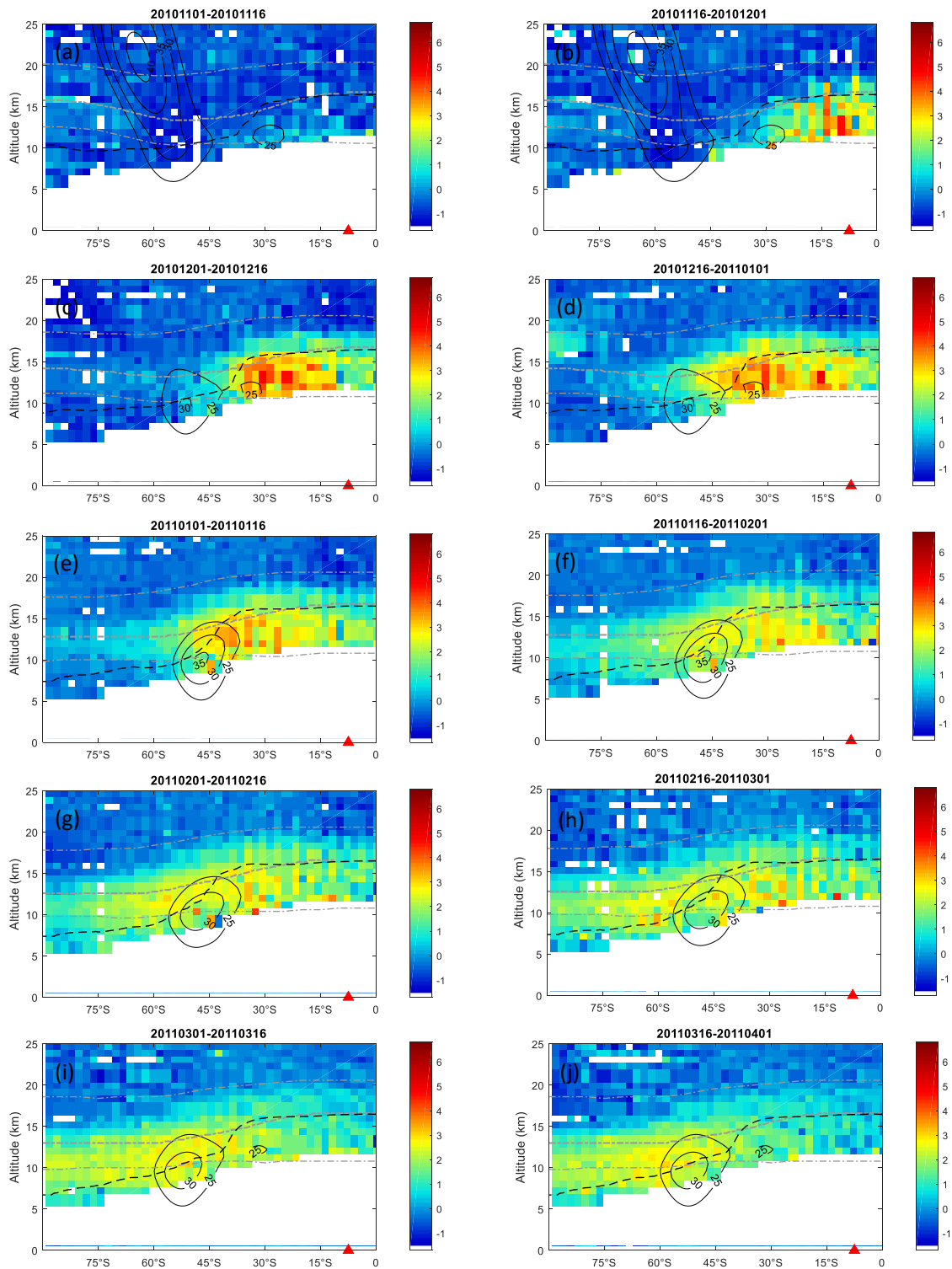


Figure 6: The change of aerosol load MIPAS ACI values after the eruption of Merapi in 2010, overlaid with monthly mean zonal winds (black contours), the thermal tropopause (black dashed line), the 380 K potential temperature isotherm (thick gray dashed line) and 350 and 480 K potential temperature isotherms (thin gray dashed lines). Positive values indicate an increase of the aerosol load and negative values indicate a decrease of the aerosol load. Results are binned every 2° in latitude and 1 km in altitude. The red triangle denotes the latitude of the Mount Merapi. Please see title of each figure for the time period covered.

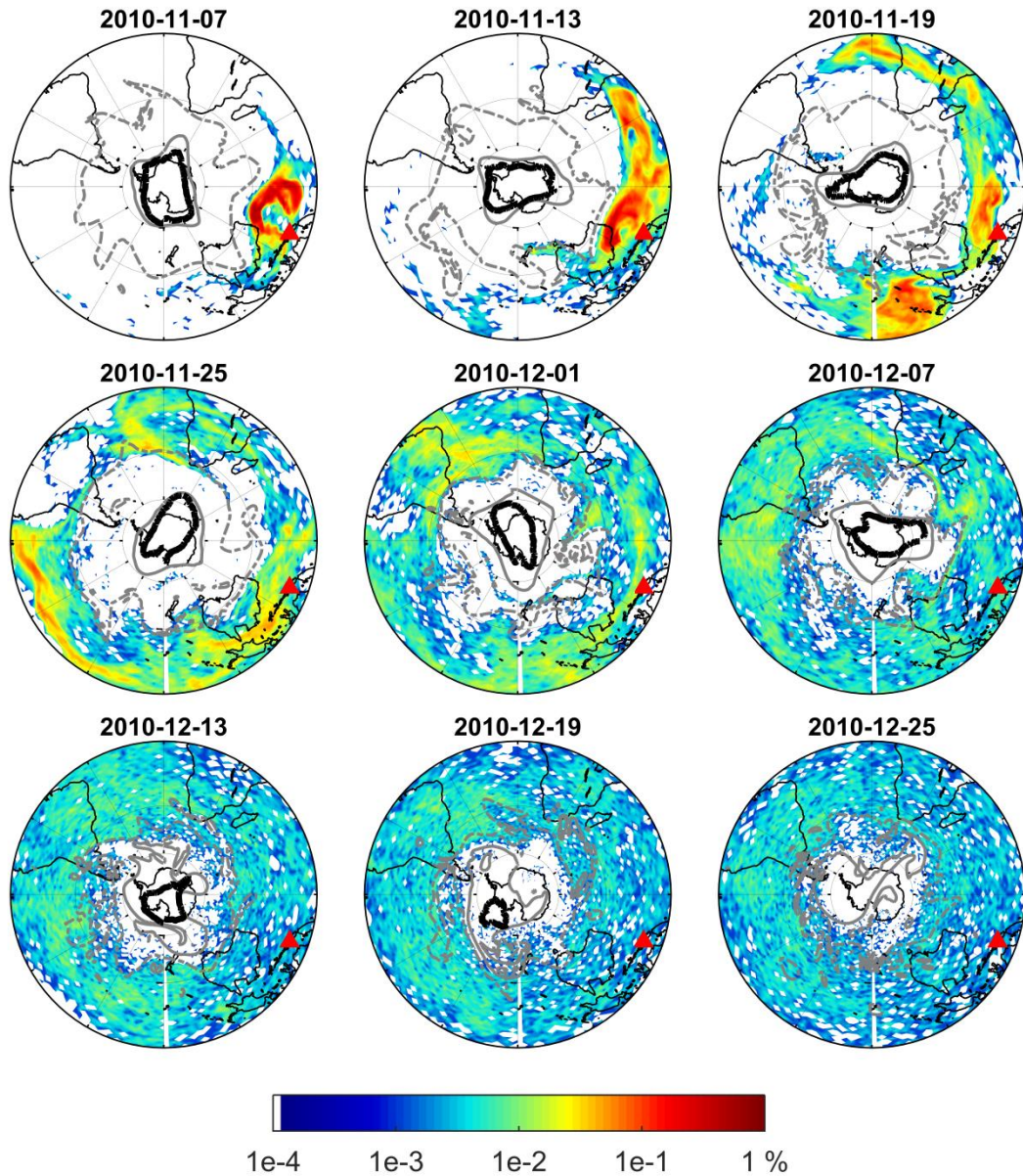


Figure 7: Percentage (%) of air parcels between the isentropic surfaces of 350 and 480 K in proportion to the total number of air parcels released in the Lagrangian forward simulation. All results are at 12:00 UTC on selected dates and binned every 2° in longitude and 1° in latitude. The black contours indicate the 220 DU contour lines of daily mean ozone column density provided by OMI. PV contours marked with gray dashed and solid lines show PV boundaries on the 350 and 480 K isentropic surfaces respectively (Kunz et al., 2015). The red triangle denotes the location of Mount Merapi.

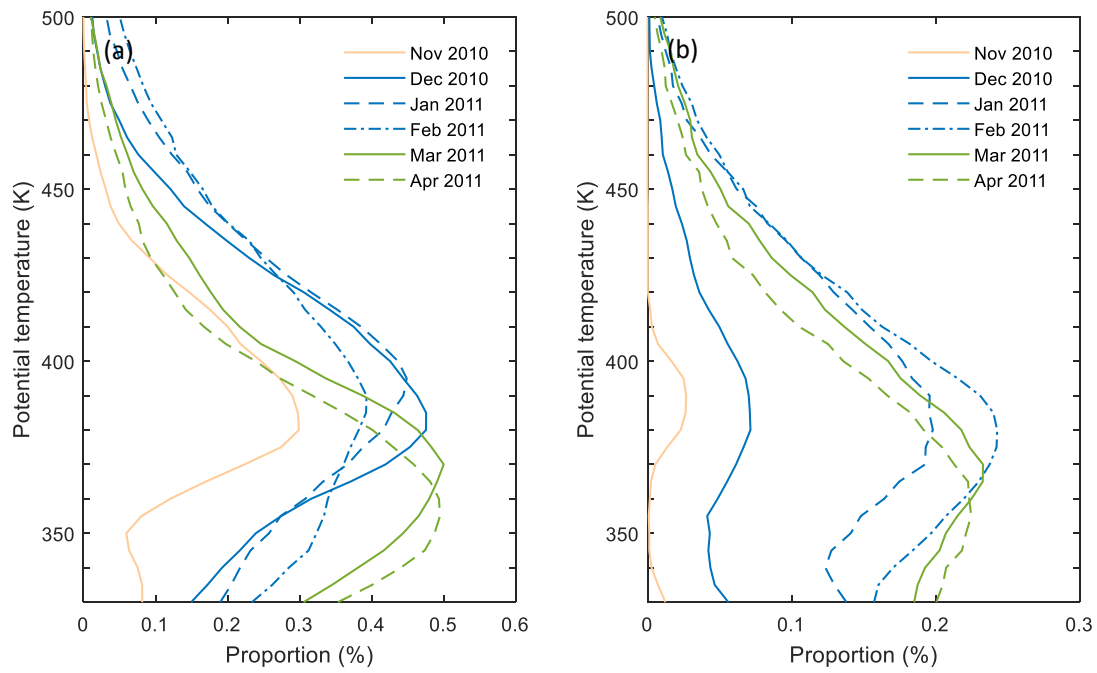


Figure 8: (a) Proportion (%) of the air parcels poleward of the PV-based transport boundaries at the end of each month; (b) proportion (%) of the air parcels south of 60°S.

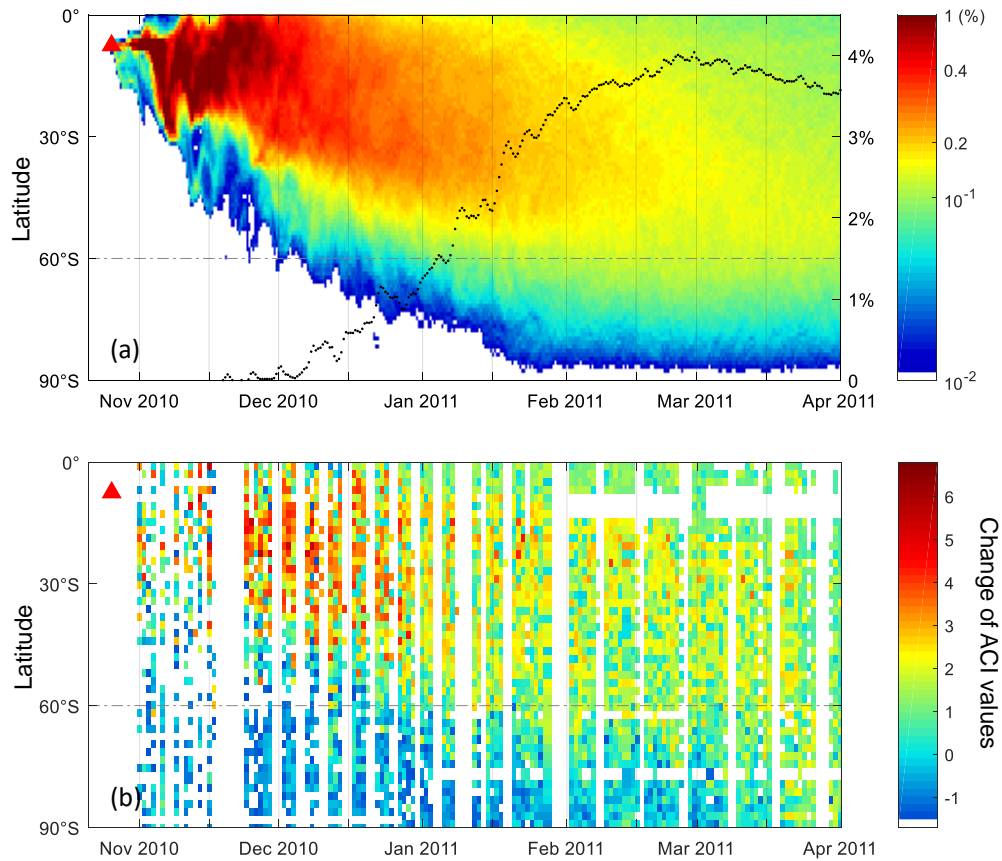


Figure 9: Time and latitude evolution of the (a) percentage (%) of air parcels between the isentropic surfaces of 350 and 480 K from the Lagrangian simulations (shading, only percentages larger than 0.05% are shown; bin size: 12h and 1 ° in latitude) and the proportion (%) of air parcels south of 60 °S (black dots); (b) the change of MIPAS measured aerosol load ACI values after the eruption of Merapi in 2010 between 350 and 480 K. Positive values indicate an increase and negative values indicate a decrease of the aerosol load (bin size: 24h and 2 ° in latitude). The red triangle denotes the time and latitude of the Merapi eruption.

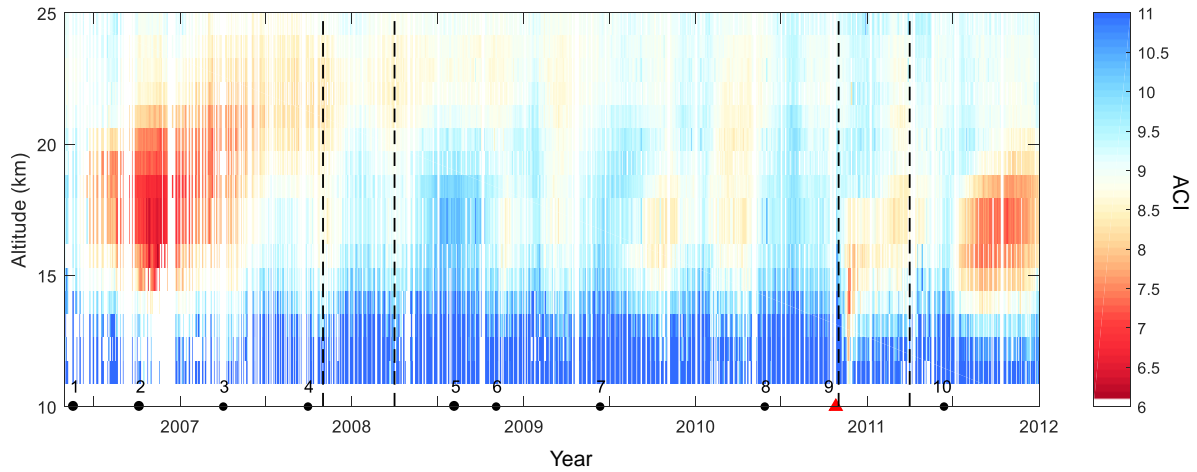


Figure A1: MIPAS 9-day running median of ACI between 10°N and 10°S from May 2006 to December 2011. The dashed vertical lines indicate the reference state from November 2007 to March 2008, and the investigation period for the Merapi eruption from November 2010 to March 2011. The red triangle indicates the time of the Merapi eruption (No. 9). The black dots indicate 1 Soufriere Hills, 2 Tavurvur (Rabaul), 3 Piton de la Fournaise, 4 Jebel at Tair, 5 Kasatochi, 6 Dalaffilla, 7 Sarychev, 8 Pacaya, 10, Nabro.

1 **Long-range transport of volcanic aerosol from the 2010 Merapi** 2 **tropical eruption to Antarctica**

3 Xue Wu^{1,2}, Sabine Griessbach¹, Lars Hoffmann¹

4 ¹Jülich Supercomputing Centre, Forschungszentrum Jülich, Jülich, Germany

5 ²Key Laboratory of Middle Atmosphere and Global Environment Observation, Institute of Atmospheric
6 Physics, Chinese Academy of Sciences, Beijing, China

7 *Correspondence to:* Xue Wu (xu.wu@fz-juelich.de)

8 **Abstract**

9 Volcanic sulfate aerosol is an important source of sulfur for Antarctica where other local sources of
10 sulfur are rare. Mid- and high latitude volcanic eruptions can directly influence the aerosol budget of the
11 polar stratosphere. However, tropical eruptions can also enhance polar aerosol load following
12 long-range transport. In the present work, we analyze the volcanic plume of a tropical eruption, Mount
13 Merapi in October 2010, and investigate the transport pathway of the volcanic aerosol from the tropical
14 tropopause layer (TTL) to the lower stratosphere over Antarctica. We use the Lagrangian particle
15 dispersion model Massive-Parallel Trajectory Calculations (MPTRAC) and Atmospheric Infrared
16 Sounder (AIRS) SO₂ measurements to reconstruct the altitude-resolved SO₂ injection time series during
17 the explosive eruption period and simulate the transport of the volcanic plume using the MPTRAC
18 model. AIRS SO₂ and aerosol measurements, the aerosol-cloud-index values provided by Michelson
19 Interferometer for Passive Atmospheric Sounding (MIPAS) are used to verify and complement the
20 simulations. The Lagrangian transport simulation of the volcanic plume is compared with MIPAS
21 aerosol measurements and shows good agreement. Both the simulations and the observations presented
22 in this study suggest that volcanic plumes from the Merapi eruption were transported to the south of
23 60°S one month after the eruption and even further to Antarctica in the following months. This
24 relatively fast meridional transport of volcanic aerosol was mainly driven by quasi-horizontal mixing
25 from the TTL to the extratropical lower stratosphere and the most of the quasi-horizontal mixing
26 occurred between the isentropic surfaces of 360 to 430 K. When the plume went to Southern
27 Hemisphere high latitudes, the polar vortex was displaced from the South Pole, so that the volcanic
28 plume was carried to the South Pole without penetrating the polar vortex. Although only 4% of the
29 sulfur injected by the Merapi eruption was transported into the lower stratosphere south of 60°S, the
30 Merapi eruption contributed up to 8800 tons of sulfur to the Antarctic lower stratosphere. This indicates

31 that the long-range transport under favorable meteorological conditions enables a moderate tropical
32 volcanic eruption to be an important remote source of sulfur for the Antarctic stratosphere.

33 **1 Introduction**

34 Over the past two decades, multiple volcanic eruptions injected sulfur into the upper troposphere and
35 lower stratosphere, which has been the dominant source of the stratospheric sulfate aerosol load
36 (Vernier et al., 2011), preventing the background level from other sources ever being seen (Solomon et
37 al., 2011). Stratospheric sulfate aerosol mainly reflects solar radiation and absorbs infrared radiation,
38 causing cooling of the troposphere and heating of the stratosphere. Stratospheric sulfate aerosol also has
39 an impact on chemical processes in the lower stratosphere (Jäger and Wege, 1990; Solomon et al.,
40 1993), in particular on polar ozone depletion (e.g. McCormick et al., 1982; Solomon et al., 1986, 1999,
41 2016; Portmann et al., 1996; Tilmes et al., 2008; Drdla and Müller, 2012). The presence of H₂SO₄ in the
42 polar stratosphere in combination with cold temperatures facilitates the formation of polar stratospheric
43 clouds (PSCs), which increase heterogeneous ozone depletion chemistry (Solomon et al., 1999; Zuev et
44 al., 2015). Recent healing of Antarctic ozone depletion was constantly disturbed by moderate volcanic
45 eruptions (Solomon et al., 2016). Mid- and high latitude explosive volcanic eruptions may directly
46 influence the polar stratosphere and may have an effect on ozone depletion in the next austral spring.
47 For example, the aerosol plume from the Calbuco eruption in 2015, including various volcanic gases,
48 penetrated the polar vortex and caused an Antarctic ozone hole with the largest daily averaged size on
49 record in October 2015 (Solomon et al., 2016; Ivy et al., 2017; Stone et al., 2017).

50 Usually, Antarctica is relatively free of local aerosol sources, but aerosol from low latitudes can reach
51 Antarctica through long-range transport (Sand et al., 2017). Most of the sulfate found in ice cores can be
52 attributed to volcanic eruptions (Mazzera et al., 2001; Gao et al., 2007; Sigl et al., 2015). Measurements
53 of enhanced aerosol in the lower Antarctic stratosphere right above the tropopause were made in
54 October/November 1983, 1984 and 1985. These enhanced aerosol number concentrations were
55 attributed to aerosol transported to Antarctica from the eruption of the tropical volcano El Chichón in
56 1982 (Hofman and Rosen, 1985; Hofmann et al., 1988). Model results indicated that numerous
57 moderate eruptions affected ozone distributions over Antarctica, including the Merapi tropical eruption
58 in October 2010 (Solomon et al., 2016). However, due to the limit of spatial and temporal resolution of
59 satellite data and in-situ observations, it is difficult to investigate transport process as well as the
60 influence of the location of the eruption, the plume height and the background meteorological

61 conditions. Thus the transport mechanism is not well represented in present global climate models and
62 the uncertainties of the modeled AOD in polar regions are large (Sand et al., 2017).

63 Mount Merapi (7.5 °S, 110.4 °E, elevation: 2930 m) is an active stratovolcano located in Central Java,
64 Indonesia. Merapi has a long record of eruptive activities. The most recent large eruption with a
65 volcanic explosivity index of 4 occurred between 26 October and 7 November 2010 (Pallister et al.,
66 2013), with SO₂ emission rates being a few orders of magnitude higher than previous eruptions.
67 Following the Merapi eruption in 2010, evidence of poleward transport of sulfate aerosol towards the
68 Southern Hemisphere high latitudes was found in time series of aerosol measurements by the Michelson
69 Interferometer for Passive Atmospheric Sounding (MIPAS) (Günther et al., 2018) and Cloud-Aerosol
70 Lidar with Orthogonal Polarization (CALIOP) (Khaykin et al., 2017; Friberg et al., 2018) .

71 There are three main ways for transport out of the tropical tropopause layer (TTL): the deep and shallow
72 branches of the Brewer-Dobson circulation (BDC) and horizontal mixing (Vogel et al., 2011). There is
73 considerable year-to-year seasonal variability in the amount of irreversible transport from the tropics to
74 high latitudes, which is related to the phase of the quasi-biennial oscillation (QBO) and the state of the
75 polar vortex (Olsen et al., 2010). The BDC plays a large role in determining the distributions of many
76 constituents in the extratropical lower stratosphere. The faster quasi-horizontal transport between the
77 tropics and polar regions also significantly contributes to determining these distributions. The efficiency
78 of transporting constituents quasi-horizontally depends on wave breaking patterns and varies with the
79 time of the year (Toohey et al., 2011; Wu et al., 2017). Better knowledge of the transport pathways and
80 an accurate representation of volcanic sulfur injections into the upper troposphere and lower
81 stratosphere (UTLS) are key elements for estimating the global stratospheric aerosol budget, the cooling
82 effects and the ozone loss linked to volcanic activity.

83 The aim of the present study is to reveal the transport process and the influence of meteorological
84 conditions by combining satellite observations with model simulations in a case study. We investigate
85 the quasi-horizontal transport by tracing the volcanic plume of the Merapi eruption from the tropics to
86 Antarctica and quantifying its contribution to the sulfur load in the Antarctic lower stratosphere. In Sect.
87 2, the new Atmospheric Infrared Sounder (AIRS) SO₂ measurements (Hoffmann et al., 2014), the
88 MIPAS aerosol measurements (Griessbach et al., 2016) and the method for reconstructing the SO₂
89 injection time series of the Merapi eruption are introduced. In Sect. 3 the results are presented: first, the
90 reconstructed time series of the Merapi eruption is discussed; second, the dispersion of the Merapi
91 plume is investigated using long Lagrangian forward trajectories initialized with the reconstructed SO₂
92 time series; third, the simulation results are compared with MIPAS aerosol measurements and the plume

93 dispersion is investigated using MIPAS aerosol detections. In Sect.4 the results are discussed and the
94 conclusions are given in Sect. 5.

95 **2 Satellite data, model and method**

96 **2.1 MIPAS aerosol measurements**

97 MIPAS (Fischer et al., 2008) is an infrared limb emission spectrometer aboard the European Space
98 Agency's (ESA's) Envisat, which provided nearly 10 years of measurements from July 2002 to April
99 2012. MIPAS spectral measurements cover the wavelength range from 4.15 to 14.6 microns. The
100 vertical coverage of MIPAS nominal measurement mode during the optimized resolution phase from
101 January 2005 to April 2012 was 7–72 km. The field of view of MIPAS was about 3 km×30 km
102 (vertically×horizontally) at the tangent point. The extent of the measurement volume along the line of
103 sight was about 300 km, and the horizontal distance between two adjacent limb scans was about 500 km.
104 On each day, ~14 orbits with ~90 profiles per orbit were measured. From January 2005 to April 2012,
105 the vertical sampling grid spacing between the tangent altitudes was 1.5 km in the UTLS and 3 km at
106 altitudes above. In 2010 and 2011, MIPAS measured for 4 days in nominal mode followed alternately
107 by one day in middle atmosphere mode or upper atmosphere mode. In this study, we focussed on
108 measurements in the nominal mode.

109 For the aerosol detection, we used the MIPAS altitude-resolved aerosol-cloud-index (ACI) as
110 introduced by Griessbach et al. (2016) to compare with the model simulations and to analyze the
111 poleward transport of the Merapi volcanic plume.

112 ACI is the maximum value of the cloud index (CI) and aerosol index (AI):

$$ACI = \max(CI; AI), \quad (1)$$

113 The CI is an established method to detect clouds and aerosol with MIPAS. The CI is the ratio between
114 the mean radiances around the 792 cm⁻¹, where a CO₂ line is located and the atmospheric window
115 region around 833 cm⁻¹ (Spang et al., 2001):

$$CI = \frac{\bar{I}_1([788.25, 796.25 \text{ cm}^{-1}])}{\bar{I}_2([832.31, 834.37 \text{ cm}^{-1}])}, \quad (2)$$

116 where \bar{I}_1 and \bar{I}_2 are the mean radiances of each window. The AI is defined as the ratio between the mean
117 radiance around the 792 cm⁻¹ CO₂ band and the atmospheric window region between 960 and 961 cm⁻¹:

$$AI = \frac{\bar{I}_1([788.25, 796.25 \text{ cm}^{-1}])}{\bar{I}_3([960.00, 961.00 \text{ cm}^{-1}])}, \quad (3)$$

118 where \bar{I}_1 and \bar{I}_3 are the mean radiance of each window.

119 The ACI is a continuous unitless value. Small ACI values indicate a high cloud or aerosol particle load
120 and large values indicate a smaller cloud or aerosol particle load. For the CI, Sembhi et al. (2012)
121 defined a set of variable (latitude, altitude and season) thresholds to discriminate between clear and
122 cloudy air. The most advanced set of altitude and latitude dependent thresholds allows for the detection
123 of aerosol and clouds with infrared extinction coefficients larger than 10^{-5} km^{-1} . For the ACI, a
124 comparable sensitivity is achieved when using a fixed threshold value of 7 (Griessbach et al. 2016).
125 Variations in the background aerosol are also visible with larger ACI values.

126 To remove ice clouds and volcanic ash from the MIPAS aerosol measurements, we first separated the
127 data into clear air ($\text{ACI} > 7$) and cloudy air ($\text{ACI} \leq 7$). Then we applied the ice cloud filter (Griessbach et
128 al., 2016) and the volcanic ash and mineral dust filter (Griessbach et al., 2014) to the cloudy part and
129 removed all ice or ash detections. However, since the ice and ash cloud filters are not sensitive to
130 non-ice PSCs, the resulting aerosol retrieval results still contain non-ice PSCs (supercooled ternary
131 solutions and nitric acid trihydrate). We keep the non-ice PSCs in the MIPAS retrieval results in this
132 study to show the temporal and spatial extent of the PSCs, when and where the identification of
133 volcanic is not possible.

134 **2.2 AIRS**

135 AIRS (Aumann et al., 2003) is an infrared nadir sounder with across-track scanning capabilities aboard
136 the National Aeronautics and Space Administration's (NASA's) Aqua satellite. Aqua was launched in
137 2002 and operates in a nearly polar Sun-synchronous orbit at about 710 km with a period of 98 min.
138 AIRS provides nearly continuous measurement coverage with 14.5 orbits per day and with a swath width
139 of 1780 km it covers the globe almost twice a day. The AIRS footprint size is $13.5 \text{ km} \times 13.5 \text{ km}$ at nadir
140 and $41 \text{ km} \times 21.4 \text{ km}$ for the outermost scan angles respectively. The along-track distance between two
141 adjacent scans is 18 km. The AIRS measurements provide good horizontal resolution and make it ideal
142 for observing the fine filamentary structures of volcanic SO_2 plumes.

143 In this study, we use an optimized SO_2 index (SI, unit: K) to estimate the amount of SO_2 injected into the
144 atmosphere by the Merapi eruption in 2010. The SI is defined as the brightness temperature differences
145 in the $7.3 \mu\text{m}$ SO_2 waveband.

$$146 \quad \text{SI} = \text{BT} \left(1412.87 \text{ cm}^{-1} \right) - \text{BT} \left(1371.52 \text{ cm}^{-1} \right), \quad (1)$$

147 where BT is the brightness temperature measured at wavenumber ν . This SI is more sensitive to low
148 concentrations and performs better on suppressing background interfering signals than the SI provided in

149 the AIRS operational data products. It is an improvement of the SI definition given by Hoffmann et al.
150 (2014) by means of a better choice of the background channel (selecting 1412.87 cm^{-1} rather than
151 1407.2 cm^{-1}). The SI increases with increasing SO_2 column density and it is most sensitive to SO_2 at
152 altitudes above 3-5 km. SO_2 injections into the lower troposphere are usually not detectable in the infrared
153 spectral region because the atmosphere gets opaque due to the water vapor continuum. A detection
154 threshold of 1 K was used in this study to identify the Merapi SO_2 injections. AIRS detected the Merapi
155 SO_2 cloud from 3 November to 15 November 2010.

156 **2.3 MPTRAC model and reconstruction of the volcanic SO_2 injection time series of the Merapi** 157 **eruption**

158 In this study, we use the highly scalable Massive-Parallel Trajectory Calculations (MPTRAC) to
159 investigate the volcanic eruption event. In the MPTRAC model, air parcel trajectories are calculated
160 based on numerical integration using wind fields from global meteorological reanalyses (Hoffmann et
161 al., 2016; Rößler et al., 2018). The MPTRAC model can be driven by reanalyses, e.g., ERA-Interim,
162 Modern-Era Retrospective Analysis for Research and Applications (MERRA) and National Centers for
163 Environmental Prediction (NCEP)/National Center for Atmospheric Research (NCAR). Hoffmann et al.
164 (2016) showed that ERA-interim data provides the best trade-off between accuracy and computing time.
165 So in this study, our calculations are based on ERA-interim data.

166 Diffusion is modeled by uncorrelated Gaussian random displacements of the air parcels with zero mean
167 and standard deviations $\sigma_x = \sqrt{D_x \Delta t}$ (horizontally) and $\sigma_z = \sqrt{D_z \Delta t}$ (vertically). D_x and D_z are the
168 horizontal and vertical diffusivities respectively, and Δt is the time step for the trajectory calculations.
169 For the Merapi simulation, D_x and D_z were set to $50 \text{ m}^2 \text{ s}^{-1}$ and $0 \text{ m}^2 \text{ s}^{-1}$ in the troposphere and $0 \text{ m}^2 \text{ s}^{-1}$
170 and $0.1 \text{ m}^2 \text{ s}^{-1}$ in the stratosphere, respectively. In addition, sub-grid scale wind fluctuations, which are
171 particularly important for long-range simulations, are simulated by a Markov model (Stohl et al., 2005;
172 Hoffmann et al., 2016). Loss processes of chemical species, SO_2 in our case, are simulated based on an
173 exponential decay of the mass assigned to each air parcel. In the stratosphere, a constant half lifetime of
174 7 days was assumed for SO_2 . Considering that the Merapi eruption occurred in the humid tropics with a
175 high concentration of hydroxyl radical, a half lifetime of 2.5 days was assumed for the troposphere.

176 To estimate the time- and altitude-resolved SO_2 injections, we follow the approach of Hoffmann et al.
177 (2016) and Wu et al. (2017) and use backward trajectories calculated with the MPTRAC model together
178 with AIRS SO_2 measurements. Measurements from 3 to 7 November 2010 were used to estimate the
179 SO_2 injection during the explosive eruption. Since the AIRS measurements do not provide altitude

180 information, we established a column of air parcels at each AIRS SO₂ detection. The vertical range of
181 the column was set to 0–25 km, covering the possible vertical dispersion range of the SO₂ plume in the
182 first few days. The AIRS footprint size varies between 14 and 41 km, hence in the horizontal direction,
183 we chose an average of 30 km as the full width at half maximum for the Gaussian scatter of the air
184 parcels. In our simulations, a fixed total number of 100,000 air parcels was assigned to all air columns
185 and the number of air parcels in each column was scaled linearly proportional to the SO₂ index. Then
186 backward trajectories were calculated for all air parcels, and trajectories that were at least 2 days but no
187 more than 5 days long and that passed the volcano domain were recorded as emissions of Merapi. The
188 volcano domain was defined by means of a search radius of 75 km around the location of the Merapi
189 and 0–20 km in the vertical direction, covering all possible injection heights. Sensitivity experiments
190 have been conducted to optimize these pre-assigned parameters to obtain the best simulation results.
191 Our estimates of the Merapi SO₂ injection are shown in Sect. 3.

192 Starting with the reconstructed altitude-resolved SO₂ injection time series, the transport of the Merapi
193 plume is simulated for 6 months. The trajectory calculations are driven by the ERA–Interim data (Dee
194 et al., 2011) interpolated on a 1° × 1° horizontal grid on 60 model levels with the vertical range
195 extending from the surface to 0.1 hPa. The ERA–Interim data are provided at 00, 06, 12 and 18 UTC.
196 Outputs of model simulations are given every 3 hours at 00, 03, 06, 09, 12, 15, 18 and 21 UTC. The
197 impact of different meteorological analyses on MPTRAC simulations was assessed by Hoffmann et al.
198 (2016, 2017). In both studies the ERA–Interim data showed good performance.

199 **3 Results**

200 **3.1 Meteorological background conditions in Antarctica**

201 The Merapi eruption in October 2010 occurred during the seasonal transition from austral spring to
202 summer when the polar vortex typically weakens and the ozone hole shrinks. The poleward transport
203 from the tropics to the polar region is known to be modulated by the phase of the QBO and the state of
204 the polar vortex. Just before the Merapi eruption in 2010, the QBO switched from the easterly phase to
205 the westerly phase. The westerly phase of the QBO promotes meridional transport from the tropics to
206 subtropics, especially into the winter hemisphere (O'Sullivan and Dunkerton, 1997; Shuckburgh et al.,
207 2001; Jäger, 2005). However, it also results in zonal wind acceleration at the high latitudes (Holton and
208 Tan, 1980; Watson and Gray, 2014) and a less dynamically disturbed polar vortex (Baldwin and

209 Dunkerton, 1999; Anstey and Shepherd, 2014), which will make it less possible for air parcels to
210 penetrate the polar vortex.

211 Figure 1 depicts the meteorological conditions at the polar lower stratosphere (150hPa, ~12km) after the
212 eruption. The minimum temperature south of 50 °S (Fig. 1a) was much lower than the climatological
213 mean during mid-November to mid-December but still higher than the low temperature necessary for
214 the existence of PSCs. The polar mean temperature in Fig. 1b, defined as the temperature averaged over
215 latitudes south of 60 °S, stayed lower than the climatological mean from November 2010 until February
216 2011. Corresponding to the low temperatures, the average zonal wind speed at 60 °S (Fig. 1c) was
217 significantly larger than the climatological mean value from November 2010 to mid-January 2011. The
218 eddy heat flux in Fig. 1d is the product of meridional wind departures and temperature departures from
219 the respective zonal mean values. A more negative value of the eddy heat flux indicates that wave
220 systems are propagating into the stratosphere and are warming the polar region (Edmon et al., 1980;
221 Newman and Nash, 2000). There is a strong anticorrelation between temperature and the 45-day
222 average of the eddy heat flux lagged prior to the temperature. Compared with the climatological mean
223 state, the polar vortex was more disturbed during mid-July to end of August, but from mid-October to
224 late November, the heat flux was much smaller than the long-term average, which meant a reduction in
225 dynamical disturbances. Considering the temperature, the subpolar wind speed and the heat flux, the
226 polar vortex was colder and stronger in November and early December 2010 than it was at the same
227 time in other years (see Fig. 1e). Consistent with the large wind speed and low temperature, the polar
228 vortex was stable after the Merapi eruption until early December 2010. Afterwards, it shrunk abruptly
229 and was destructed in by mid-January 2011. In accordance with the strength of the polar vortex, in
230 November and early December 2010 the ozone hole area in Fig. 1f, defined as the region of ozone
231 values below 220 Dobson Units (DU) located south of 40 °S, was larger than the climatological mean.
232 Meanwhile, the low polar mean temperature and stable polar vortex resulted in a long-lasting ozone
233 hole, which disappeared in the last week of December. The polar vortex broke down by mid-January
234 2011 when the subpolar wind speed decreased below 15 m/s (Fig. 1c).

235 **3.2 Merapi eruption and SO₂ injection time series**

236 According to the chronology of the Merapi eruption that combined satellite observations from AIRS, the
237 Infrared Atmospheric Sounding Interferometer (IASI), the Ozone Monitoring Instrument (OMI) and a
238 limited number of Ground-based ultra-violet Differential Optical Absorption Spectroscopy (DOAS)
239 measurements (Surono et al., 2012), the explosive eruption first occurred between 10:00 and 12:00 UTC

240 on 26 October and this eruption generated an ash plume that reached 12 km altitude. A period of
241 relatively small explosive eruptions continued from 26 October to 31 October. On 3 November, the
242 eruptive intensity increased again accompanied by much stronger degassing and a series of explosions.
243 The intermittent explosive eruptions occurred during 4–5 November with the climactic eruption on 4
244 November, producing an ash column that reached up to 17 km altitude. From 6 November, explosive
245 activity decreased slowly and the degassing declined.

246 Figure 2 shows the time- and altitude-resolved SO₂ injections of the Merapi eruption retrieved using the
247 AIRS SO₂ index data and the backward-trajectory approach. It agrees well with the chronology of the
248 Merapi eruption as outlined by Surono et al. (2012). SO₂ was injected into altitudes below 8 km during
249 the initial explosive eruptions on 26–30 October. Starting from 31 October the plume reached up to 12
250 km. During 1–2 November the SO₂ injections into altitudes below 12 km continued but the mass was
251 less than the mass at the initial phase. On 3 November the intensity increased again and peaked on 4
252 November. Before 3 November the reconstruction indicates a minor fraction of SO₂ right above the
253 tropopause. The SO₂ above the tropopause is not reported in the study Surono et al. (2012), but is quite
254 robust in our simulations. Further, CALIOP profiles from 27 October 2010 to 10 November 2010 show
255 that some dust appeared at the height from about 14 to 18 km around Mount Merapi on 2, 3, 5
256 November 2010, and between 3 and 17 km on 6 November 2010. It could be a fraction of volcanic
257 plume elevated by the updraft in the convection associated with the tropical storm Anggrek. The center
258 of the tropical storm Anggrek was on the Indian ocean about 1000 km southwest of the Mount Merapi.
259 The SO₂ mass above the tropopause is very small compared with the total SO₂ mass.

260 To study the long-range transport of the Merapi plume, we initialized 100,000 air parcels as the SO₂
261 injection time series shown in Fig. 2. A total SO₂ mass of 0.44 Tg is assigned to these air parcels as
262 provided in Surono et al. (2012). Then the trajectories are calculated forward for 6 months. Here, we
263 only considered the plume in the upper troposphere and stratosphere where the lifetime of both SO₂ and
264 sulfate aerosol is longer than their lifetime in the lower troposphere. Further, the SO₂ was converted into
265 sulfate aerosol within a few weeks (von Glasow et al., 2009; also confirmed by the AIRS SO₂ and
266 MIPAS aerosol data), and we assumed that the sulfate aerosol remained collocated with the SO₂ plume.
267 Figure 3 shows the evolution of the simulated Merapi plume and compares the plume altitudes to the
268 aerosol top altitudes measured by MIPAS between 7 and 23 November. Immediately after the eruption,
269 the majority of the plume moved towards the southwest and was entrained by the circulation of the
270 tropical storm Anggrek. After Anggrek weakened and dissipated, the majority of the plume parcels in
271 the upper troposphere moved eastward and those in the lower stratosphere moved westward. In general,

272 the altitudes of the simulated plume agree with the MIPAS measurements. The remaining discrepancies
273 of air parcel altitudes being higher than the altitudes of MIPAS aerosol detections can be attributed to
274 the fact that the MIPAS tends to underestimate aerosol top cloud altitudes, which is about 0.9 km in
275 case of low extinction aerosol layers and can reach down to 4.5 km in case of broken cloud conditions
276 (Höpfner et al., 2009).

277 **3.3 Lagrangian simulation and satellite observation of the transport of the Merapi plume**

278 The early plume evolution until about one month after the initial eruption is shown on the maps in Fig.
279 3 together with MIPAS measurements of volcanic aerosol (only aerosol detections with $ACI < 7$ are
280 shown). Within about one month after the initial eruption, the plume is nearly entirely transported
281 around the globe in the tropics, moving west at altitudes of about 17 km. The lower part of the plume,
282 below about 17 km is transported south-eastward and reaches latitudes south of 30 °S by mid-November.
283 The simulated long-term transport of the Merapi plume is illustrated in Fig. 4, showing the proportion
284 of air parcels reaching a latitude-altitude bin every half a month.

285 The simulation results show that during the first month after the eruption (Fig. 4a–b), the majority of the
286 plume was transported southward roughly along the isentropic surfaces. The most significant pathway is
287 above the core of the subtropical jet in the Southern Hemisphere. However, because of the transport
288 barrier of the polar jet during austral spring, the plume was confined to the north of 60 °S. In December
289 2010 (Fig. 4c–d), a larger fraction of the plume was transported southward above the subtropical jet
290 core and deep into the polar region south of 60 °S as the polar jet broke down. Until the end of January
291 2011, the majority of the plume entered the mid- and high latitudes in the Southern Hemisphere.
292 Substantial quasi-horizontal poleward transport from the TTL towards the extratropical lowermost
293 stratosphere (LMS) in Antarctica was found from November 2010 to February 2011 (Fig. 4a–h),
294 approximately between 350 and 480 K (~10–20 km). In March 2011 (Fig. 4i–j), the proportion of the
295 plume that went across 60 °S stopped increasing and the maxima of the proportion descended below 380
296 K. Besides this transport towards Antarctica, a slow upward transport could also be seen. The top of the
297 simulated plume was below the 480 K isentropic surface at around 18 km in Fig. 4a and then the top of
298 the plume went up to 25 km five months later in Fig. 4j. This slow upward transport was mainly located
299 in the tropics and can be attributed to the tropical upwelling.

300 MIPAS aerosol detections (ACI values) are used to compare with the simulations. Figure 5 displays the
301 time-latitude section of the median value of the MIPAS ACI within the vertical range of 12 and 18 km
302 from January 2005 to April 2012, covering the TTL and the LMS. Only ACI values from 4 to 8 are

303 shown in Fig.5. The MIPAS data show all the key events that contributed to the aerosol load in the
304 UTLS, i.e., moderate volcanic eruptions from 2005 to 2012 and one large bushfire in 2009, as well as
305 the subsequent dispersion and change of aerosol load over time. The poleward transport of aerosol from
306 the Merapi eruption in 2010, marked by the red triangle in Fig. 5, caused the most long-lasting aerosol
307 signals in the Southern Hemisphere mid- and high latitudes. The small ACI values in the winter months
308 of both hemispheres are attributed to the non-ice PSCs.

309 To show the change of aerosol load in the Southern Hemisphere due to the Merapi eruption, we first
310 removed the seasonal cycle from the MIPAS aerosol data. Therefore, we selected a time period from
311 November 2007 to March 2008 with no major SO₂ emission in the Southern Hemisphere UTLS (as
312 shown in Fig. 5) as a “reference state”. We calculated the biweekly median ACI between November
313 2010 and March 2011 and subtracted it from the biweekly ACI median of the “reference state”. The
314 results are shown in Fig. 6. Since in the MIPAS retrievals, small ACI values represent large aerosol
315 extinction coefficients and large ACI values represent small aerosol extinction coefficients, in Fig. 6 the
316 positive values indicate an increase of the aerosol load and negative values indicate a decrease of the
317 aerosol load. Reference time periods from November 2003 to March 2004 and November 2005 to
318 March 2006 were also tested and they all showed qualitatively comparable results.

319 In the first half of November, the zonal median (Fig. 6a) does not show a signal of the Merapi eruption,
320 because during the initial time period, the plume was confined to longitudes around the volcano (see Fig.
321 3), and the MIPAS tracks did not always sample the maximum concentration, so the median ACI values
322 are large (low concentration or clear air). In the second half of November, the plume was transported
323 zonally around the globe, and hence the largest aerosol increase appeared in the upper troposphere at the
324 latitude of the Mount Merapi (Fig. 6b) and then moved quasi-horizontally southward into the UTLS
325 region at ~30–40 °S (Figs. 6c–d), confirming the simulation result in Fig. 4c–d. The increase of the
326 aerosol load south of 60 °S started to become prominent after December 2010, and the poleward
327 movement is most obvious above the 350 K isentropic surface (Figs. 6e–h). The observations confirm
328 the temporal and spatial characteristics of the poleward movement of the aerosol in the simulation in
329 Fig. 4. Later in March 2011, the enhanced aerosol load in the tropics phased out and the aerosol load
330 maxima descended to around the 350 K isentropic surface.

331 However, the background aerosol level in the tropical upper troposphere and stratosphere is constantly
332 disturbed by tropical and extratropical volcanic eruptions. The reference time period we chose
333 (November 2007 to March 2008) is relatively free of large aerosol sources in the Southern Hemisphere,
334 but the aerosol load in the tropical stratosphere is already elevated by previous volcanic eruptions, e.g.,

335 Soufriere Hills (May 2006), Tavorvur (October 2006), Piton de la Fournaise (April 2007), Jebel at Tair
336 (September 2007). So the change of the aerosol load in Fig.6 underestimates the increase of aerosol load
337 in the tropical stratosphere after the Merapi eruption. The slow upward transport in the tropics shown in
338 Fig. 4 is about 7 km in five months. It is not visible in Fig. 6, but time series of the MIPAS
339 measurements in the tropical stratosphere reveals a similar upward transport trend (see Fig. A1 in the
340 appendix).

341 **3.4 Quasi-horizontal transport from the tropics to Antarctica**

342 The MPTRAC simulations and the MIPAS measurements show the transport in the “surf zone” that
343 reaches from the subtropics to high latitudes (Holton et al., 1995), where air masses are affected by both
344 fast meridional transport and the slow BDC. The reconstructed emission time series in Fig. 2 and the
345 MIPAS aerosol measurements in Figs. 3 and 6 show that the volcanic plume was injected into the TTL.
346 Hence, the main transport pathway towards Antarctica is the quasi-horizontal mixing in the lower
347 extratropical stratosphere between 350 and 480 K (see Fig. 4 and Fig. 6). Figure 7 illustrates how the
348 volcanic plume between 350 and 480 K approached Antarctica over time. Kunz et al. (2015) derived a
349 climatology of potential vorticity (PV) streamer boundaries on isentropic surfaces between 320 and
350 500K using ERA-Interim reanalyses for the time period from 1979 to 2011. This boundary is derived
351 from the maximum product of the meridional PV gradient and zonal wind speed on isentropic surfaces,
352 which identifies a PV contour that best represents the dynamical discontinuity on each isentropic
353 surface. It can be used as an isentropic transport barrier and to determine the isentropic cross-barrier
354 transport related to Rossby wave breaking (Haynes and Shuckburgh, 2000; Kunz et al., 2011a,b). In Fig.
355 7, gray dashed lines mark PV boundaries on the 350 K isentropic surface. On isentropic surfaces below
356 380 K, the PV boundaries represent the dynamical discontinuity near the core of the subtropical jet
357 stream. Isentropic transport of air masses across these boundaries indicates exchange between the
358 tropics and extratropics due to Rossby wave breaking. On isentropic surfaces above 400 K, PV
359 boundaries represent a transport barrier in the lower stratosphere, in particular, due to the polar vortices
360 in winter (Kunz et al., 2015). For comparison, we also show the 220 DU contour lines of ozone column
361 density (black isolines in Fig. 7), obtained from OMI on satellite Aura, indicating the boundary and size
362 of the ozone hole. The PV boundary on 480 K is in most cases collocated with the area of the ozone
363 hole, showing that both quantities provide a consistent representation of the area of the polar vortex.
364 The Merapi volcanic plume first reached the transport barrier on the 350 K isentropic surface in
365 mid-November and went close to the transport barrier on the 480 K isentropic surface in December. The

366 long-lasting polar vortex prevented the volcanic plume from crossing the transport barrier at 480 K in
367 early December. But from mid-December, the polar vortex became more disturbed and displaced from
368 the South Pole, resulting in a shrinking ozone hole. As mentioned in Sect.3.1, the ozone hole broke
369 down at the end of December 2010 and the polar vortex broke down by mid-January 2011.

370 The fraction of the volcanic plume that crosses the individual transport barrier or the latitude of 60°S on
371 each isentropic surface are shown in Fig. 8. In both cases, the proportion increased from November
372 2010 to January 2011. In November and December 2010 the largest plume transport across the transport
373 barriers occurred between the 360 and 430 K isentropic surface (Fig. 8a), with a peak at 380–390 K. In
374 January and February 2011 the peak was slightly elevated to 390–400 K. In November 2010, the
375 volcanic plume did not cross the 480 K transport barrier of the polar vortex at high altitudes, especially
376 above about 450 K. The high-latitude fraction increased from December 2010 to February 2011 as the
377 weakening of the polar vortex made the transport barrier more permeable. In March and April 2011, the
378 total proportion decreased and the peak descended to 370 K in March and further to 360 K in April. The
379 proportion of the volcanic plume south of 60°S (Fig. 8b) increased slightly from November to
380 December 2010, and then increased significantly from December 2010 to January and February 2011 at
381 all altitudes as the polar vortex displaced and broke down. Finally, the transport to the south of 60°S
382 started to decrease in March 2011. From November 2010 to February 2011 the peak was around 370–
383 400 K, but in March and April 2011 the peak resided around 350–370 K.

384 Figure 9a summarizes the simulated poleward transport of the volcanic plume between the isentropic
385 surfaces of 350 and 480 K from November 2010 to March 2011 and the percentage of air parcels south
386 of 60°S. The percentage was calculated by dividing the number of SO₂ parcels between 350 and 480 K
387 south of 60°S by the total number of SO₂ parcels released for the forward trajectory simulation. Figure
388 9b demonstrates the change of aerosol load in the same vertical range for MIPAS aerosol detections. As
389 in Sect. 3.3, we calculated the median ACI between November 2010 and March 2011 and subtracted it
390 from the ACI median of the “reference state” between November 2007 and March 2008. The
391 simulations show that the plume reached 60°S in December 2010. Correspondingly, the aerosol load
392 south of 60°S was elevated. The percentage fluctuated, but increased until the end of February 2011,
393 with a maximum percentage of about 4%. A steep increase occurred from mid-December 2010 to end of
394 January 2011, following the displacement and breakdown of the polar vortex. The elevated aerosol load
395 south of 60°S decreased from March 2011, and part of the plume descended to altitudes below 350 K as
396 shown by Fig. 8b. The MIPAS aerosol measurements in Fig. 9b where a positive ACI difference
397 indicates an increase in the aerosol load, confirm the simulated transport pattern in Fig. 9a. Overall,

398 simulations and observations indicate the largest increase of the aerosol load in the tropics and
399 mid-latitudes, but also show a significant enhancement over the south polar region after December
400 2010.

401 **4 Discussion**

402 The results presented in Sect. 3 show that the main transport pathway for the poleward transport of the
403 Merapi volcanic plume to Antarctica was between the isentropic surfaces of 350 and 480 K (about 10 to
404 20 km), covering the TTL and the lower stratosphere at mid- and high latitudes. For this long-range
405 transport on timescales of a few months, fast isentropic transport associated with quasi-horizontal
406 mixing played the main role in transporting the volcanic aerosol from the TTL to the Antarctic lower
407 stratosphere. The Merapi eruption occurred in austral spring and fast poleward transport was facilitated
408 by the weakening of the subtropical jet and active Rossby wave breaking events. The polar vortex was
409 relatively stable when the Merapi erupted, but by the time the volcanic plume reached the south polar
410 region, the polar vortex was displaced from the South Pole and distorted because more wave systems
411 propagated into the polar stratosphere and warmed the polar region, so that the volcanic plume was
412 transported from the tropics deep into Antarctica.

413 Based on the simulation results in Sect. 3.4, up to 4% of the volcanic plume air parcels was transported
414 from the TTL to the lower stratosphere in the south polar region till the end of February 2011. Based on
415 previous research on the Merapi case, we assigned a total mass of 0.44 Tg to all SO₂ parcel released,
416 which means the Merapi eruption contributed about 8800 tons of sulfur to the polar lower stratosphere
417 within 4 months after the eruption, assuming that the sulfate aerosol converted from the SO₂ remained
418 in the plume. Although the MPTRAC model we used to simulate the 3D movement of air parcels in the
419 volcanic plumes can estimate the conversion of SO₂ to sulfate aerosol during the transport process,
420 however, it does not resolve the chemical processes of aerosol formation. Hence, the estimated 8800
421 tons of sulfur are the maximum value since processes as e.g. wet deposition remove sulfur from the
422 atmosphere. But in the lower stratosphere, the atmosphere is relatively dry and clean compared with the
423 lower troposphere, so the sulfate aerosol has a lower possibility to interact with clouds or to be washed out.
424 In fact, in the polar lower stratosphere usually sedimentation and downward transport by the BDC are the
425 main removal processes. Clouds and washout processes usually cannot be expected in the lower
426 stratosphere. However, the amount of sulfate aerosol in the plume could also be affected by other
427 mechanisms that speed up the loss of sulfur, for example, coagulation in the volcanic plume, or the

428 absorption of sulfur onto fine ash particles. But for the moderate eruption Merapi in 2010, sulfuric
429 particle growth may not be as significant as it is in a large volcanic eruption, so the scavenging
430 efficiency of sulfur will be low. So generally, our estimation may be larger than the actual value, but this
431 number may be considered as the upper limit of the contribution of the Merapi eruption.

432 Besides, a kinematic trajectory model like MPTRAC, in which reanalysis vertical wind is used as
433 vertical velocity, typically shows higher vertical dispersion in the equatorial lower stratosphere
434 compared with a diabatic trajectory model (Schoeberl et al., 2003; Wohltmann and Rex, 2008; Liu et al.,
435 2010; Ploeger et al., 2010, 2011). However, the ERA–Interim reanalysis data used in this study to drive
436 the model may constrain the vertical dispersion much better than older reanalyses (Liu et al., 2010;
437 Hoffmann et al., 2017). The meridional transport in this study was mainly quasi-horizontal transport in
438 the mid- and high latitude UTLS region, so the effect of the vertical speed scheme is limited.

439 The aerosol transported to the polar lower stratosphere will finally descend with the downward flow and
440 have a chance to become a nonlocal source of sulfur for Antarctica by dry and wet deposition, following
441 the general precipitation patterns. Quantifying the sulfur deposition flux onto Antarctica is beyond the
442 scope of this study, though. Model results of Solomon et al. (2016) suggest that the Merapi eruption
443 made a small but significant contribution to the ozone depletion over Antarctica in the vertical range of
444 100–200 hPa, roughly between 10 and 14 km. This altitude range is in agreement with our results,
445 where we found transport into the Antarctic stratosphere between 10 and 20 km. When the volcanic
446 plume was transported to Antarctica in December 2010, the polar synoptic temperature at these low
447 height levels was already too high for the formation of PSCs. The additional ozone depletion found by
448 Solomon et al. (2016) together with the fact that sulfate aerosol was transported from the Merapi into
449 the Antarctic stratosphere between November and February where no PSCs are present during polar
450 summer, may support the study that suggested that significant ozone depletion can also occur on cold
451 binary aerosol (Drdla and Müller, 2012). The Merapi eruption in 2010 could be an interesting case
452 study for more sophisticated geophysical models to study the aftermath of volcanic eruptions on polar
453 processes.

454 **5 Summary and conclusion**

455 In this study, we analyzed the poleward transport of volcanic aerosol released by the Merapi eruption in
456 2010 from the tropics to the Antarctic lower stratosphere. The analysis was based on AIRS SO₂
457 measurements, MIPAS sulfate aerosol detections and MPTRAC transport simulations. First, we

458 estimated altitude-resolved SO₂ injection time series during the explosive eruption period using AIRS
459 data together with a backward trajectory approach. Second, the long-range transport of the volcanic
460 plume from the initial eruption to April 2011 was simulated based on the derived SO₂ injection time
461 series. Then the evolution and the poleward migration of the volcanic plume were analyzed using the
462 forward trajectory simulations and MIPAS aerosol measurements. The simulations are compared with
463 and verified by the MIPAS aerosol measurements.

464 Results of this study suggest that the volcanic plume from the Merapi eruption was transported from the
465 tropics to the south of 60 °S within a time scale of one month. Later on, in the UTLS region a fraction of
466 the volcanic plume (~4%) crossed 60 °S, even further to Antarctica until the end of February 2011. As a
467 result, the aerosol load in the Antarctic lower stratosphere was significantly elevated. This relatively fast
468 meridional transport of volcanic aerosol was mainly carried out by quasi-horizontal mixing from the
469 TTL to the extratropical lower stratosphere. Based on the simulations, most of the quasi-horizontal
470 mixing occurred between the isentropic surfaces of 360 to 430 K. This transport was in turn facilitated
471 by the weakening of the subtropical jet and the breakdown of the polar vortex in the seasonal transition
472 from austral spring to summer. The polar vortex in late austral spring 2010 was relatively strong
473 compared to the climatological mean state. However, in December 2010 the polar vortex was displaced
474 off the South Pole and later on broke down when the plume went to the high latitudes, so the volcanic
475 plume did not penetrate the polar vortex but entered the South Pole with the breakdown of the polar
476 vortex.

477 Overall, after the Merapi eruption, the largest increase of aerosol load occurred in the Southern
478 Hemisphere midlatitudes and a relatively small but significant fraction of the volcanic plume (4%) was
479 further transported to the Antarctic lower stratosphere within 4 months after the eruption. As a
480 maximum estimation, it contributed up to 8800 tons of sulfur to the Antarctic stratosphere, which
481 indicates that long-range transport under favorable meteorological conditions can make moderate
482 tropical volcanic eruptions an important remote source of sulfur to Antarctica.

483
484 *Code and data availability.* AIRS data are distributed by the NASA Goddard Earth Sciences Data
485 Information and Services Center. The SO₂ index data used in this study (Hoffmann et al., 2014) are
486 available for download at <https://datapub.fz-juelich.de/slcs/airs/volcanoes/> (last access: 26 March 2018).
487 Envisat MIPAS Level-1B data are distributed by the European Space Agency. The ERA–Interim
488 reanalysis data (Dee et al., 2011) were obtained from the European Centre for Medium-Range Weather
489 Forecasts. The code of the Massive-Parallel Trajectory Calculations (MPTRAC) model is available

490 under the terms and conditions of the GNU General Public License, Version 3 from the repository at
491 <https://github.com/slcs-jsc/mptrac> (last access: 31 January 2018).

492

493 *Appendix*

494 Figure A1 shows the 9-day running median values of the MIPAS ACI between 10 °N and 10 °S. During
495 the time period of the reference state (November 2007 to March 2008), the aerosol load in the tropical
496 stratosphere from 20 to 25 km is elevated by a couple of previous volcanic eruptions. The aerosol load
497 at this vertical range after the Merapi eruption in 2010 is apparently smaller compared with the
498 reference state.

499 It should be noted that there are semiannual data oscillations in the MIPAS ACI aerosol detections. This
500 periodic pattern is caused by the aerosol index that uses the atmospheric window region between 960
501 and 961 cm⁻¹. Around this window region, there are CO₂ laser bands. Due to the semiannual
502 temperature changes at about 50 km (semiannual oscillation), the CO₂ radiance contribution to this
503 window region also oscillates. As this window is generally very clear of other trace gases, this
504 oscillation is not only visible at higher altitudes but also in the lower stratosphere, because the satellite
505 line of sight looks through the whole layer (Wu et al., 2017). But even though with the semiannual data
506 oscillations, the upward transport of the aerosol from the Merapi eruption in the tropical stratosphere is
507 still visible and the vertical speed is estimated to about 7–8 km in five months (November 2010 to
508 March 2011).

509

510 *Competing interests.* The authors declare that they have no conflict of interest.

511

512 *Acknowledgments.* This work was supported by National Natural Science Foundation of China under
513 grant no. 41605023, China Postdoctoral Science Foundation under grant no. 2018T110131 and
514 International Postdoctoral Exchange Fellowship Program 2015 under grant no. 20151006.

515 **Reference**

- 516 Anstey, J. A., and Shepherd, T. G.: High-latitude influence of the quasi-biennial oscillation, *Q. J. R.*
517 *Meteorol. Soc.*, 140, 1-21, doi: 10.1002/qj.2132, 2014.
- 518 Aumann, H. H., Chahine, M. T., Gautier, C., Goldberg, M. D., Kalnay, E., McMillin, L. M., Revercomb,
519 H., Rosenkranz, P. W., Smith, W. L., Staelin, D. H., Strow, L. L., and Susskind, J.: AIRS/AMSU/HSB
520 on the Aqua mission: design, science objectives, data products, and processing systems, *IEEE Trans.*
521 *Geosci. Remote Sens.*, 41, 253-264, doi: 10.1109/TGRS.2002.808356, 2003.

522 Baldwin, M. P., and Dunkerton, T. J.: Propagation of the Arctic Oscillation from the stratosphere to the
523 troposphere, *J. Geophys. Res. Atmos.*, 104, 30937-30946, doi: 10.1029/1999JD900445, 1999.

524 Bosilovich, M., Akella, S., Coy, L., Cullather, R., Draper, C., Gelaro, R., Kovach, R., Liu, Q., Molod,
525 A., Norris, P., Wargan, K., Chao, W., Reichle, R., Takacs, L., Vikhliav, Y., Bloom, S., Collow, A.,
526 Firth, S., Labow, G., Partyka, G., Pawson, S., Reale, O., Schubert, S. D., and Suarez, M.: MERRA-2:
527 Initial evaluation of the climate, Tech. rep., NASA, series on Global Modeling and Data
528 Assimilation, NASA/TM-2015-104606, Vol. 43, 2015.

529 Dee, D. P., Uppala, S. M., Simmons, A. J., Berrisford, P., Poli, P., Kobayashi, S., Andrae, U.,
530 Balmaseda, M. A., Balsamo, G., Bauer, P., Bechtold, P., Beljaars, A. C. M., van de Berg, L., Bidlot,
531 J., Bormann, N., Delsol, C., Dragani, R., Fuentes, M., Geer, A. J., Haimberger, L., Healy, S. B.,
532 Hersbach, H., Holm, E. V., Isaksen, L., Kallberg, P., Kohler, M., Matricardi, M., McNally, A. P.,
533 Monge-Sanz, B. M., Morcrette, J. J., Park, B. K., Peubey, C., de Rosnay, P., Tavolato, C., Thepaut, J.
534 N., and Vitart, F.: The ERA-Interim reanalysis: configuration and performance of the data
535 assimilation system, *Q. J. R. Meteorol. Soc.*, 137, 553-597, doi: 10.1002/qj.828, 2011.

536 Drdla, K., and Müller, R.: Temperature thresholds for chlorine activation and ozone loss in the polar
537 stratosphere, *Ann. Geophys.*, 30, 1055-1073, doi: 10.5194/angeo-30-1055-2012, 2012.

538 Edmon, H. J. J., Hoskins, B. J., and McIntyre, M. E.: Eliassen-Palm Cross Sections for the Troposphere,
539 *J. Atmos. Sci.*, 37, 2600-2616, doi: 10.1175/1520-0469(1980)037<2600:epcsft>2.0.co;2, 1980.

540 Fischer, H., Birk, M., Blom, C., Carli, B., Carlotti, M., von Clarmann, T., Delbouille, L., Dudhia, A.,
541 Ehhalt, D., Endemann, M., Flaud, J. M., Gessner, R., Kleinert, A., Koopman, R., Langen, J.,
542 López-Puertas, M., Mosner, P., Nett, H., Oelhaf, H., Perron, G., Remedios, J., Ridolfi, M., Stiller, G.,
543 and Zander, R.: MIPAS: an instrument for atmospheric and climate research, *Atmos. Chem. Phys.*, 8,
544 2151-2188, doi: 10.5194/acp-8-2151-2008, 2008.

545 Friberg, J., Martinsson, B. G., Andersson, S. M., and Sandvik, O. S.: Volcanic impact on the climate –
546 the stratospheric aerosol load in the period 2006–2015, *Atmos. Chem. Phys.*, 18, 11149-11169, doi:
547 10.5194/acp-18-11149-2018, 2018.

548 Gao, C., Oman, L., Robock, A., and Stenchikov, G. L.: Atmospheric volcanic loading derived from
549 bipolar ice cores: Accounting for the spatial distribution of volcanic deposition, *J. Geophys. Res.*
550 *Atmos.*, 112, D09109, doi: 10.1029/2006JD007461, 2007.

551 Griessbach, S., L. Hoffmann, R. Spang and M. Riese: Volcanic ash detection with infrared limb
552 sounding: MIPAS observations and radiative transfer simulations, *Atmos. Meas. Tech.* 7,
553 1487-1507, doi: 10.5194/amt-7-1487-2014, 2014.

554 Griessbach, S., Hoffmann, L., Spang, R., von Hobe, M., Müller, R., and Riese, M.: Infrared limb
555 emission measurements of aerosol in the troposphere and stratosphere, *Atmos. Meas. Tech.*, 9,
556 4399-4423, doi:10.5194/amt-9-4399-2016, 2016.

557 Günther, A., Höpfner, M., Sinnhuber, B. M., Griessbach, S., Deshler, T., von Clarmann, T., and Stiller,
558 G.: MIPAS observations of volcanic sulphate aerosol and sulphur dioxide in the stratosphere, *Atmos.*
559 *Chem. Phys.*, 2017, 1-32, doi: 10.5194/acp-18-1217-2018, 2018.

560 Haynes, P., and Shuckburgh, E.: Effective diffusivity as a diagnostic of atmospheric transport: 2.
561 Troposphere and lower stratosphere, *J. Geophys. Res. Atmos.*, 105, 22795-22810, doi:
562 10.1029/2000JD900092, 2000.

563 Heng, Y., Hoffmann, L., Griessbach, S., Rößler, T., and Stein, O.: Inverse transport modeling of volcanic
564 sulfur dioxide emissions using large-scale simulations, *Geosci. Model Dev.*, 9, 1627-1645,
565 doi:10.5194/gmd-9-1627-2016, 2016.

566 Hoffmann, L., Griessbach, S., and Meyer, C. I.: Volcanic emissions from AIRS observations: detection
567 methods, case study, and statistical analysis, in: *Remote Sensing of Clouds and the Atmosphere XIX*
568 *and Optics in Atmospheric Propagation and Adaptive Systems XVII*, edited by: Comeron, A.,

569 Kassianov, E. I., Schafer, K., Picard, R. H., Stein, K., and Gonglewski, J. D., Proceedings of SPIE,
570 Spie-Int Soc Optical Engineering, Bellingham, doi: 92421410.1117/12.2066326, 2014.

571 Hoffmann, L., Hertzog, A., Rößler, T., Stein, O., and Wu, X.: Intercomparison of meteorological
572 analyses and trajectories in the Antarctic lower stratosphere with Concordiasi superpressure balloon
573 observations, *Atmos. Chem. Phys.*, 17, 8045-8061, doi: 10.5194/acp-17-8045-2017, 2017.

574 Hoffmann, L., Rößler, T., Griessbach, S., Heng, Y., and Stein, O.: Lagrangian transport simulations of
575 volcanic sulfur dioxide emissions: Impact of meteorological data products, *J. Geophys. Res. Atmos.*,
576 121, 4651-4673, doi: 10.1002/2015JD023749, 2016.

577 Hofmann, D. J., Rosen, J. M., and Gringel, W.: Delayed production of sulfuric acid condensation nuclei
578 in the polar stratosphere from El Chichon volcanic vapors, *J. Geophys. Res. Atmos.*, 90, 2341-2354,
579 doi:10.1029/JD090iD01p02341, 1985.

580 Hofmann, D. J., Rosen, J. M., and Harder, J. W.: Aerosol measurements in the winter/spring Antarctic
581 stratosphere: 1. Correlative measurements with ozone, *J. Geophys. Res. Atmos.*, 93, 665-676,
582 doi:10.1029/JD093iD01p00665, 1988.

583 Holton, J. R., Haynes, P. H., McIntyre, M. E., Douglass, A. R., Rood, R. B., and Pfister, L.:
584 Stratosphere-troposphere exchange, *Rev. Geophys.*, 33, 403-439, doi: 10.1029/95RG02097, 1995.

585 Holton, J. R., and Tan, H. C.: The Influence of the Equatorial Quasi-Biennial Oscillation on the Global
586 Circulation at 50 mb, *J. Atmos. Sci.*, 37, 2200-2208, doi:
587 10.1175/1520-0469(1980)037<2200:tioteq>2.0.co;2, 1980.

588 Höpfner, M., Pitts, M. C., and Poole, L. R.: Comparison between CALIPSO and MIPAS observations
589 of polar stratospheric clouds, *J. Geophys. Res. Atmos.*, 114, doi:10.1029/2009JD012114, 2009.

590 Ivy, D. J., Solomon, S., Kinnison, D., Mills, M. J., Schmidt, A., and Neely, R. R.: The influence of the
591 Calbuco eruption on the 2015 Antarctic ozone hole in a fully coupled chemistry-climate model,
592 *Geophys. Res. Lett.*, 44, 2556-2561, doi: 10.1002/2016GL071925, 2017.

593 Jäger, H.: Long-term record of lidar observations of the stratospheric aerosol layer at
594 Garmisch-Partenkirchen, *J. Geophys. Res. Atmos.*, 110, D08106, doi: 10.1029/2004JD005506, 2005.

595 Jäger, H., and Wege, K.: Stratospheric ozone depletion at northern midlatitudes after major volcanic
596 eruptions, *J. Atmos. Chem.*, 10, 273-287, doi: 10.1007/bf00053863, 1990.

597 Kalnay, E., Kanamitsu, M., Kistler, R., Collins, W., Deaven, D., Gandin, L., Iredell, M., Saha, S., White,
598 G., Woollen, J., Zhu, Y., Chelliah, M., Ebisuzaki, W., Higgins, W., Janowiak, J., Mo, K. C.,
599 Ropelewski, C., Wang, J., Leetmaa, A., Reynolds, R., Jenne, R., and Joseph, D.: The NCEP/NCAR
600 40-Year Reanalysis Project, *Bull. Am. Meteorol. Soc.* 77, 437-472, doi:
601 10.1175/1520-0477(1996)077<0437:tnyrp>2.0.co;2, 1996.

602 Khaykin, S. M., Godin-Beekmann, S., Keckhut, P., Hauchecorne, A., Jumelet, J., Vernier, J. P.,
603 Bourassa, A., Degenstein, D. A., Rieger, L. A., Bingen, C., Vanhellemont, F., Robert, C., DeLand,
604 M., and Bhartia, P. K.: Variability and evolution of the midlatitude stratospheric aerosol budget from
605 22 years of ground-based lidar and satellite observations, *Atmos. Chem. Phys.*, 17, 1829-1845, doi:
606 10.5194/acp-17-1829-2017, 2017.

607 Kunz, A., Konopka, P., Müller, R., and Pan, L. L.: Dynamical tropopause based on isentropic potential
608 vorticity gradients, *J. Geophys. Res. Atmos.*, 116, D01110, doi: 10.1029/2010JD014343, 2011a.

609 Kunz, A., Pan, L. L., Konopka, P., Kinnison, D. E., and Tilmes, S.: Chemical and dynamical
610 discontinuity at the extratropical tropopause based on START08 and WACCM analyses, *J. Geophys.
611 Res. Atmos.*, 116, D24302, doi: 10.1029/2011JD016686, 2011b.

612 Kunz, A., Sprenger, M., and Wernli, H.: Climatology of potential vorticity streamers and associated
613 isentropic transport pathways across PV gradient barriers, *J. Geophys. Res. Atmos.*, 120, 3802-3821,
614 doi: 10.1002/2014jd022615, 2015.

615 Levelt, P. F., Oord, G. H. J. v. d., Dobber, M. R., Malkki, A., Huib, V., Johan de, V., Stammes, P.,
616 Lundell, J. O. V., and Saari, H.: The ozone monitoring instrument, *IEEE Trans. Geosci. Remote*
617 *Sens.*, 44, 1093-1101, doi: 10.1109/TGRS.2006.872333, 2006.

618 Liu, Y. S., Fueglistaler, S., and Haynes, P. H.: Advection-condensation paradigm for stratospheric water
619 vapor, *J. Geophys. Res. Atmos.*, 115, D24307, doi: 10.1029/2010JD014352, 2010.

620 Mazzera, D. M., Lowenthal, D. H., Chow, J. C., and Watson, J. G.: Sources of PM10 and sulfate aerosol
621 at McMurdo station, Antarctica, *Chemosphere*, 45, 347-356, doi:
622 [https://doi.org/10.1016/S0045-6535\(00\)00591-9](https://doi.org/10.1016/S0045-6535(00)00591-9), 2001.

623 McCormick, M. P., Steele, H. M., Hamill, P., Chu, W. P., and Swissler, T. J.: Polar Stratospheric Cloud
624 Sightings by SAM II, *J. Atmos. Sci.*, 39, 1387-1397, doi:
625 10.1175/1520-0469(1982)039<1387:pscsbs>2.0.co;2, 1982.

626 Newman, P. A., and Nash, E. R.: Quantifying the wave driving of the stratosphere, *J. Geophys. Res.*
627 *Atmos.*, 105, 12485-12497, doi: 10.1029/1999JD901191, 2000.

628 Olsen, M. A., Douglass, A. R., Schoeberl, M. R., Rodriguez, J. M., and Yoshida, Y.: Interannual
629 variability of ozone in the winter lower stratosphere and the relationship to lamina and irreversible
630 transport, *J. Geophys. Res. Atmos.*, 115, 10.1029/2009jd013004, 2010.

631 O'Sullivan, D., and Dunkerton, T. J.: The influence of the quasi-biennial oscillation on global
632 constituent distributions, *J. Geophys. Res. Atmos.*, 102, 21731-21743, doi: 10.1029/97JD01689,
633 1997.

634 Pallister, J. S., Schneider, D. J., Griswold, J. P., Keeler, R. H., Burton, W. C., Noyles, C., Newhall, C.
635 G., and Ratdomopurbo, A.: Merapi 2010 eruption—Chronology and extrusion rates monitored with
636 satellite radar and used in eruption forecasting, *J. Volcanol. Geotherm. Res.*, 261, 144-152, doi:
637 <http://dx.doi.org/10.1016/j.jvolgeores.2012.07.012>, 2013.

638 Ploeger, F., Konopka, P., Gunther, G., Grooss, J. U., and Muller, R.: Impact of the vertical velocity
639 scheme on modeling transport in the tropical tropopause layer, *J. Geophys. Res. Atmos.*, 115, 14, doi:
640 10.1029/2009jd012023, 2010.

641 Ploeger, F., Fueglistaler, S., Grooss, J. U., Gunther, G., Konopka, P., Liu, Y. S., Muller, R., Ravegnani,
642 F., Schiller, C., Ulanovski, A., and Riese, M.: Insight from ozone and water vapour on transport in
643 the tropical tropopause layer (TTL), *Atmos. Chem. Phys.*, 11, 407-419, doi:
644 10.5194/acp-11-407-2011, 2011.

645 Portmann, R. W., Solomon, S., Garcia, R. R., Thomason, L. W., Poole, L. R., and McCormick, M. P.:
646 Role of aerosol variations in anthropogenic ozone depletion in the polar regions, *J. Geophys. Res.*
647 *Atmos.*, doi: 10.1029/96JD02608, 1996.

648 Rößler, T., Stein, O., Heng, Y., Baumeister, P., and Hoffmann, L.: Trajectory errors of different
649 numerical integration schemes diagnosed with the MPTRAC advection module driven by ECMWF
650 operational analyses, *Geosci. Model Dev.*, 11, 575-592, doi: 10.5194/gmd-11-575-2018, 2018.

651 Sand, M., Samset, B. H., Balkanski, Y., Bauer, S., Bellouin, N., Berntsen, T. K., Bian, H., Chin, M.,
652 Diehl, T., Easter, R., Ghan, S. J., Iversen, T., Kirkevåg, A., Lamarque, J. F., Lin, G., Liu, X., Luo, G.,
653 Myhre, G., Noije, T. V., Penner, J. E., Schulz, M., Seland, Ø., Skeie, R. B., Stier, P., Takemura, T.,
654 Tsigaridis, K., Yu, F., Zhang, K., and Zhang, H.: Aerosols at the poles: an AeroCom Phase II
655 multi-model evaluation, *Atmos. Chem. Phys.*, 17, 12197-12218, doi: 10.5194/acp-17-12197-2017,
656 2017.

657 Schoeberl, M. R., Douglass, A. R., Zhu, Z. X., and Pawson, S.: A comparison of the lower stratospheric
658 age spectra derived from a general circulation model and two data assimilation systems, *J. Geophys.*
659 *Res. Atmos.*, 108, 16, doi: 10.1029/2002jd002652, 2003.

660 Sembhi, H., Remedios, J., Trent, T., Moore, D. P., Spang, R., Massie, S., and Vernier, J. P.: MIPAS
661 detection of cloud and aerosol particle occurrence in the UTLS with comparison to HIRDLS and
662 CALIOP, *Atmos. Meas. Tech.*, 5, 2537-2553, doi: 10.5194/amt-5-2537-2012, 2012.

663 Shuckburgh, E., Norton, W., Iwi, A., and Haynes, P.: Influence of the quasi-biennial oscillation on
664 isentropic transport and mixing in the tropics and subtropics, *J. Geophys. Res. Atmos.*, 106,
665 14327-14337, doi: 10.1029/2000JD900664, 2001.

666 Sigl, M., Winstrup, M., McConnell, J. R., Welten, K. C., Plunkett, G., Ludlow, F., Buntgen, U., Caffee,
667 M., Chellman, N., Dahl-Jensen, D., Fischer, H., Kipfstuhl, S., Kostick, C., Maselli, O. J., Mekhaldi,
668 F., Mulvaney, R., Muscheler, R., Pasteris, D. R., Pilcher, J. R., Salzer, M., Schupbach, S., Steffensen,
669 J. P., Vinther, B. M., and Woodruff, T. E.: Timing and climate forcing of volcanic eruptions for the
670 past 2,500 years, *Nature*, 523, 543-549, doi:
671 10.1038/nature14565 [http://www.nature.com/nature/journal/v523/n7562/abs/nature14565.html#suppl](http://www.nature.com/nature/journal/v523/n7562/abs/nature14565.html#supplementary-information)
672 [ementary-information](http://www.nature.com/nature/journal/v523/n7562/abs/nature14565.html#supplementary-information), 2015.

673 Solomon, S.: Stratospheric ozone depletion: A review of concepts and history, *Rev. Geophys.*, 37,
674 275-316, doi: 10.1029/1999RG900008, 1999.

675 Solomon, S., Daniel, J. S., Neely, R. R., Vernier, J.-P., Dutton, E. G., and Thomason, L. W.: The
676 Persistently Variable “Background” Stratospheric Aerosol Layer and Global Climate Change,
677 *Science*, 333, 866-870, doi: 10.1126/science.1206027, 2011.

678 Solomon, S., Garcia, R. R., Rowland, F. S., and Wuebbles, D. J.: On the depletion of Antarctic ozone,
679 *Nature*, 321, 755, doi: 10.1038/321755a0, 1986.

680 Solomon, S., Ivy, D. J., Kinnison, D., Mills, M. J., Neely, R. R., and Schmidt, A.: Emergence of healing
681 in the Antarctic ozone layer, *Science*, doi: 10.1126/science.aae0061, 2016.

682 Solomon, S., Sanders, R. W., Garcia, R. R., and Keys, J. G.: Increased chlorine dioxide over Antarctica
683 caused by volcanic aerosols from Mount-Pinatubo, *Nature*, 363, 245–248, doi:
684 <https://doi.org/10.1038/363245a0>, 1993.

685 Spang, R., Riese, M., and Offermann, D.: CRISTA-2 observations of the south polar vortex in winter
686 1997: A new dataset for polar process studies, *Geophys. Res. Lett.*, 28, 3159–3162, doi:
687 10.1029/2000GL012374, 2001.

688 Stohl, A., Forster, C., Frank, A., Seibert, P., and Wotawa, G.: Technical note: The Lagrangian particle
689 dispersion model FLEXPART version 6.2, *Atmos. Chem. Phys.*, 5, 2461-2474,
690 doi:10.5194/acp-5-2461-2005, 2005.

691 Stone, K. A., Solomon, S., Kinnison, D. E., Pitts, M. C., Poole, L. R., Mills, M. J., Schmidt, A., Neely,
692 R. R., Ivy, D., Schwartz, M. J., Vernier, J.-P., Johnson, B. J., Tully, M. B., Klekociuk, A. R.,
693 König-Langlo, G., and Hagiya, S.: Observing the Impact of Calbuco Volcanic Aerosols on South
694 Polar Ozone Depletion in 2015, *J. Geophys. Res. Atmos.*, 122, 11,862-811,879, doi:
695 10.1002/2017JD026987, 2017.

696 Suroño, Jousset, P., Pallister, J., Boichu, M., Buongiorno, M. F., Budisantoso, A., Costa, F., Andreastuti,
697 S., Prata, F., Schneider, D., Clarisse, L., Humaida, H., Sumarti, S., Bignami, C., Griswold, J., Carn,
698 S., Oppenheimer, C., and Lavigne, F.: The 2010 explosive eruption of Java's Merapi volcano—A
699 ‘100-year’ event, *J. Volcanol. Geotherm. Res.*, 241, 121-135, doi:
700 <http://dx.doi.org/10.1016/j.jvolgeores.2012.06.018>, 2012.

701 Tilmes, S., Müller, R., and Salawitch, R.: The sensitivity of polar ozone depletion to proposed
702 geoengineering schemes, *Science*, 320, 1201-1204, doi: 10.1126/science.1153966, 2008.

703 Toohey, M., Krüger, K., Niemeier, U., and Timmreck, C.: The influence of eruption season on the
704 global aerosol evolution and radiative impact of tropical volcanic eruptions, *Atmos. Chem. Phys.*, 11,
705 doi: 12351-12367, 10.5194/acp-11-12351-2011, 2011.

706 Vernier, J. P., Thomason, L. W., Pommereau, J. P., Bourassa, A., Pelon, J., Garnier, A., Hauchecorne,
707 A., Blanot, L., Trepte, C., Degenstein, D., and Vargas, F.: Major influence of tropical volcanic
708 eruptions on the stratospheric aerosol layer during the last decade, *Geophys. Res. Lett.*, 38, L12807,
709 doi: 10.1029/2011GL047563, 2011.

710 Vogel, B., Pan, L. L., Konopka, P., Gunther, G., Muller, R., Hall, W., Campos, T., Pollack, I.,
711 Weinheimer, A., Wei, J., Atlas, E. L., and Bowman, K. P.: Transport pathways and signatures of
712 mixing in the extratropical tropopause region derived from Lagrangian model simulations, *J.*
713 *Geophys. Res. Atmos.*, 116, 16, doi: 10.1029/2010jd014876, 2011.

714 von Glasow, R., Bobrowski, N., and Kern, C.: The effects of volcanic eruptions on atmospheric
715 chemistry, *Chem. Geol.*, 263, 131-142, doi: <http://dx.doi.org/10.1016/j.chemgeo.2008.08.020>, 2009.

716 Watson, P. A. G., and Gray, L. J.: How Does the Quasi-Biennial Oscillation Affect the Stratospheric
717 Polar Vortex?, *J. Atmos. Sci.*, 71, 391-409, doi: 10.1175/jas-d-13-096.1, 2014.

718 Wohltmann, I., and Rex, M.: Improvement of vertical and residual velocities in pressure or hybrid
719 sigma-pressure coordinates in analysis data in the stratosphere, *Atmos. Chem. Phys.*, 8, 265-272, doi:
720 10.5194/acp-8-265-2008, 2008.

721 Wu, X., Griessbach, S., and Hoffmann, L.: Equatorward dispersion of a high-latitude volcanic plume
722 and its relation to the Asian summer monsoon: a case study of the Sarychev eruption in 2009, *Atmos.*
723 *Chem. Phys.*, 17, 13439-13455, doi: 10.5194/acp-17-13439-2017, 2017.

724 Zuev, V. V., Zueva, N. E., Savelieva, E. S., and Gerasimov, V. V.: The Antarctic ozone depletion
725 caused by Erebus volcano gas emissions, *Atmos. Environ.*, 122, 393-399, doi:
726 <https://doi.org/10.1016/j.atmosenv.2015.10.005>, 2015.

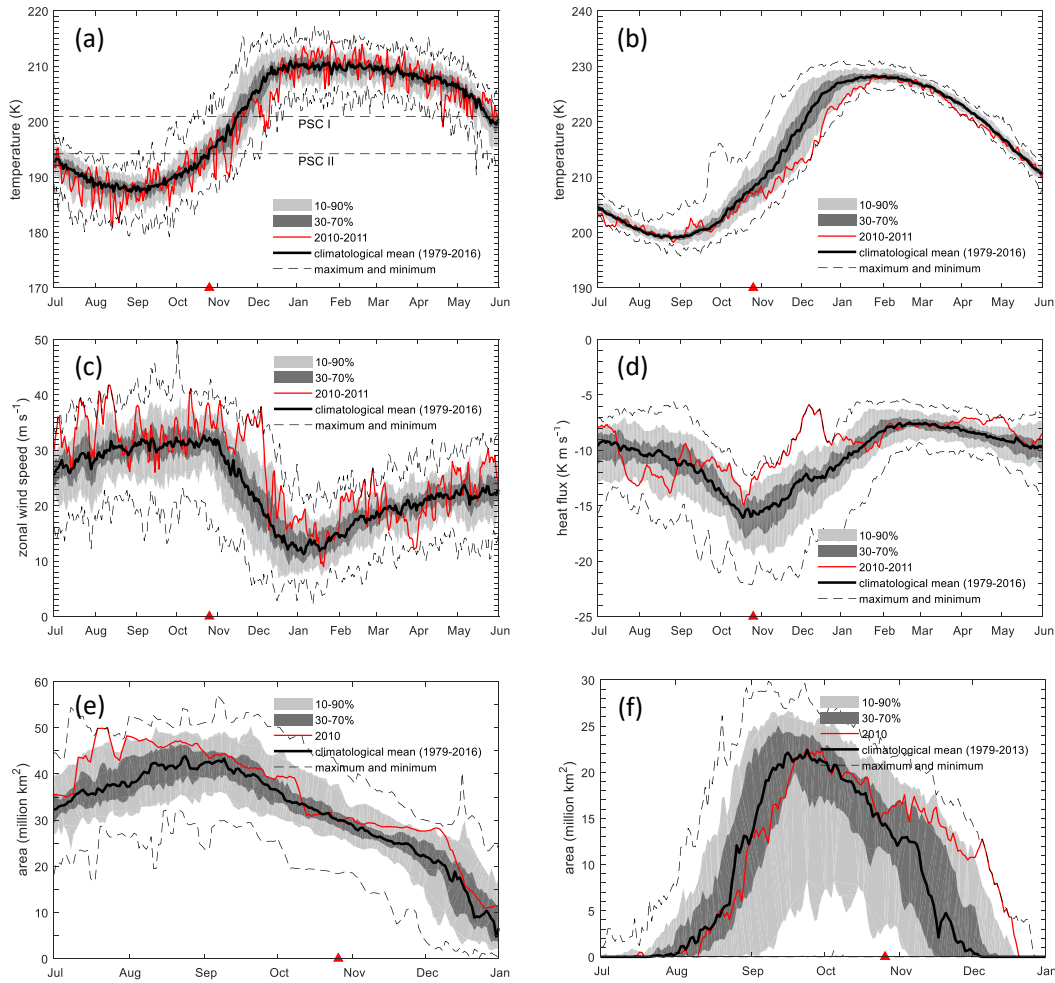


Figure 1: (a) Minimum temperature south of 50°S at 150 hPa; (b) temperature averaged over the polar cap for latitudes south of 60°S at 150 hPa; (c) zonal wind speed at 60°S at 150 hPa; (d) eddy heat flux averaged between 45°S and 75°S for the 45-day period prior to the date indicated at 150 hPa; (e) the area of the polar vortex for 1 July–31 December 2010 on the 460 K isentropic surface; (f) ozone hole area for 1 July 2010–31 December 2010. Temperatures for PSC existence in (a) are determined by assuming a nitric acid concentration of 6 ppbv and a water vapor concentration of 4.5 ppmv. (a)–(f) are based on Modern-Era Retrospective analysis for Research and Applications reanalysis version 2 (MERRA2) data (Bosilovich et al., 2015). The ozone hole area in (f) is determined from OMI ozone satellite measurements (Levelt et al., 2006). The red triangles indicate the time of the Merapi eruption.

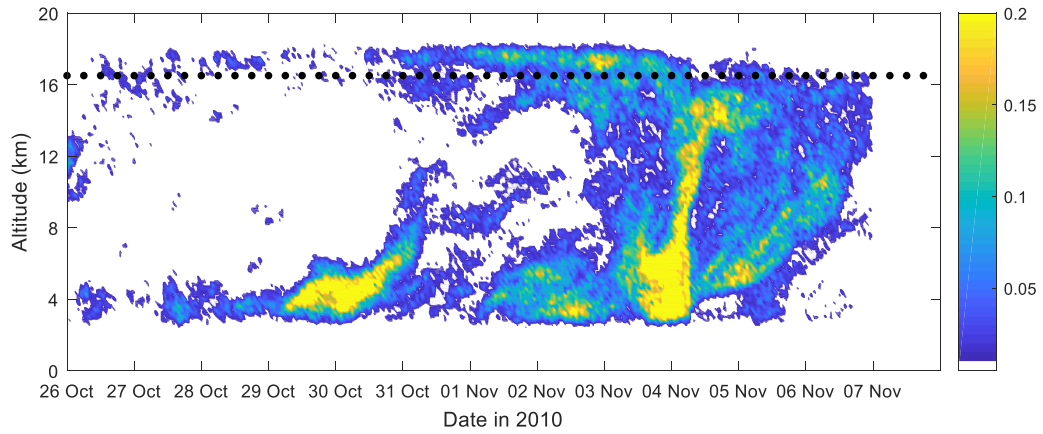


Figure 2: Merapi SO₂ emission time series (unit: kg m⁻¹ s⁻¹) derived from AIRS measurements using a backward trajectory approach (see text for details). The emission data are binned every 1 h and 0.2 km. The ticks for the horizontal axis mark 0 UTC on each day. Black dots denote the height of the thermal tropopause (based on the ERA–Interim reanalysis).

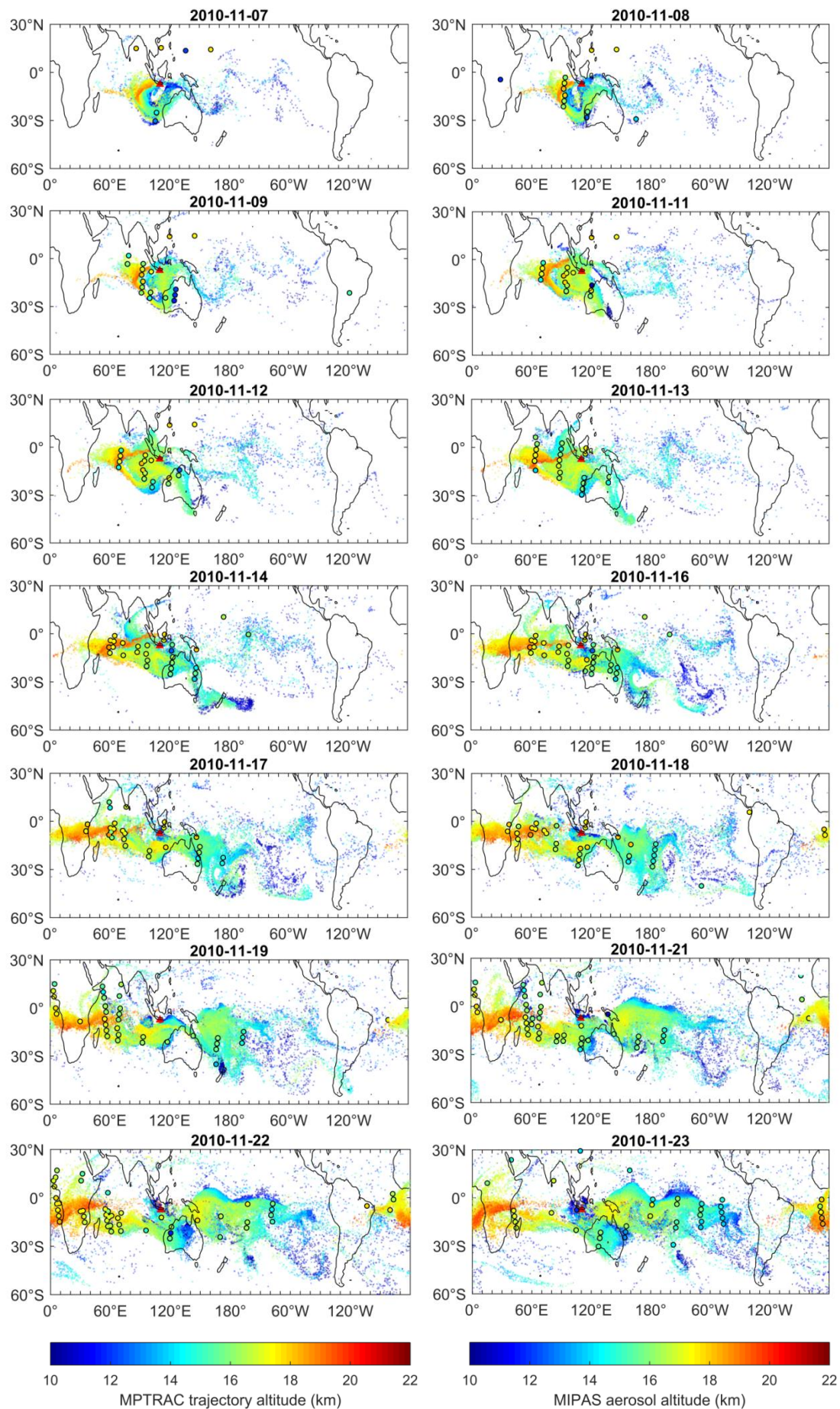


Figure 3: Distribution of the volcanic plume (showing only air parcels higher than 10 km, shading) from MPTRAC simulations (shown for 00:00UTC on selected days) and MIPAS aerosol detections ($ACI < 7$) within ± 6 h (color-filled circles). The altitudes of all

air parcels, regardless of their SO₂ values, are shown. The red triangle denotes the location of Mount Merapi.

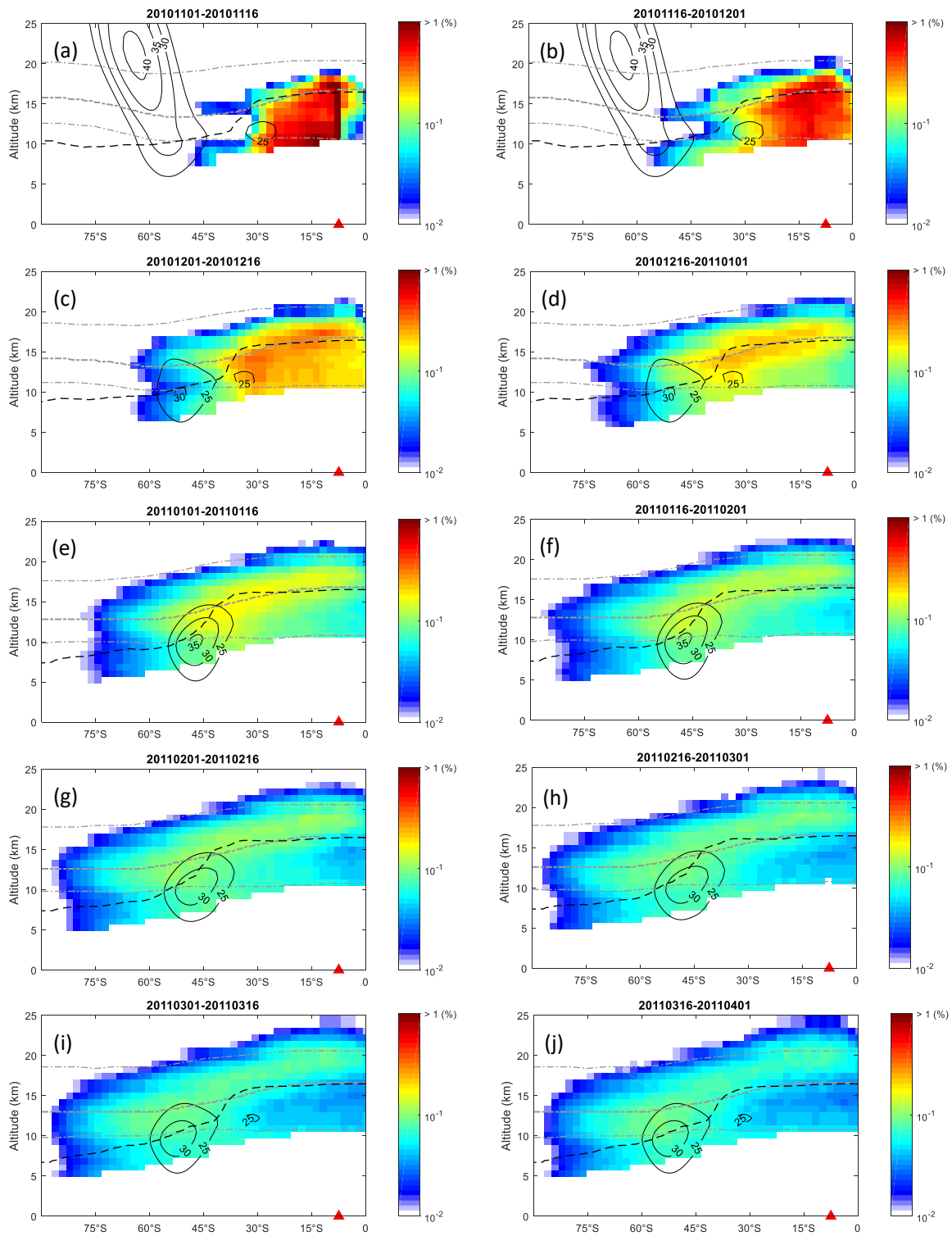


Figure 4: Percentage (%) of air parcels in proportion to the total number of air parcels released in the Lagrangian forward simulation, overlaid with monthly mean zonal winds (black contours), the thermal tropopause (black dashed line), the 380 K potential temperature isoline (thick gray dashed line) and 350 and 480 K potential temperature isolines (thin gray dashed lines). Results are binned every 2° in latitude and 1 km in altitude. The red triangle denotes the latitude of the Mount Merapi. Please see title of each figure for the time period covered.

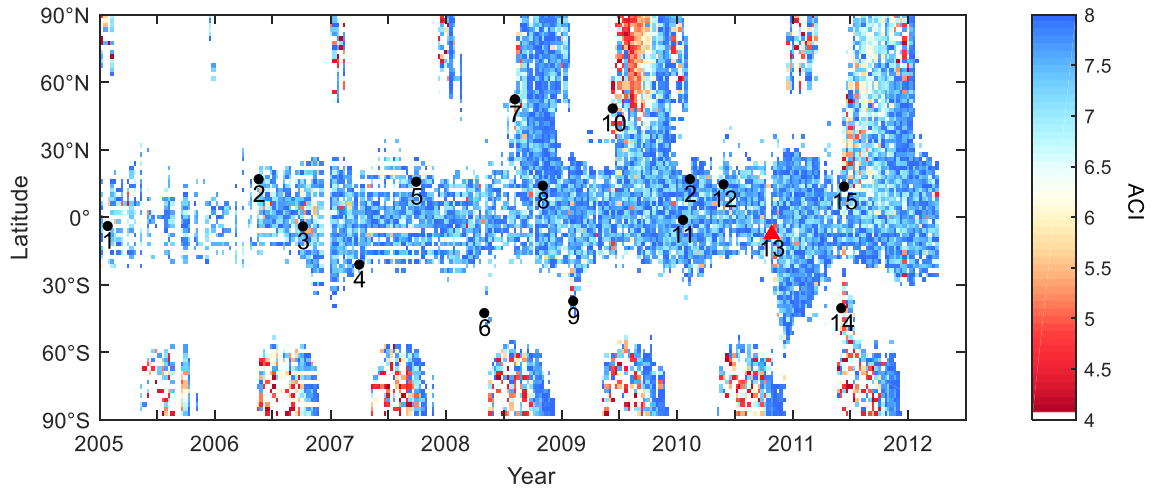


Figure 5: Median value of MIPAS ACI detections between 12–18 km (bin size: 10 days and 2° in latitude) from January 2005 to April 2012. Only ACI values from 4 to 8 are shown. The red triangle indicates the eruption of Mount Merapi (No. 13). The black filled circles indicate 1 Manam, 2 Soufriere Hills, 3 Tavurvur (Rabaul), 4 Piton de la Fournaise, 5 Jebel at Tair, 6 Chaitén, 7 Kasatochi, 8 Dalaffilla, 9 Australian bushfire, 10 Sarychev Peak, 11 Nyamuragira, 12 Pacaya, 14 Puyehue-Cordón Caulle, 15 Nabro.

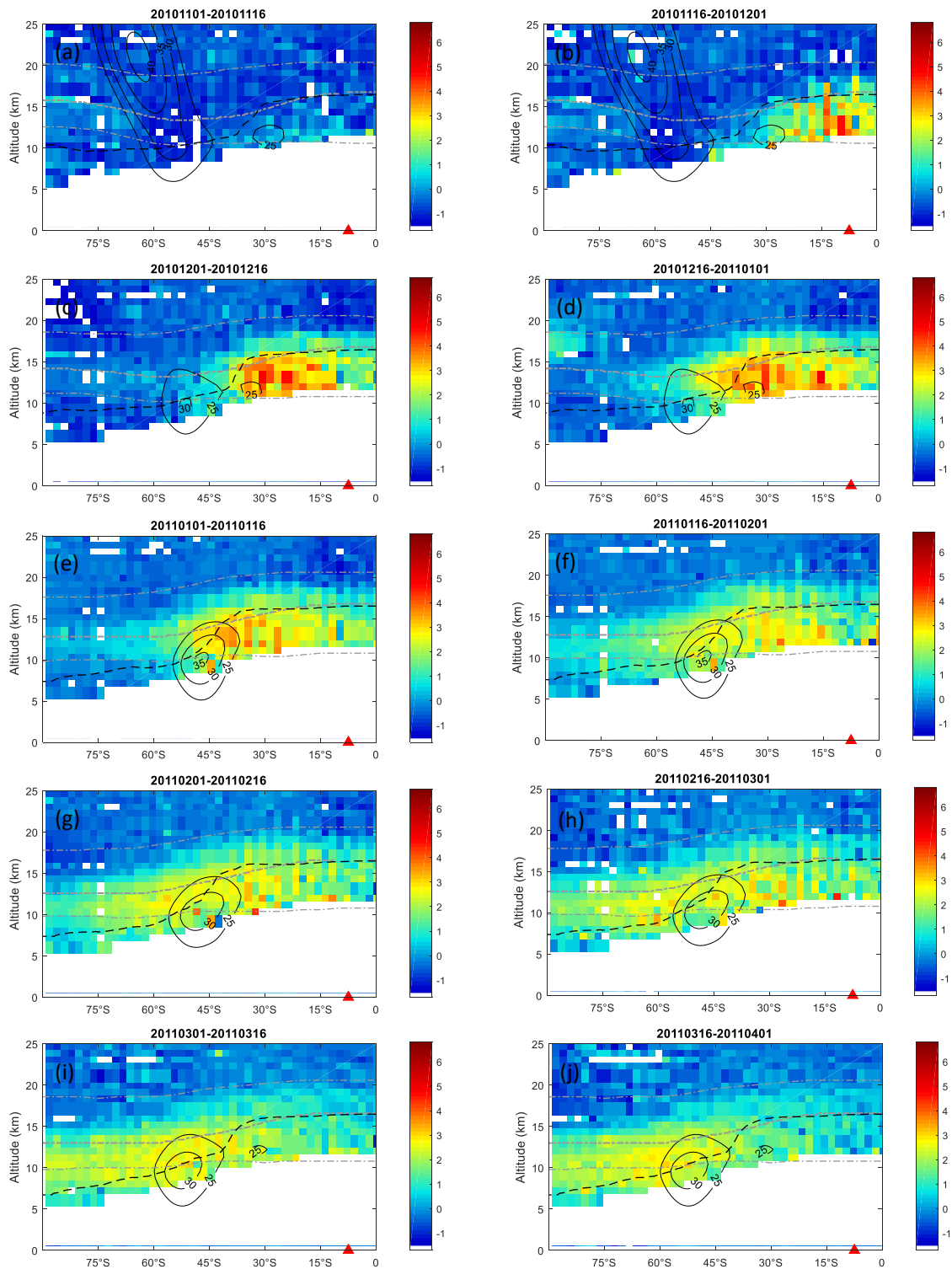


Figure 6: The change of MIPAS ACI values after the eruption of Merapi in 2010, overlaid with monthly mean zonal winds (black contours), the thermal tropopause (black dashed line), the 380 K potential temperature isoline (thick gray dashed line) and 350 and 480 K potential temperature isolines (thin gray dashed lines). Positive values indicate an increase of the aerosol load and negative values indicate a decrease of the aerosol load. Results are binned every 2° in latitude and 1 km in altitude. The red triangle denotes the latitude of the Mount Merapi. Please see title of each figure for the time period covered.

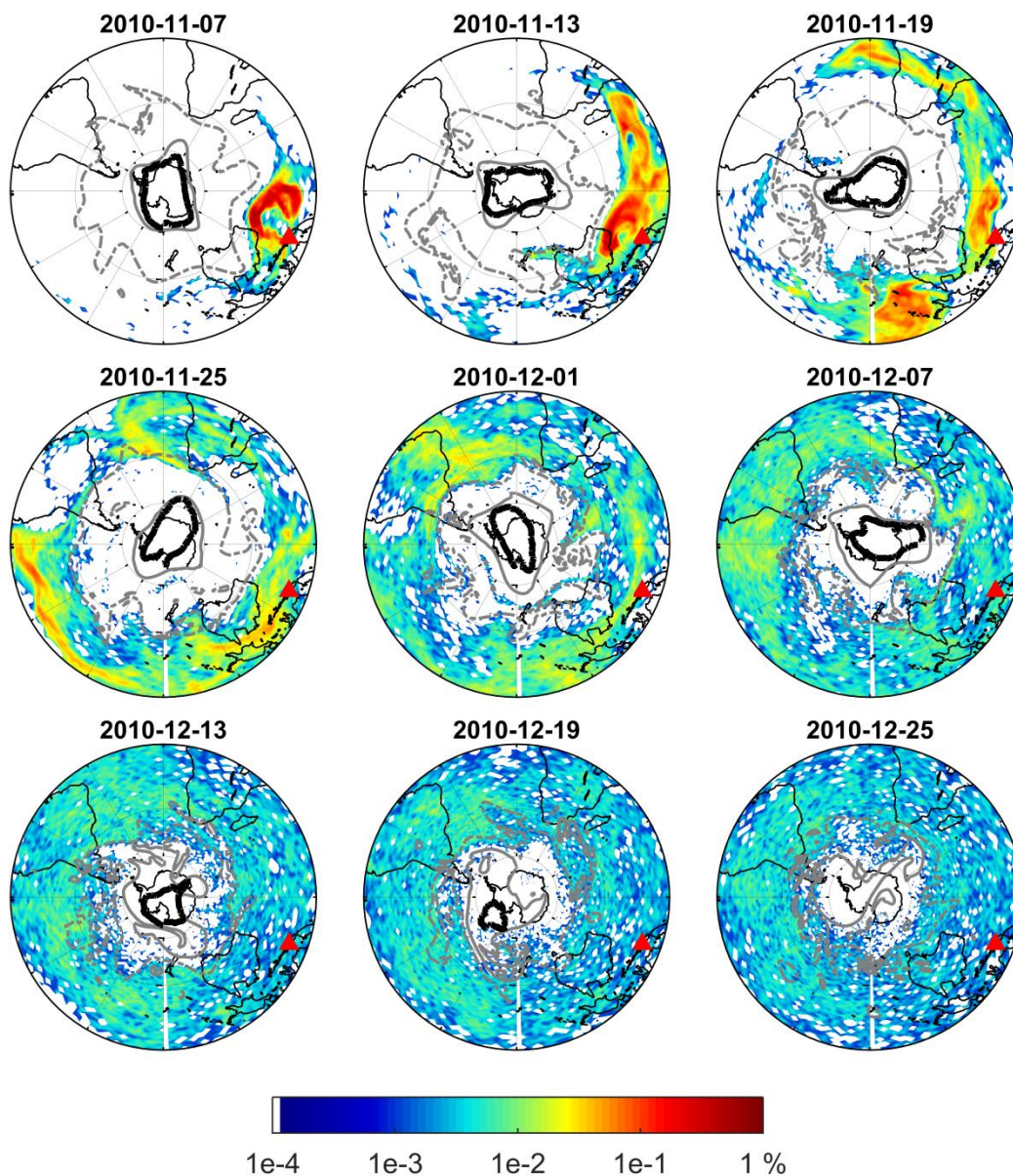


Figure 7: Percentage (%) of air parcels between the isentropic surfaces of 350 and 480 K in proportion to the total number of air parcels released in the Lagrangian forward simulation. All results are at 12:00 UTC on selected dates and binned every 2° in longitude and 1° in latitude. The black contours indicate the 220 DU contour lines of daily mean ozone column density provided by OMI. PV contours marked with gray dashed and solid lines show PV boundaries on the 350 and 480 K isentropic surfaces respectively (Kunz et al., 2015). The red triangle denotes the location of Mount Merapi.

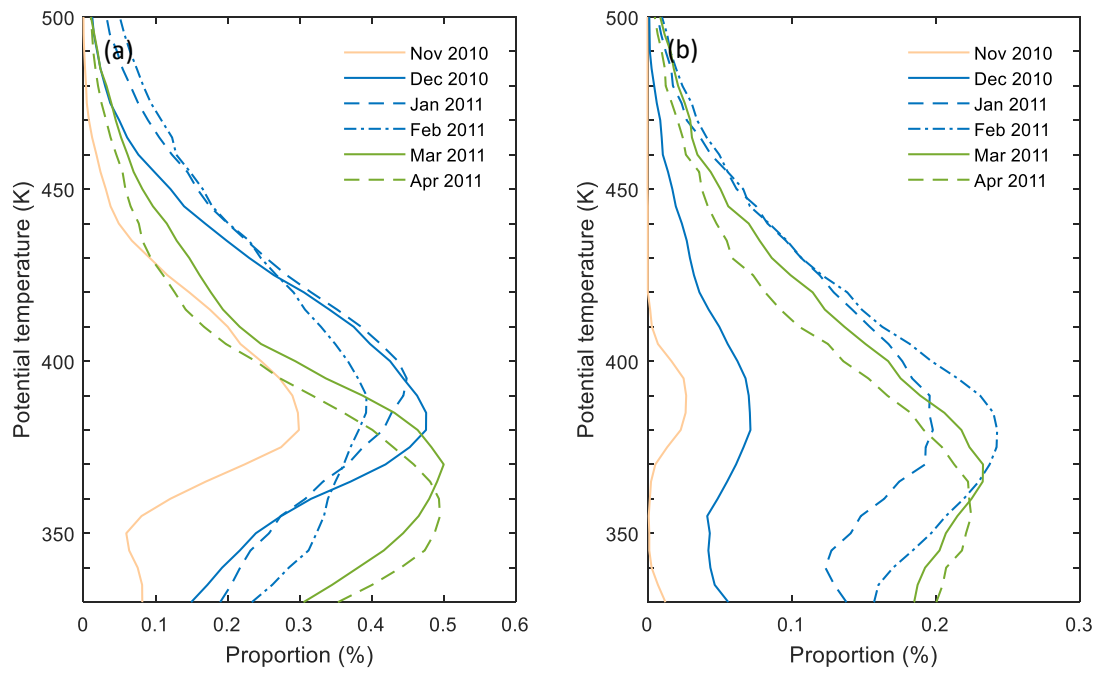


Figure 8: (a) Proportion (%) of the air parcels poleward of the PV-based transport boundaries at the end of each month; (b) proportion (%) of the air parcels south of 60°S.

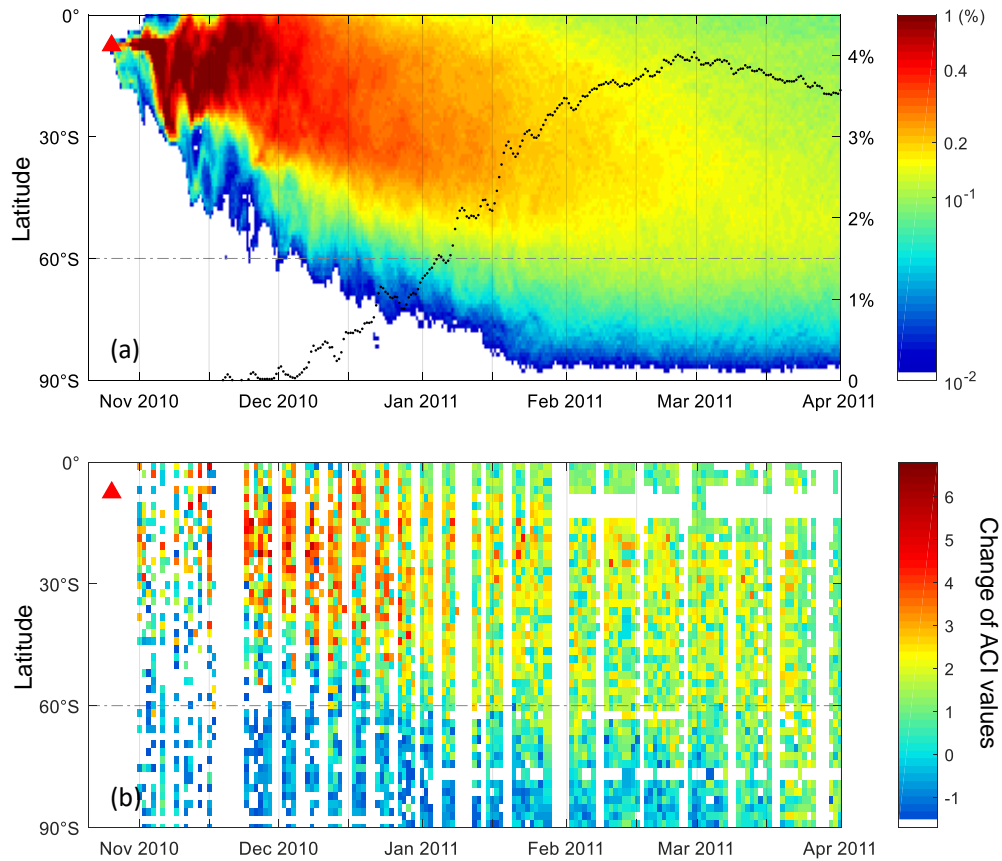


Figure 9: Time and latitude evolution of the (a) percentage (%) of air parcels between the isentropic surfaces of 350 and 480 K from the Lagrangian simulations (shading, only percentages larger than 0.05% are shown; bin size: 12h and 1 ° in latitude) and the proportion (%) of air parcels south of 60 °S (black dots); (b) the change of MIPAS ACI values after the eruption of Merapi in 2010 between 350 and 480 K. Positive values indicate an increase and negative values indicate a decrease of the aerosol load (bin size: 24h and 2 ° in latitude). The red triangle denotes the time and latitude of the Merapi eruption.

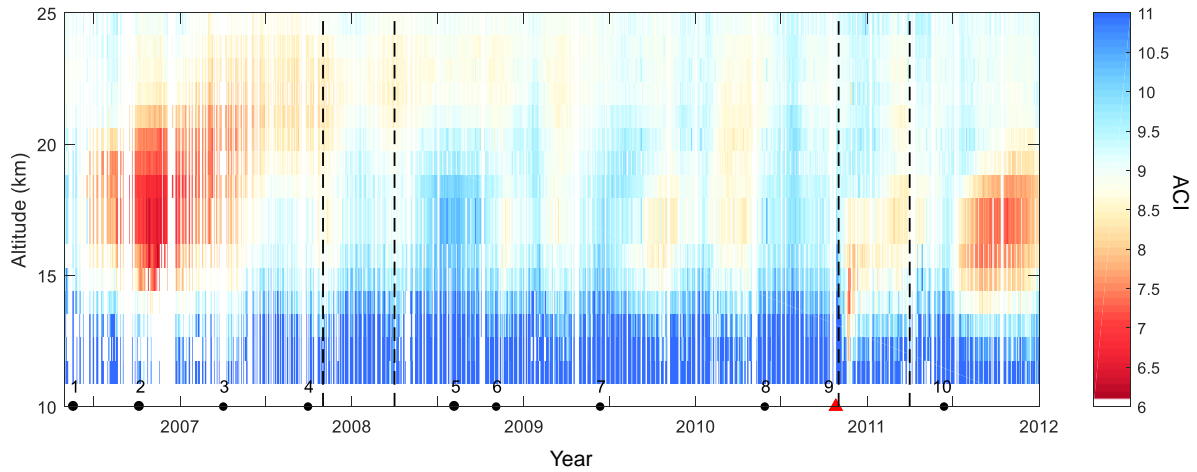


Figure A1: MIPAS 9-day running median of ACI between 10°N and 10°S from May 2006 to December 2011. The dashed vertical lines indicate the reference state from November 2007 to March 2008, and the investigation period for the Merapi eruption from November 2010 to March 2011. The red triangle indicates the time of the Merapi eruption (No. 9). The black dots indicate 1 Soufriere Hills, 2 Tavurvur (Rabaul), 3 Piton de la Fournaise, 4 Jebel at Tair, 5 Kasatochi, 6 Dalaffilla, 7 Sarychev, 8 Pacaya, 10 Nabro.